Title page

Functional coupling between TRPV4 channel and TMEM16F modulates human trophoblast fusion

Yang Zhang[1], Pengfei Liang[1], Liheng Yang[2], Ke Zoe Shan[1], Liping Feng[3,4], Yong Chen[5], Wolfgang Liedtke[5-9], Carolyn B. Coyne[2,10], Huanghe Yang[1,6,*]

[1]Department of Biochemistry, Duke University Medical Center, Durham, NC 27710, USA
[2]Department of Molecular Genetics and Microbiology, Duke University Medical Center, Durham, NC 27710, USA
[3]Department of Obstetrics and Gynecology, Duke University Medical Center, Durham, NC, 27710, USA
[4]MOE-Shanghai Key Laboratory of Children's Environmental Health, Xinhua Hospital, Shanghai, China
[5]Department of Neurology, Duke University Medical Center, Durham, NC 27710, USA
[6]Department of Neurobiology, Duke University Medical Center, Durham, NC 27710, USA
[7]Department of Anesthesiology, Duke University Medical Center, Durham, NC 27710, USA
[8]College of Dentistry, Department of Molecular Pathobiology, NYU, New York, NY 10021
[9]Global Development Scientific Council, Regeneron Pharmaceuticals, Tarrytown NY 10591
[10]Duke Human Vaccine Institute, Duke University, Durham, NC, 27710, USA

* Corresponding author: Huanghe Yang. Email: huanghe.yang@duke.edu

Conflict of interest: The authors declare no conflict of interests.

Abstract

TMEM16F, a Ca^{2+}-activated phospholipid scramblase (CaPLSase), is critical for placental trophoblast syncytialization, HIV infection, and SARS-CoV2-mediated syncytialization, however, how TMEM16F is activated during cell fusion is unclear. Here, using trophoblasts as a model for cell fusion, we demonstrate that Ca^{2+} influx through the Ca^{2+} permeable transient receptor potential vanilloid channel TRPV4 is critical for TMEM16F activation and plays a role in subsequent human trophoblast fusion. GSK1016790A, a TRPV4 specific agonist, robustly activates TMEM16F in trophoblasts. We also show that TRPV4 and TMEM16F are functionally coupled within Ca^{2+} microdomains in a human trophoblast cell line using patch clamp electrophysiology. Pharmacological inhibition or gene silencing of TRPV4 hinders TMEM16F activation and subsequent trophoblast syncytialization. Our study uncovers the functional expression of TRPV4 and one of the physiological activation mechanisms of TMEM16F in human trophoblasts, thus providing us with novel strategies to regulate CaPLSase activity as a critical checkpoint of physiologically- and disease-relevant cell fusion events.

Introduction

Phospholipids are essential building blocks of mammalian cell membranes and are asymmetrically distributed between the inner and outer leaflets (1, 2). TMEM16F is a Ca^{2+}-activated phospholipid scramblase (CaPLSase), that catalyzes trans-bilayer movement of the phospholipids down their concentration gradients (3, 4). In response to increased intracellular Ca^{2+}, phosphatidylserine (PS), an anionic phospholipid that is usually sequestered in the inner membrane leaflet, can rapidly permeate through a hydrophilic pathway of TMEM16F and become exposed on the cell surface (5-8). In platelets, TMEM16F CaPLSase-mediated PS exposure facilitates clotting factor assembly to catalyze thrombin generation and blood coagulation (1, 3, 9). Consistent with its important role in blood coagulation, TMEM16F deficiency leads to defective thrombin generation and prolonged bleeding in Scott syndrome patients (3, 10, 11) and in TMEM16F knockout mice (9). Besides blood coagulation, TMEM16F-mediated PS exposure has been increasingly reported to be important in cell-cell fusion and viral-cell fusion events including placental trophoblast syncytialization (12), SARS-CoV2-mediated syncytialization (13) and HIV infection (14). To elucidate the physiological and pathological roles of TMEM16F in cell-cell and viral-cell fusion events, one hitherto missing prerequisite is to understand the cellular mechanisms of TMEM16F activation.

Ca^{2+} is required for TMEM16 activation (4, 15-18). Ca^{2+} binds to the highly conserved Ca^{2+} binding sites to activate TMEM16 proteins including TMEM16F CaPLSase and TMEM16A and TMEM16B Ca^{2+}-activated Cl^- channels (CaCCs) (4, 9, 18). However, the apparent Ca^{2+} sensitivity of TMEM16F is lower than that of TMEM16A and TMEM16B. Differing from CaCCs that are readily activated by elevated cytosolic Ca^{2+} from either cell surface Ca^{2+} channels or from internal stores (9, 19-24), TMEM16F activation requires more

robust and sustained intracellular Ca^{2+} elevation (3, 4, 8, 9, 25-29). Ca^{2+} ionophores are widely used to artificially trigger TMEM16F activation and these pharmacological tools allow us to study the biophysical properties or functional expression of TMEM16F in native cells (3, 5, 8, 12). Nevertheless, how TMEM16F is activated under physiological conditions remains unclear, greatly hindering our understanding of TMEM16F biology and subsequent modulation strategies.

We recently showed that TMEM16F is highly expressed in placenta trophoblasts and plays an essential role in human trophoblast syncytialization both *in vitro* and in mouse placental development *in vivo* (12). Our TMEM16F knockout mice displayed deficient trophoblast syncytialization, signs of intrauterine growth restriction, and partial perinatal lethality. Our animal experiments suggested that the extremely rare incidence of Scott syndrome patients exhibiting only mild bleeding tendencies (30, 31) could be derived from pregnancy complications due to *TMEM16F* loss-of-function in trophoblasts. To further understand the underlying mechanism of TMEM16F-mediated trophoblast fusion, it is critical to elucidate how TMEM16F is activated under physiological conditions. Ca^{2+}-permeable TRPV6 and L-type voltage-gated Ca^{2+} (Ca_V) channel expression has been reported in trophoblasts (32-36). Due to its fast inactivation kinetics upon Ca^{2+} entry (37), TRPV6 involves in trans-placental Ca^{2+} transport (CaT) instead of sustained Ca^{2+} signaling (38-41). L-type Cav channels, on the other hand, require strong membrane depolarization (42), which can hardly be achieved in non-excitable trophoblasts. Therefore, these known trophoblast Ca^{2+} channels are unlikely to play a major role in activating TMEM16F during trophoblast fusion.

Here we report that Ca^{2+} influx through Ca^{2+}-permeable TRPV4 channels in human trophoblasts plays a key role in activating TMEM16F CaPLSase to modulate trophoblast fusion. Using Ca^{2+} imaging and patch clap electrophysiology, we showed that TRPV4 channel is

functionally expressed in human trophoblasts. GSK-1016790A (GSK101), a TRPV4 specific agonist, causes robust Ca^{2+} entry, which triggers TMEM16F CaPLSase activation and subsequent PS exposure. Furthermore, using the different Ca^{2+} chelating kinetics of EGTA and BAPTA, our patch clamp recording further demonstrated that trophoblast TPRV4 and TMEM16F are functionally coupled within microdomains. We also show that gene silencing of *TRPV4* or pharmacological inhibition of TRPV4 channels hinders trophoblast syncytialization in a human trophoblast cell line and a human trophoblast stem cell-derived organoid model. Thus, manipulating Ca^{2+} channels can serve as an effective approach to control TMEM16F activities, thereby helping to dissect the biological functions of the CaPLSases. We anticipate that these findings will advance our understanding of the cellular activation mechanisms of TMEM16 CaPLSases in different physiological and pathological fusion processes, while also inspiring new therapeutic strategies to target TMEM16F-mediated diseases.

Results

TRPV4 is functionally expressed in human trophoblasts

As a contiguous multinucleated cell layer in the chorionic villi, the placental syncytiotrophoblast establish the most important materno-fetal exchange interface and perform vital barrier, transport, and secretion functions to sustain fetal development and maternal health (Figure 1A) (43, 44). The syncytiotrophoblast is formed and maintained by continuous cell fusion of underlying mononucleated cytotrophoblasts into the syncytial layer during placental development (44). Besides the trophoblast CaT encoded by *TRPV6* (38, 39), the single cell RNA sequencing results from the Human Protein Atlas show that *TRPV4* is also highly expressed in cytotrophoblasts and syncytiotrophoblasts in the human placenta among TRPV channels (Figure 1—figure supplement 1) (45, 46). Consistent with the database, our RT-qPCR experiment also

showed that *TRPV4* transcripts are expressed in human primary trophoblasts and BeWo cells, a human choriocarcinoma trophoblast cell line (Figure 1B-C). Immunofluorescence with a specific anti-TRPV4 antibody (Figure 1—figure supplement 2A-B) further demonstrates that TRPV4 is expressed in the multi-nucleated syncytiotrophoblasts and single-nucleated cytotrophoblasts in human placenta villi (Figure 1D), as well as in BeWo cells (Figure 1—figure supplement 2C).

TRPV4 is a Ca^{2+} permeable, non-selective cation channel with less pronounced inactivation than TRPV6 (37, 47, 48). Thus, TRPV4 activation might lead to sustained Ca^{2+} elevation in trophoblasts, which would subsequently activate TMEM16F. The availability of selective and potent TRPV4 agonists such as GSK101 and antagonists including GSK-2193874 (GSK219) (49, 50) enabled us to explicitly confirm TRPV4's functional expression in human trophoblasts and examine its capability to activate TMEM16F. We found that 20 nM GSK101 robustly increases intracellular Ca^{2+} in BeWo cells, sustaining for no less than 10 minutes (Figure 1E, 1G). Application of 20 μM 4α-phorbol-12,13-didecanoate (4α-PDD), another TRPV4 agonist, also induced sustained intracellular Ca^{2+} increase in BeWo cells (Figure 1—figure supplement 3). On the other hand, 500 nM TRPV4 antagonist GSK219 abolished the intracellular Ca^{2+} elevation induced by 20 nM GSK101, yet it failed to inhibit Ca^{2+} increase from ionomycin (Figure 1F-G). Our Ca^{2+} imaging experiments using specific pharmacological tools thus support TRPV4 functional expression in human trophoblasts and that TRPV4 activation can lead to sustained intracellular Ca^{2+} increase.

To further validate our Ca^{2+} imaging results, we used outside-out patch clamp to record GSK101-induced current from BeWo cell membranes. Indeed, GSK101 robustly elicits an outward rectifying cation current that is rapidly inhibited by co-application of GSK219 (Figure 1H-J). In addition to pharmacological inhibition, silencing *TRPV4* with siRNAs (Figure 1—

figure supplement 4) also greatly reduced GSK101-induced Ca^{2+} elevation (Figure 1—figure supplement 5A-B) and the non-selective, outward rectifying current (Figure 1—figure supplement 5C-E). Taken together, our Ca^{2+} imaging and patch clamp results established that Ca^{2+} permeable TRPV4 is functionally expressed in human trophoblasts and that TRPV4 activation can lead to sustained Ca^{2+} elevation in these cells.

Ca^{2+} entry through TRPV4 activates TMEM16F in human trophoblasts *in vitro*

Using TMEM16F's dual function as a Ca^{2+}-activated (i) phospholipid scramblase and (ii) a non-selective ion channel, we applied a fluorescence imaging-based CaPLSase assay (5, 8, 12) and patch clamp technique to investigate whether TRPV4-mediated Ca^{2+} influx activates endogenous TMEM16F in human trophoblasts. Upon GSK101 application, Ca^{2+} increased in both BeWo cells (Figure 2A, 2C) and primary human term placental trophoblasts (Figure 2—figure supplement 1), followed by phospholipid scrambling as evidenced by robust cell surface accumulation of the fluorescently tagged PS sensor Annexin-V (AnV) (Figure 2A, 2D, Video 1). In addition, the plasma membrane was dramatically remodeled and released numerous PS positive microparticles, which is consistent with the essential role of TMEM16F in mediating microparticle release in platelets (51). In stark contrast, TMEM16F deficient BeWo (KO) cells did not exhibit CaPLSase activity, despite robust Ca^{2+} elevation in response to GSK101 application (Figure 2B, 2C-D, Video 2). Neither membrane remodeling nor microparticle release occurred in the TMEM16F KO BeWo cells. Our fluorescence imaging experiments thus indicate that TRPV4 activation can robustly activate TMEM16F CaPLSases in human trophoblasts.

We also used patch clamp to monitor whole cell current in BeWo cells in response to GSK101 stimulation. GSK101 rapidly triggered outward-rectifying TRPV4 current that plateaus in both wildtype (WT) and TMEM16F KO BeWo cells (Figure 3A-C). A much larger, voltage-,

and time-dependent conductance developed after a delay of 6-8 minutes. Distinct from the initial TRPV4 current, a larger voltage- and time-dependent conductance developed after a 6–8-minute delay (Figure 3A, D & E), showing slow activation and deactivation kinetics (Figure 3B-C). The biophysical characteristics of the second conductance closely resemble TMEM16F current recorded in heterologous expression systems (25-27) and endogenous TMEM16F current recorded in WT BeWo cells under whole-cell (Figure 3—figure supplement 1A-C) or outside-out configurations (Figure 3—figure supplement 1D-F). TMEM16F KO BeWo cells lack Ca^{2+}-, voltage- and time-dependent TMEM16F conductance (Figure 3—figure supplement 1); and GSK101 only triggers small, outward-rectifying TRPV4 conductance (Figure 3). It is worth noting that, for reasons unclear, there is always a long delay to activate TMEM16F CaPLSase and channel activities in the whole cell configuration (4, 8, 25, 27, 52). Using whole-cell patch clamp-lipid scrambling fluorometry (PCLSF) to monitor both ionic current and PS exposure (8, 26), we confirm that TMEM16F-mediated ion and phospholipid permeation happen almost simultaneously 7-10 minutes after GSK101 application (Figure 3—figure supplement **2**). Our imaging and patch clamp experiments therefore demonstrate that strong stimulation of TRPV4 activation can robustly activate TMEM16F channels in human trophoblasts.

To further support this conclusion, we used *TRPV4* siRNA and GSK219 to examine if suppressing *TRPV4* expression or TRPV4 activation prevents GSK101-induced TMEM16F activation. GSK219 indeed completely inhibits GSK101-induced Ca^{2+} elevation, eliminating TMEM16F-CaPLSase activation (Figure 4—figure supplement 1). Similarly, siRNA knockdown of *TRPV4* not only greatly suppresses the endogenous TRPV4 current and TRPV4-mediated Ca^{2+} influx in BeWo cells (Figure 4A, 4C-E and Figure 1—figure supplement 5), but also prevents TMEM16F-mediated PS exposure (Figure 4A-B) and ion permeation (Figure 4C-E).

We still observed robust ionomycin-induced phospholipid scrambling and TMEM16F current in *TRPV4* knockdown BeWo cells (Figure 4—figure supplement 2), suggesting that TMEM16F CaPLSases are not affected by *TRPV4* knockdown. Our CaPLSase imaging and patch clamp experiments thus demonstrate that TRPV4, a previously under-appreciated Ca^{2+}-permeable channel in human trophoblasts, can serve as an upstream Ca^{2+}-source for trophoblast TMEM16F activation.

TRPV4 and TMEM16F are functionally coupled within microdomains

To overcome TMEM16F's relatively low Ca^{2+} sensitivity (8, 9, 25), its Ca^{2+} sources must be nearby. Unfortunately, the validated antibodies for TRPV4 (Figure 1—figure supplement 2) and TMEM16F (12) are incompatible, which prevents us from using standard biochemical or imaging analyses to demonstrate their spatial relationship under native conditions. Instead, we used a quantitative patch clamp approach to estimate the proximity between endogenous TRPV4 and TMEM16F in trophoblasts, taking advantage of EGTA and BAPTA's differential Ca^{2+} buffering kinetics to distinguish between TRPV4 Ca^{2+} micro-domains and nano-domains (53-58). Because we and others have shown that TMEM16F ionic current is instantaneously elicited by Ca^{2+} without delay in excised inside-out (9, 52), we conducted outside-out patch recording to i) enable extracellular application of GSK101 and, ii) avoid complications derived from the long delay of TMEM16F activation in the whole cell configuration (Figure 3A and Figure 3—figure supplement 2) (8, 25, 27, 52).

In the presence of GSK101, we varied the duration of a -100 mV pre-pulse to facilitate Ca^{2+} influx through TRPV4 channels (Figure 5A). 30 nM GSK101 elicited a small outward-rectifying TRPV4 current in the absence of extracellular Ca^{2+} (Figure5B, #1) or without TMEM16F expression (Figure 5B, #5). As this current depends on GSK101 but not on the

duration of the pre-pulse (Figure 5—figure supplement 1), it is largely mediated by TRPV4. Under 2.5 mM extracellular Ca^{2+} and in the presence of 0.2 mM intracellular EGTA from the electrode, GSK101 rapidly elicited a large, time dependent current in WT (Figure 5B-C, #2) but not TMEM16F-KO BeWo cells (Figure 5B, #5), implying that TMEM16F is responsible for the GSK101-induced time dependent current. Interestingly, TMEM16F current amplitudes remain stable regardless of pre-pulse duration, suggesting that Ca^{2+} influx through TRPV4 can activate nearby TMEM16F channels and then rapidly diffuse into the bulk pipette solution without obvious accumulation (Figure 5B, #2). When the intracellular EGTA concentration was increased to 2 mM, TMEM16F current after GSK101 stimulation was drastically delayed, suggesting that a higher concentration of EGTA in the electrode efficiently buffers Ca^{2+} influx through TRPV4 channels, hindering TMEM16F activation (Figure 5B-C, #3). When the -100 mV pre-pulse was prolonged, more Ca^{2+} entered through TRPV4, overcoming EGTA's buffer capacity within Ca^{2+} microdomains, ultimately activating nearby TMEM16F (Figure 5B, 5D, #3). In stark contrast, 2 mM BAPTA, which has much faster Ca^{2+} chelating kinetics (54-56), completely ablates TMEM16F current development; only TRPV4 current is observed under this condition (Figure 5B-D, #4). The effectiveness of BAPTA but not EGTA to abolish GSK101-induced TMEM16F channel activation demonstrates that TMEM16F and TRPV4 function together in shared microdomain.

TRPV4-TMEM16F coupling enables spatiotemporal CaPLSase activity

TRPV4-TMEM16F microdomain coupling suggests that Ca^{2+} influx through TRPV4 can efficiently activate TMEM16F CaPLSases without requiring sustained global Ca^{2+} increase. To test this hypothesis, we applied an extremely low concentration of GSK101 to BeWo cells. We found that 0.2 nM GSK101 triggered a mild global increase of Ca^{2+}, which rapidly decayed.

Following the Ca^{2+} transient, AnV fluorescence accumulated on a small membrane process and then rapidly disappeared (Figure 6A-B and Video 3). As opposed to strong 20-30 nM GSK101 induced irreversible PS exposure (Fig. 2 and video 1), 0.2 nM GSK101 induced local CaPLSase activity that can be fully reversible (Figure 6), reflecting the synergistic action of CaPLSases and lipid flippases in maintaining membrane phospholipid asymmetry under physiological conditions (2). In addition, mild TRPV4 stimulation-induced CaPLSase activity did not result in obvious membrane remodeling and microparticle release, which are usually evident after strong CaPLSase activation (Figure 2 and Video 1). Comparing with global PS exposure in response to 20 nM GSK101 (Figure. 2A, 2C, 2D and Figure 2—figure supplement 1), 0.2 nM GSK101 triggered local PS exposure in 7 out of 18 WT BeWo cells tested (Figure 6C). In stark contrast, 0.2 nM GSK101 did not stimulate any local CaPLSase activity in TMEM16F KO BeWo cells, albeit normal transient increase of global Ca^{2+} as WT BeWo cells (Figure 6C, Figure 6—figure supplement 1 and Video 4). It is worth noting that no local and transient PS exposure was observed in the *TRPV4* siRNA-treated BeWo cells even in the presence of saturating 20 nM GSK101 (Figure 1—figure supplement 5A-B), albeit weak increase of intracellular Ca^{2+} through the residual TRPV4 channels. Our experiment thus demonstrates that transient opening of TRPV4 is sufficient to activate TMEM16F CaPLSase in some subcellular locations. TRPV4-TMEM16F coupling likely plays a key role in spatiotemporal activation of TMEM16F CaPLSase in trophoblast under physiological conditions. Our experiment also shows that TMEM16F CaPLSase can be activated under physiologically relevant Ca^{2+} concentrations without requiring extremely high Ca^{2+} concentration of 20-200 μM as estimated by whole-cell patch clamp studies.

Inhibiting TRPV4 hinders human trophoblast fusion *in vitro*

We recently showed that TMEM16F plays an indispensable role in controlling trophoblast fusion.(12). To elucidate a physiological function of TRPV4-TMEM16F coupling in trophoblasts, we examined the impacts of TRPV4 inhibition on forskolin-induced BeWo cell fusion *in vitro*. Consistent with the critical role of TRPV4 in mediating Ca^{2+} influx and TMEM16F-mediated PS externalization, the fusion index of BeWo cells was significantly decreased when cells were exposed to the TRPV4 inhibitor, GSK219 (Figure 7A-B). Furthermore, *TRPV4* siRNA knockdown also significantly hinders BeWo cell fusion (Figure 7C-D). Our cell-based fusion measurements suggest that TRPV4-TMEM16F coupling plays a critical role in controlling trophoblast fusion.

Next, we attempted to understand the physiological function of TRPV4-TMEM16F coupling *in vivo* by examining the histology of the *Trpv4* deficient (KO) mouse placentas. We do not observe obvious defects on the gross morphology of the placentas (Figure 7—figure supplement 1A-B). Using MCT1 and MCT2 as markers for the SynT-1 and SynT-2 syncytiotrophoblast layers in the mouse labyrinth (Figure 7—figure supplement 1C), no obvious change in syncytiotrophoblast layer integrity was observed between the WT and *Trpv4* KO placentas (Figure 7—figure supplement 1D-E). The lack of fusion defect in mouse placentas is likely due to distinct expression profiles of *TRPV4* in human and mouse placentas. According to recent systematic mapping of Trp channel expression in the mouse placenta (59), *Trpv4* is only expressed in the maternal decidua but not the junctional zone nor the labyrinth, where cytotrophoblasts fuse and form the two syncytiotrophoblast layers (59). Interestingly, the species-specific differential expression profiles are not just limited to *TRPV4*. *Trpv6*, encoding a long-established Ca^{2+} transporter in human trophoblasts (60, 61) (Figure 1—figure supplement 1), is only weakly expressed in the mouse labyrinth and more prominently expressed in the

intraplacental yolk sac (59, 60). *Tprv2*, on the other hand, is highly expressed in the mouse labyrinth (59), yet only weakly expressed in human cytotrophoblasts and the syncytiotrophoblast according to the Human Protein Atlas (Figure 1—figure supplement 1). The species-specific differential expression of TRPV channels is possibly rooted in the fact that the placenta is a recently evolved organ (62). Therefore, TRPV4 might play a key role in the human placenta and a more marginal role in the mouse placenta. Future studies are therefore needed to systematically compare the physiological functions of other TRPV channels in human and murine trophoblasts.

The species-dependent expression of *Trpv4* in the murine placenta prevents us from using mice as an animal model. Therefore, we used a recently developed human trophoblast organoid *ex vivo* model (63) to further examine TRPV4-TMEM16F coupling in human trophoblast fusion (Figure 7E). An imaging method to directly quantify fusion indexes in 3D human trophoblast organoids has yet to be developed. Therefore, we evaluate the fusion efficiency by measuring the expression of the placental syncytiotrophoblast marker genes, *CSH1* and *CGB*, which encode human placental lactogen (hPL) and hormone-specific β-subunit of human chorionic gonadotropin (βhCG), respectively (Figure 7F). As both hPL and βhCG are specifically secreted by the syncytiotrophoblast (64), these markers have been widely used to as the biomarkers of trophoblast fusion (65-67). We found that incubation of human trophoblast organoids derived from two unique donor tissues with GSK219 abolished *CSH1* and *CGB* expression, indicating that pharmacological inhibition of TRPV4 can hinder human trophoblast fusion in the organoid model. Interestingly, TRPV4 inhibition even resulted in slight upregulation of *SYNCYTIN-1* (*SYN1*) in the human trophoblast organoids (Figure 7F). This suggests that the trophoblast fusion defect in the presence of TRPV4 inhibitor GSK219 is not derived from the reduction of fusogene

SYN1 expression. Our experiments using human trophoblast organoids and BeWo cells thus demonstrate that TRPV4 plays an important role in human trophoblast fusion *in vitro*.

Discussion

Using TRPV4-specific pharmacological and gene silencing tools, fluorescence imaging, and patch clamp recording with Ca^{2+} chelators, we show that TRPV4 and TMEM16F are functionally coupled within local Ca^{2+} microdomains in a human trophoblast cell line and their coupling plays an important role in trophoblast fusion. The spatial proximity between TRPV4 and TMEM16F ensures higher and more sustained Ca^{2+} elevation, which is required for spatiotemporal TMEM16F activation. When TRPV4 is strongly stimulated by 20-30 nM of GSK101, BeWo cells show a sustained global increase of Ca^{2+} and robust Ca^{2+}-dependent phospholipid scrambling and membrane remodeling (Figure 2). Distinct from delayed TMEM16F channel and scramblase activation under the invasive whole-cell patch clamp configuration (Figures 3A, 4C and Figure 3—figure supplement 2), there is a minimal delay in TMEM16F CaPLSase activation when intact BeWo cells are treated with the same concentration of GSK101 (Figures 2D, 4B and Figure 4—figure supplement 2). This observation suggests that 1) membrane break-in to form the whole-cell configuration likely disrupts the intracellular environment, alters some cellular factors or structures, which subsequently hinder TMEM16F activation; and 2) the previously reported low Ca^{2+} sensitivity (20 -200 μM) for TMEM16F channel activation in whole-cell patches may underestimate TMEM16F CaPLSase's Ca^{2+} affinity (7). Consistent with this hypothesis, our observation of spatiotemporal activation of CaPLSases in local membrane processes under 0.2 nM GSK101 stimulation further supports that extremely high, global increase of Ca^{2+} is not required for TMEM16F CaPLSase activation under physiological conditions. Future studies are needed to accurately measure the Ca^{2+}

sensitivity of native TMEM16F CaPLSase in different cell type and pinpoint the exact cellular factors and/or structures that hamper TMEM16F activation.

The transient and reversible CaPLSase activity observed under mild TRPV4 stimulation suggests that TMEM16F CaPLSase activity is likely dynamically regulated in a spatiotemporal fashion under physiological conditions. This highlights the importance of further understanding TMEM16F activation mechanisms to decipher its physiological and pathological functions. We anticipate that our study will inspire future investigations to examine if the functional coupling between Ca^{2+} permeable channels and TMEM16F is a generalized mechanism for TMEM16F activation across different cell types. Ca^{2+}-permeable channels other than TRPV4 may be identified as new Ca^{2+} sources for TMEM16F activation. TMEM16A and TMEM16B CaCCs are readily activated by Ca^{2+} entry and Ca^{2+} release from internal stores in both excitable and non-excitable cells (20-23). Future studies are also needed to examine if Ca^{2+} store release is sufficient to transiently activate TMEM16F at the plasma membrane.

As a polymodal temperature, chemical and osmotic sensors in vertebrates, TRPV4 Ca^{2+} permeable channel is widely expressed and has been reported to be important for vascular function, joint biology and disease, nociception, itch, central nervous system regulation of systemic tonicity, neuroprotection, skin barrier, immune and neurosensory function, lung fibrosis, and skeletal integrity (68). TRPV4's importance for reproduction was first demonstrated in an elegant study of the uterus, in which Ying, et al. demonstrated that TRPV4 in the myometrium modulates uterine tone during pregnancy and contributes to preterm birth (69). However, TRPV4's expression and physiological function in the human placenta remained unexplored. In our present study, we demonstrate for the first time that TRPV4 is functionally

expressed in human trophoblasts and plays an important role in regulating trophoblast Ca^{2+} signaling, activating TMEM16F to subsequently mediate trophoblast fusion (Figure 7G).

Our discovery of TRPV4 expression in human trophoblasts also opens a new avenue to further understand TRPV4 in reproductive biology and pregnancy complications. Future studies are needed to understand how TRPV4 is activated under physiological and pathological conditions and whether TRPV4 contributes to trophoblast functions besides activating TMEM16F (Figure 7G). As a polymodal sensor, TRPV4 senses temperature, osmolarity, and it can be activated by endogenous signaling molecules including bioactive lipid, such as glycerophospholipids (70) and endocannabinoids (68). It is plausible that TRPV4 may sense physiological cues, and respond to changing concentrations of endogenous lipid mediators, to maintain trophoblasts function. On the other hand, inappropriate activation mechanisms of TRPV4 might contribute pregnancy complications. Moreover, some dominant gain-of-function (GOF) mutations of *TRPV4* are lethal, up to this point, were considered as critically-severe skeletal malformation. Our data suggest that gain-of-function of TRPV4 may contribute to placental malfunction, resulting perinatal lethality (71, 72), another interesting subject for future studies.

Cell fusion including cell-cell fusion and viral-cell fusion requires the synergistic action of multiple fusion machineries and is tightly regulated (73-75). In addition to known fusogens, recent studies from our and others show that TMEM16F CaPLSase plays essential roles in trophoblast fusion (12), HIV-host cell fusion (14), and SARS-CoV2-mediated syncytialization (13). Although a detailed mechanism for TMEM16F-mediated cell-cell fusion remains to be determined, it is plausible that PS exposure mediated by TMEM16F CaPLSase serves as a ‘fuse-me’ signal to prime the fusogenic sites or fusogenic synapses to facilitate these cell fusion events.

Our current finding that TMEM16F is functionally coupled to TRPV4 channels raises a provocative question of the molecular identities of Ca^{2+} sources that activate TMEM16F in viral diseases where TMEM16F plays a significant role in syncytium-formation, namely HIV infection (14) and SARS-CoV2-mediated pathological syncytialization (13). Targeting functional coupling between Ca^{2+}-permeable channels (76) and TMEM16F might complement current therapeutic strategies for HIV-AIDS and COVID19.

Taken together, we reveal functional expression of a previously unrecognized Ca^{2+}-permeable channel, TRPV4 in human trophoblasts and demonstrate that microdomain-coupled Ca^{2+} entry through TRPV4 directly activates TMEM16F CaPLSase and contributes to trophoblast fusion. Our study thus uncovers a new physiological activation mechanism for TMEM16F, demonstrating one approach to understand TMEM16F's biological functions in wide-ranging physiological and pathological processes, including blood coagulation, bone mineralization, HIV infection, trophoblast fusion and SARS-CoV2-mediated syncytialization.

Materials and Methods

Cell lines. The BeWo cell line was a gift from Dr. Sallie Permar at Duke University and was authenticated by the Duke University DNA Analysis Facility. The TMEM16F KO BeWo cell line was generated by sgRNAs targeting exon 2 as described previously (12). The HEK293T cells are authenticated by Duke Cell Culture Facility. BeWo cells were cultured in Dulbecco's Modified Eagle Medium-Hams F12 (DMEM/F12) medium (Gibco, REF 11320-033) and HEK293T cells were cultured in Dulbecco's modified Eagle medium (Gibco, REF 11995-065). Both media were supplemented with 10% FBS (Sigma, cat. F2442) and 1% penicillin/streptomycin (Gibco, REF 15-140-122) and cells were cultured in a 5% CO_2-95% air incubator at 37°C.

Human placenta tissue and primary cultured human trophoblast cells. Placental tissues were collected under the Institutional Review Board approval (IRB# PRO00014627 and XHEC-C-2018-089). Informed consent was obtained following the IRBs. Placental cytotrophoblast cells from human term placenta were prepared using a modified method of Kliman as described previously (12). The cytotrophoblasts were plated in fibronectin coated cover glass and supplied with DMEM/F12 medium, 10% FBS, and 1% penicillin/streptomycin.

siRNA transfection. BeWo cells were seeded on coverslips coated with poly-L-lysine (Sigma, # P2636). One day after seeding, BeWo cells were transfected with *TRPV4* siRNAs (Horizon, # MQ-004195-00-0002) using Lipofectamine RNAiMAX Transfection Reagent (Invitrogen, # 13778075) following the manufacturer's instructions. After siRNA transfection for 24 hours, the medium was changed to fresh DMEM-F12 and the cells were cultured for another 24 hours before confocal imaging.

Trophoblast Organoids (TOs) Culture. TOs lines used in this study were derived as described (63). Briefly, TOs lines were plated into the Matrigel (Corning 356231) 'domes', then submerged with prewarmed complete growth media as described (63). TO cultures were maintained in a 37°C humidified incubator with 5% CO_2. The medium was renewed every 2-3 days. About 5-7 days after seeding, TOs were collected from Matrigel 'domes', digested in prewarmed Stem Pro Accutase (Gibco, A11105-01) at 37°C for 5-7 min, then mechanically dissociated into small fragments using electronic automatic pipette. If necessary, digested TOs can be further pipetted manually and then re-seeded into fresh Matrigel 'domes' in 24-well tissue culture plates (Corning 3526). Propagation was performed at 1:3-6 splitting ratio once every 5-7 days. During the first four days after re-seeding, the complete growth media was supplemented with additional 5 μM Y-27632 (Sigma, Y0503). For TRPV4 inhibition, the dissociated TOs were directly plated onto the top of 20 μL of Matrigel coating in each well of a regular 24-well plate and cultured for 5 days prior to GSK219 treatment in complete growth media. After 96 hrs, supernatant media was removed and coat seeding TOs were lysed with lysis buffer from Sigma Total RNA purification kit for total RNA purification. RT-qPCR were performed as described (63). Primer sequences can be found in Supplemental File 1.

Mice. The TRPV4 deficient mouse line was reported previously (77). PCR genotyping was performed using tail DNA extraction. Mouse handling and usage were carried out in a strict compliance with protocols approved by the Institutional Animal Care and Use Committee at Duke University, in accordance with National Institute of Health guideline.

Mouse placenta histological analysis. Isoflurane was used for deep anesthesia of mice. Placentas and embryos were freshly collected and fixed in 4% paraformaldehyde (Electron Microscopy Sciences, cat. 15710) overnight at 4 °C and embedded in paraffin (HistoCore

Arcadia H and Arcadia C, Leica Biosystems) and then sectioned at 5 μm by using Leica RM2255 (Leica Biosystems, Buffalo Grove, IL) for histological staining. Immunofluorescence staining against MCT1 (EMD Millipore, #AB1286-I) and MCT4 (Santa Cruz Biotechnology, #sc-376140) were performed on TRPV4 WT and KO placenta by using MCT1 antibody (Millipore-Sigma, AB1286-I) and MCT4 antibody (Santa Cruz Biotechnology, Inc., sc-376140). Images were collected using Zeiss 780 inverted confocal microscope.

Fluorescence imaging of Ca^{2+} and PS exposure. Ca^{2+} dynamics were monitored using a calcium indicator Calbryte 520 AM (AAT Bioquest, # 20701). BeWo cells were stained with 1 μM Calbryte 520 AM in DMEM-F12 for 15 minutes at 37°C and 5% CO_2. PS exposure was detected using CF 594–tagged Annexin V (AnV, Biotium, # 29011). To monitor Ca^{2+} and PS dynamics before stimulation, Calbryte 520 AM-stained cells were loaded on the cover glass and incubated in AnV (1:175 diluted in Hank's balanced salt solution) and image for 50 seconds. To stimulate TRPV4 activity, 20 nM or 0.2 nM TRPV4 agonist GSK101 (Sigma, #G0798) was used. To inhibit TRPV channel activities, 500 nM TRPV4 antagonist GSK219 (Sigma, #SML0694) was applied to trophoblasts. Cells were continually imaged for another 10 minutes. Zeiss 780 inverted confocal microscope was used to image Ca^{2+} and PS dynamics at a 5-second interval. MATLAB was used to quantify the cytosolic calcium and AnV binding.

BeWo cell fusion and quantification of fusion index. After seeding cells for 24 hours, BeWo cells were treated with 30 μM forskolin (Cell Signaling Technology, #3828s) for 48 hours to induce cell fusion, with forskolin-containing media changed every 24 hours. After forskolin treatment, cells were stained with Hoechst (Invitrogen™, #H3570, 1:2000) and Di-8-ANEPPS (Biotium, #61012, 2 μM) or Wheat Germ Agglutinin Alexa Fluor™-488 Conjugate (Invitrogen™, #W11261, 1:1000) for 15 min at 37°C and 5% CO_2. For each treatment group, six

random fields of view were acquired using Zeiss 780 inverted confocal microscope. Cell fusion is quantified by calculating the fusion index (FI) as described previously (12). FI is calculated as:

$$FI = \frac{\sum_1^6 fi}{6} = \frac{\sum_1^6 \left(\frac{\sum nf}{N}\right)}{6}$$

where *fi* represents the fusion index of each field; *nf*, the number of fused nuclei in each field; *N*, the total nuclei number in each field. To avoid the instances of cell division, cells with two nuclei were not considered as fused cells.

Immunostaining. The mCherry-TMEM16F expressing BeWo TMEM16F knockout (KO) cells were generated by transduction of mCherry-TMEM16F containing lentiviral particles as described previously (12). Flag-tagged R. norvegicus TRPV4 plasmids (Addgene, # 45751) were transiently transfected to HEK293T cells by using X-tremeGENE360 transfection reagent (Millipore-Sigma). Medium was replaced with regular culture medium 4 hours after transfection. Ruthenium red (Sigma, #R2751, 10μM) was add into the culture medium to inhibit TRPV4 activation. Cells were fixed with 1% paraformaldehyde in phosphate-buffered saline (PBS) for 10 minutes, permeabilized with 0.1% Triton X-100 in PBS, and blocked with 5% goat serum in PBS for an hour. Coverslips were incubated in primary antibodies, anti-TRPV4 (1:200, Alomone, #ACC-034) and anti-mCherry (1:500, NOVUS, #NBP1-96752) or anti-Flag (1:1000, Sigma, #F1804), at 4 °C overnight. Secondary antibodies, Alexa Fluor 488 or Alexa Fluor 640 fluorescence system (Molecular Probes, #35552), were used for fluorescent staining. After staining nuclei with 4′,6-diamidino-2-phenylindole (DAPI), coverslips were mounted using ProLong™ Diamond Antifade Mountant (Invitrogen, #P36961) and imaged with Zeiss 780 inverted confocal microscope.

Electrophysiology. All currents were recorded in either outside-out or whole-cell configurations on BeWo cells using an Axopatch 200B amplifier (Molecular Devices) and the pClamp software package (Molecular Devices). The glass pipettes were pulled from borosilicate capillaries (Sutter Instruments) and fire-polished using a microforge (Narishge) to reach resistance of 2–3 MΩ. The pipette solution contained (in mM): 140 CsCl, 10 HEPES, 1 $MgCl_2$, adjusted to pH 7.2 (CsOH), 0.2 or 2 mM EGTA or 2mM BAPTA as indicated. The bath solution contained 140 CsCl, 10 HEPES, 0 or 2.5 $CaCl_2$ as indicated, adjusted to pH 7.4 (CsOH). Pharmacological reagents were applied from extracellular side including 30 nM GSK101 (Sigma, #G0798), 500 nM GSK219 (Sigma, #SML0694) as indicated. Procedures for solution application were as employed previously (5, 26). Briefly, a perfusion manifold with 100–200 μm tip was packed with eight PE10 tubes. Each tube was under separate valve control (ALA-VM8, ALA Scientific Instruments), and solution was applied from only one PE10 tube at a time onto the excised patches or whole-cell clamped cells. All experiments were at room temperature (22–25°C). All the other chemicals for solution preparation were obtained from Sigma-Aldrich.

Patch clamp-lipid scrambling fluorometry assay (PCLSF). This assay combined patch clamp recoding with phospholipid scrambling assay as reported previously (8, 26). Briefly, cells were seeded and transfected on poly-L-lysine (Sigma)-coated coverslips prior to the experiments. Fluorescence-tagged (CF 594) Annexin V (Annexin V-CF 594, Biotium # 29011) was diluted at 0.5 μg ml^{-1} with extracellular recording solutions (140 mM CsCl, 2.5 mM $CaCl_2$, 10 mM HEPES, 30nM GSK101, pH 7.4) and then added into one of the perfusion tubes. Glassed pipettes were prepared and filled with internal solution as mentioned previously in the electrophysiology part. After focusing on the cell surface, switching the filter to CF594 (Annexin V signal). Then a whole-cell patch was achieved, following with application of designed voltage protocol at an

inter-sweep interval of 5 s. Simultaneously, imaging recordings about Annexin V signal was initiated also with 5 seconds interval.

Statistical analysis. All statistical analyses were performed with Clampfit 10.7 (Molecular Devices), Excel (Microsoft), or Prism software (GraphPad). A two-tailed Student's t-test was used for single comparisons between two groups (paired or unpaired). One-way ANOVA following by Tukey's test was used for multiple comparisons. Data were represented as mean ± standard error of the mean (SEM) unless stated otherwise. Symbols *, **, ***, **** and ns denote statistical significance corresponding to p-value <0.05, <0.01, <0.001, <0.0001 and no significance, respectively.

Data Availability. All study data are included in the article and/or supporting information. All the numerical data can be found in the Source data Excel files associated with each figure. The MATLAB code supporting the present study is available at GitHub https://github.com/YZ299/matlabcode/blob/main/matlabcode.m.

Acknowledgments: We appreciate Dr. Hua Pan for technical support and Augustus Lowry for critical reading of the manuscript. This work was supported by NIH-DP2GM126898 grant (to H.Y.).

References:

1. E. M. Bevers, P. L. Williamson, Getting to the Outer Leaflet: Physiology of Phosphatidylserine Exposure at the Plasma Membrane. *Physiol Rev* **96**, 605-645 (2016).
2. S. Nagata, J. Suzuki, K. Segawa, T. Fujii, Exposure of phosphatidylserine on the cell surface. *Cell Death Differ* **23**, 952-961 (2016).
3. J. Suzuki, M. Umeda, P. J. Sims, S. Nagata, Calcium-dependent phospholipid scrambling by TMEM16F. *Nature* **468**, 834-U135 (2010).
4. S. C. Le, P. Liang, A. J. Lowry, H. Yang, Gating and Regulatory Mechanisms of TMEM16 Ion Channels and Scramblases. *Front Physiol* **12**, 787773 (2021).
5. T. Le *et al.*, An inner activation gate controls TMEM16F phospholipid scrambling. *Nat Commun* **10**, 1846 (2019).
6. S. Feng *et al.*, Cryo-EM Studies of TMEM16F Calcium-Activated Ion Channel Suggest Features Important for Lipid Scrambling. *Cell Rep* **28**, 567-579 e564 (2019).
7. C. Alvadia *et al.*, Cryo-EM structures and functional characterization of the murine lipid scramblase TMEM16F. *Elife* **8** (2019).
8. K. Yu *et al.*, Identification of a lipid scrambling domain in ANO6/TMEM16F. *Elife* **4**, e06901 (2015).
9. H. Yang *et al.*, TMEM16F forms a Ca2+-activated cation channel required for lipid scrambling in platelets during blood coagulation. *Cell* **151**, 111-122 (2012).
10. P. Boisseau *et al.*, A new mutation of ANO6 in two familial cases of Scott syndrome. *Br J Haematol* **180**, 750-752 (2018).
11. E. Castoldi, P. W. Collins, P. L. Williamson, E. M. Bevers, Compound heterozygosity for 2 novel TMEM16F mutations in a patient with Scott syndrome. *Blood* **117**, 4399-4400 (2011).
12. Y. Zhang *et al.*, TMEM16F phospholipid scramblase mediates trophoblast fusion and placental development. *Sci Adv* **6**, eaba0310 (2020).
13. L. Braga *et al.*, Drugs that inhibit TMEM16 proteins block SARS-CoV-2 spike-induced syncytia. *Nature* **594**, 88-+ (2021).
14. E. Zaitseva *et al.*, Fusion Stage of HIV-1 Entry Depends on Virus-Induced Cell Surface Exposure of Phosphatidylserine. *Cell Host Microbe* **22**, 99-110 e117 (2017).
15. J. Tien *et al.*, A comprehensive search for calcium binding sites critical for TMEM16A calcium-activated chloride channel activity. *Elife* **3** (2014).
16. K. Yu, C. Duran, Z. Qu, Y. Y. Cui, H. C. Hartzell, Explaining calcium-dependent gating of anoctamin-1 chloride channels requires a revised topology. *Circ Res* **110**, 990-999 (2012).
17. J. D. Brunner, N. K. Lim, S. Schenck, A. Duerst, R. Dutzler, X-ray structure of a calcium-activated TMEM16 lipid scramblase. *Nature* **516**, 207-212 (2014).
18. N. Pedemonte, L. J. Galietta, Structure and function of TMEM16 proteins (anoctamins). *Physiol Rev* **94**, 419-459 (2014).
19. I. Cabrita *et al.*, Differential effects of anoctamins on intracellular calcium signals. *The FASEB Journal* **31**, 2123-2134 (2017).
20. M. Genovese *et al.*, TRPV4 and purinergic receptor signalling pathways are separately linked in airway epithelia to CFTR and TMEM16A chloride channels. *J Physiol-London* **597**, 5859-5878 (2019).

21. X. Jin *et al.*, Activation of the Cl- Channel ANO1 by Localized Calcium Signals in Nociceptive Sensory Neurons Requires Coupling with the IP3 Receptor. *Science Signaling* **6**, ra73-ra73 (2013).
22. S. Shah *et al.*, Local Ca2+ signals couple activation of TRPV1 and ANO1 sensory ion channels. *Sci Signal* **13** (2020).
23. Y. Zhang *et al.*, Inferior Olivary TMEM16B Mediates Cerebellar Motor Learning. *Neuron* **95**, 1103-+ (2017).
24. Y. Takayama, K. Shibasaki, Y. Suzuki, A. Yamanaka, M. Tominaga, Modulation of water efflux through functional interaction between TRPV4 and TMEM16A/anoctamin 1. *FASEB J* **28**, 2238-2248 (2014).
25. S. Grubb *et al.*, TMEM16F (Anoctamin 6), an anion channel of delayed Ca2+ activation. *Journal of General Physiology* **141**, 585-600 (2013).
26. P. Liang, H. Yang, Molecular underpinning of intracellular pH regulation on TMEM16F. *J Gen Physiol* **153** (2021).
27. T. Shimizu *et al.*, TMEM16F is a component of a Ca2+-activated Cl- channel but not a volume-sensitive outwardly rectifying Cl- channel. *American Journal of Physiology - Cell Physiology* **304** (2013).
28. W. L. Ye *et al.*, Phosphatidylinositol-(4,5)-bisphosphate regulates calcium gating of small-conductance cation channel TMEM16F. *P Natl Acad Sci USA* **115**, E1667-E1674 (2018).
29. W. L. Ye, T. W. Han, M. He, Y. N. Jan, L. Y. Jan, Dynamic change of electrostatic field in TMEM16F permeation pathway shifts its ion selectivity. *Elife* **8** (2019).
30. R. F. Zwaal, P. Comfurius, E. M. Bevers, Scott syndrome, a bleeding disorder caused by defective scrambling of membrane phospholipids. *Biochim Biophys Acta* **1636**, 119-128 (2004).
31. S. L. Millington-Burgess, M. T. Harper, Gene of the issue: ANO6 and Scott Syndrome. *Platelets* **31**, 964-967 (2020).
32. C. Fecher-Trost *et al.*, Maternal Transient Receptor Potential Vanilloid 6 (Trpv6) Is Involved In Offspring Bone Development. *Journal of Bone and Mineral Research* **34**, 699-710 (2019).
33. S. Meuris, B. Polliotti, C. Robyn, P. Lebrun, Ca2+ entry through L-type voltage-sensitive Ca2+ channels stimulates the release of human chorionic gonadotrophin and placental lactogen by placental explants. *Biochim Biophys Acta* **1220**, 101-106 (1994).
34. S. Miura, K. Sato, M. Kato-Negishi, T. Teshima, S. Takeuchi, Fluid shear triggers microvilli formation via mechanosensitive activation of TRPV6. *Nat Commun* **6**, 8871 (2015).
35. C. Niger, A. Malassine, L. Cronier, Calcium channels activated by endothelin-1 in human trophoblast. *J Physiol-London* **561**, 449-458 (2004).
36. Y. Suzuki *et al.*, Calcium channel TRPV6 is involved in murine maternal-fetal calcium transport. *J Bone Miner Res* **23**, 1249-1256 (2008).
37. A. K. Singh, L. L. McGoldrick, E. C. Twomey, A. I. Sobolevsky, Mechanism of calmodulin inactivation of the calcium-selective TRP channel TRPV6. *Sci Adv* **4**, eaau6088 (2018).
38. C. Fecher-Trost, U. Wissenbach, P. Weissgerber, TRPV6: From identification to function. *Cell Calcium* **67**, 116-122 (2017).

39. M. K. C. van Goor, J. G. J. Hoenderop, J. van der Wijst, TRP channels in calcium homeostasis: from hormonal control to structure-function relationship of TRPV5 and TRPV6. *Biochim Biophys Acta Mol Cell Res* **1864**, 883-893 (2017).
40. R. Moreau *et al.*, Calcium uptake and calcium transporter expression by trophoblast cells from human term placenta. *Biochim Biophys Acta* **1564**, 325-332 (2002).
41. T. Stumpf *et al.*, The human TRPV6 channel protein is associated with cyclophilin B in human placenta. *J Biol Chem* **283**, 18086-18098 (2008).
42. B. Hille, *Ion channels of excitable membranes* (Sinauer, Sunderland, MA, ed. 3rd, 2001).
43. K. Benirschke, S. G. Driscoll, "The pathology of the human placenta" in Placenta. (Springer, 1967), pp. 97-571.
44. B. Huppertz, M. Borges, Placenta trophoblast fusion. *Methods Mol Biol* **475**, 135-147 (2008).
45. M. Uhlen *et al.*, A genome-wide transcriptomic analysis of protein-coding genes in human blood cells. *Science* **366** (2019).
46. E. Sjostedt *et al.*, An atlas of the protein-coding genes in the human, pig, and mouse brain. *Science* **367** (2020).
47. A. Jara-Oseguera, K. E. Huffer, K. J. Swartz, The ion selectivity filter is not an activation gate in TRPV1-3 channels. *eLife* **8**, e51212 (2019).
48. B. Nilius, J. Vriens, J. Prenen, G. Droogmans, T. Voets, TRPV4 calcium entry channel: a paradigm for gating diversity. *Am J Physiol Cell Physiol* **286**, C195-205 (2004).
49. M. Cheung *et al.*, Discovery of GSK2193874: An Orally Active, Potent, and Selective Blocker of Transient Receptor Potential Vanilloid 4. *Acs Med Chem Lett* **8**, 549-554 (2017).
50. K. S. Thorneloe *et al.*, N-((1S)-1-{[4-((2S)-2-{[2,4-Dichlorophenyl)sulfonyl]amino}-3-hydroxypropanoyl)-1-piperazinyl]carbonyl}-3-methylbutyl)-1-benzothiophene-2-carboxamide (GSK1016790A), a Novel and Potent Transient Receptor Potential Vanilloid 4 Channel Agonist Induces Urinary Bladder Contraction and Hyperactivity: Part I (vol 326, pg 432, 2008). *J Pharmacol Exp Ther* **338**, 410-410 (2011).
51. T. Fujii, A. Sakata, S. Nishimura, K. Eto, S. Nagata, TMEM16F is required for phosphatidylserine exposure and microparticle release in activated mouse platelets. *Proc Natl Acad Sci U S A* **112**, 12800-12805 (2015).
52. H. Lin, J. Roh, J. H. Woo, S. J. Kim, J. H. Nam, TMEM16F/ANO6, a Ca(2+)-activated anion channel, is negatively regulated by the actin cytoskeleton and intracellular MgATP. *Biochem Biophys Res Commun* **503**, 2348-2354 (2018).
53. G. J. Augustine, F. Santamaria, K. Tanaka, Local Calcium Signaling in Neurons. *Neuron* **40**, 331-346 (2003).
54. S. L. Dargan, I. Parker, Buffer kinetics shape the spatiotemporal patterns of IP3-evoked Ca2+ signals. *J Physiol* **553**, 775-788 (2003).
55. B. Fakler, J. P. Adelman, Control of KCa Channels by Calcium Nano/Microdomains. *Neuron* **59**, 873-881 (2008).
56. E. Neher, Vesicle Pools and Ca2+ Microdomains: New Tools for Understanding Their Roles in Neurotransmitter Release. *Neuron* **20**, 389-399 (1998).
57. E. Eggermann, I. Bucurenciu, S. P. Goswami, P. Jonas, Nanodomain coupling between Ca(2)(+) channels and sensors of exocytosis at fast mammalian synapses. *Nat Rev Neurosci* **13**, 7-21 (2011).

58. E. M. Adler, G. J. Augustine, S. N. Duffy, M. P. Charlton, Alien intracellular calcium chelators attenuate neurotransmitter release at the squid giant synapse. *J Neurosci* **11**, 1496-1507 (1991).
59. K. De Clercq *et al.*, Mapping the expression of transient receptor potential channels across murine placental development. *Cell Mol Life Sci* 10.1007/s00018-021-03837-3 (2021).
60. Y. Suzuki *et al.*, Calcium channel TRPV6 is involved in murine maternal-fetal calcium transport. *J Bone Miner Res* **23**, 1249-1256 (2008).
61. C. Fecher-Trost *et al.*, Maternal Transient Receptor Potential Vanilloid 6 (Trpv6) Is Involved In Offspring Bone Development. *J Bone Miner Res* **34**, 699-710 (2019).
62. R. M. Roberts, J. A. Green, L. C. Schulz, The evolution of the placenta. *Reproduction* **152**, R179-189 (2016).
63. L. Yang *et al.*, Innate immune signaling in trophoblast and decidua organoids defines differential antiviral defenses at the maternal-fetal interface. *bioRxiv* 10.1101/2021.03.29.437467, 2021.2003.2029.437467 (2022).
64. S. Yabe *et al.*, Comparison of syncytiotrophoblast generated from human embryonic stem cells and from term placentas. *P Natl Acad Sci USA* **113**, E2598-E2607 (2016).
65. G. Pidoux *et al.*, Biochemical characterization and modulation of LH/CG-receptor during human trophoblast differentiation. *J Cell Physiol* **212**, 26-35 (2007).
66. A. Deglincerti *et al.*, Self-organization of the in vitro attached human embryo. *Nature* **533**, 251-254 (2016).
67. U. J. Gaspard, J. Hustin, A. M. Reuter, R. Lambotte, P. Franchimont, Immunofluorescent localization of placental lactogen, chorionic gonadotrophin and its alpha and beta subunits in organ cultures of human placenta. *Placenta* **1**, 135-144 (1980).
68. T. Rosenbaum *et al.*, TRPV4: A Physio and Pathophysiologically Significant Ion Channel. *Int J Mol Sci* **21** (2020).
69. L. Ying *et al.*, The transient receptor potential vanilloid 4 channel modulates uterine tone during pregnancy. *Sci Transl Med* **7**, 319ra204 (2015).
70. Y. Chen *et al.*, Epithelia-Sensory Neuron Cross Talk Underlies Cholestatic Itch Induced by Lysophosphatidylcholine. *Gastroenterology* **161**, 301-317 e316 (2021).
71. S. S. Kang, S. H. Shin, C. K. Auh, J. Chun, Human skeletal dysplasia caused by a constitutive activated transient receptor potential vanilloid 4 (TRPV4) cation channel mutation. *Exp Mol Med* **44**, 707-722 (2012).
72. N. Camacho *et al.*, Dominant TRPV4 mutations in nonlethal and lethal metatropic dysplasia. *Am J Med Genet A* **152A**, 1169-1177 (2010).
73. N. G. Brukman, B. Uygur, B. Podbilewicz, L. V. Chernomordik, How cells fuse. *J Cell Biol* **218**, 1436-1451 (2019).
74. J. M. Whitlock, L. V. J. J. o. B. C. Chernomordik, Flagging fusion: Phosphatidylserine signaling in cell-cell fusion. 100411 (2021).
75. E. H. Chen, E. N. Olson, Unveiling the mechanisms of cell-cell fusion. *Science* **308**, 369-373 (2005).
76. W. M. Kuebler, S. E. Jordt, W. B. Liedtke, Urgent reconsideration of lung edema as a preventable outcome in COVID-19: inhibition of TRPV4 represents a promising and feasible approach. *Am J Physiol Lung Cell Mol Physiol* **318**, L1239-L1243 (2020).
77. W. Liedtke, J. M. Friedman, Abnormal osmotic regulation in trpv4-/- mice. *Proc Natl Acad Sci U S A* **100**, 13698-13703 (2003).

Figures

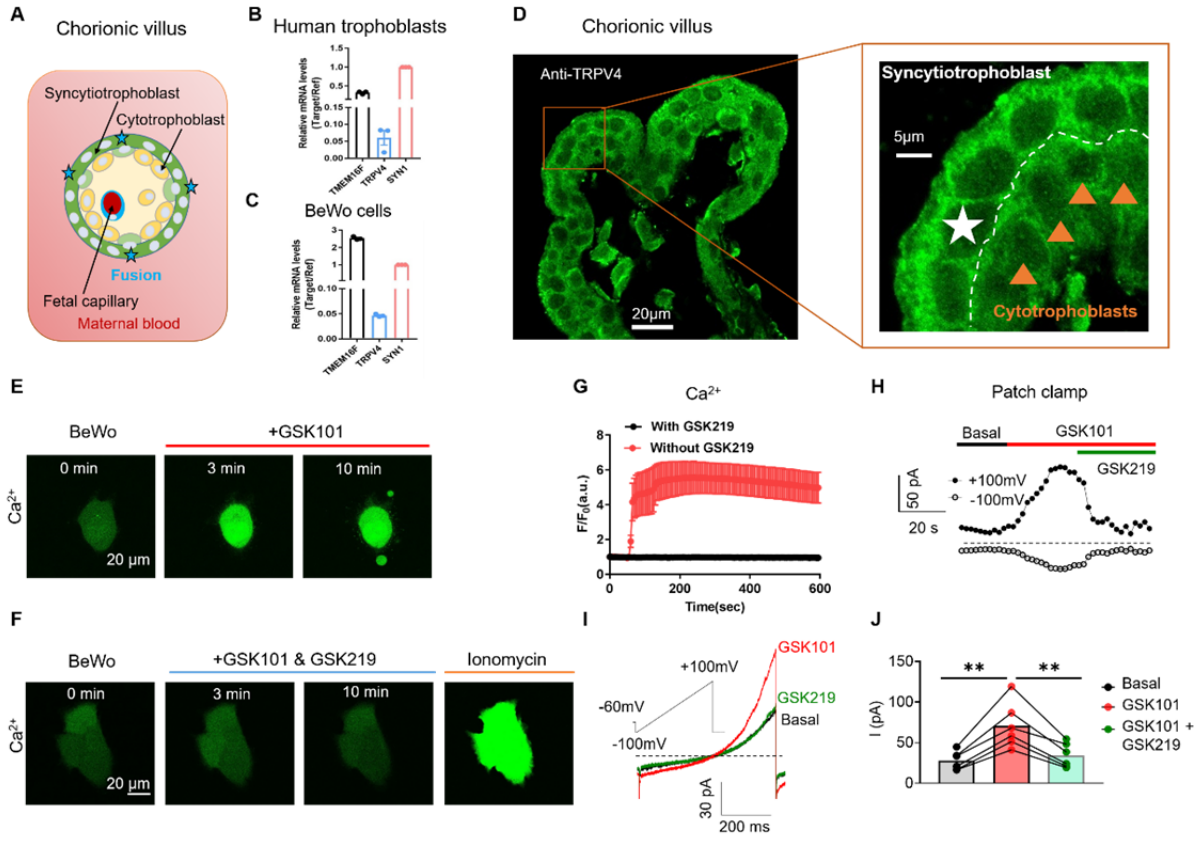

Figure 1. TRPV4 is functionally expressed in human trophoblasts. (**A**) Schematic of the first trimester placental villus and trophoblast fusion. **(B-C)** qRT-PCR of *TRPV4* in primary human trophoblasts (B) and BeWo cells (C). All genes were normalized to GAPDH and then normalized to Syncytin-1 (SYN1). **(D)** Representative immunofluorescence of TRPV4 (green) and nuclei (blue) in a human first trimester placenta villus (cross-section). TRPV4 is expressed in both cytotrophoblasts and syncytiotrophoblasts. **(E)** GSK1016790A (GSK101, 20 nM), a specific TRPV4 agonist, triggers robust intracellular Ca^{2+} elevation in BeWo cells. **(F)** GSK2193874 (GSK219, 500 nM), a selective TRPV4 antagonist, abolishes GSK101-induced Ca^{2+} influx through TRPV4 channels in BeWo cells. Ca^{2+} elevation through ionomycin is intact

in the presence of GSK219. All fluorescence images in D-F are the representatives of at least three biological replicates. **(G)** Summary of GSK101 (n = 4) and GSK219 (n = 5) effects on BeWo cell Ca^{2+} dynamics measured by Ca^{2+} dye (Calbryte 520). **(H)** Time course of outside-out currents elicited in response to 30 nM GSK101 with and without 500 nM GSK219. Current was elicited by a 500 ms ramp voltage protocol from -100 mV to +100 mV. The holding potential was set at -60 mV. **(I)** Representative current traces in the presence of GSK101 and GSK219+GSK101 from (H). **(J)** Quantification of GSK101-induced current in BeWo cells using the same voltage protocol in (H). Values represent mean ± SEM and statistics were done using Student's t-test (n=5 for each group, **: $p<0.01$).

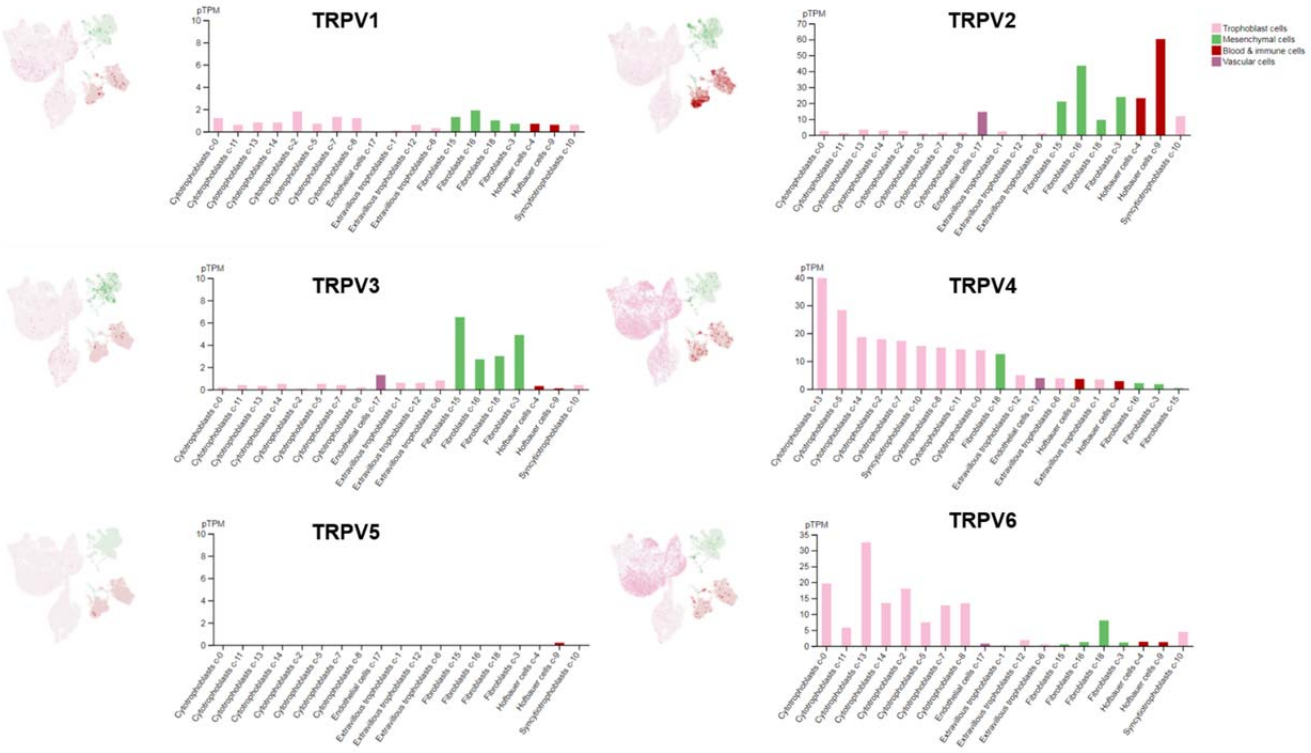

Figure 1—figure supplement 1. Single cell RNA sequencing results of *TRPV* channel genes in different cell types from human placentas. UMAP plots (left) illustrate single cell RNA expression profiles in different cell types, and bar graphs (right) show pTPM levels in each single cells cluster. All the data were from the Human Protein Atlas V20.1.proteinatlas.org.

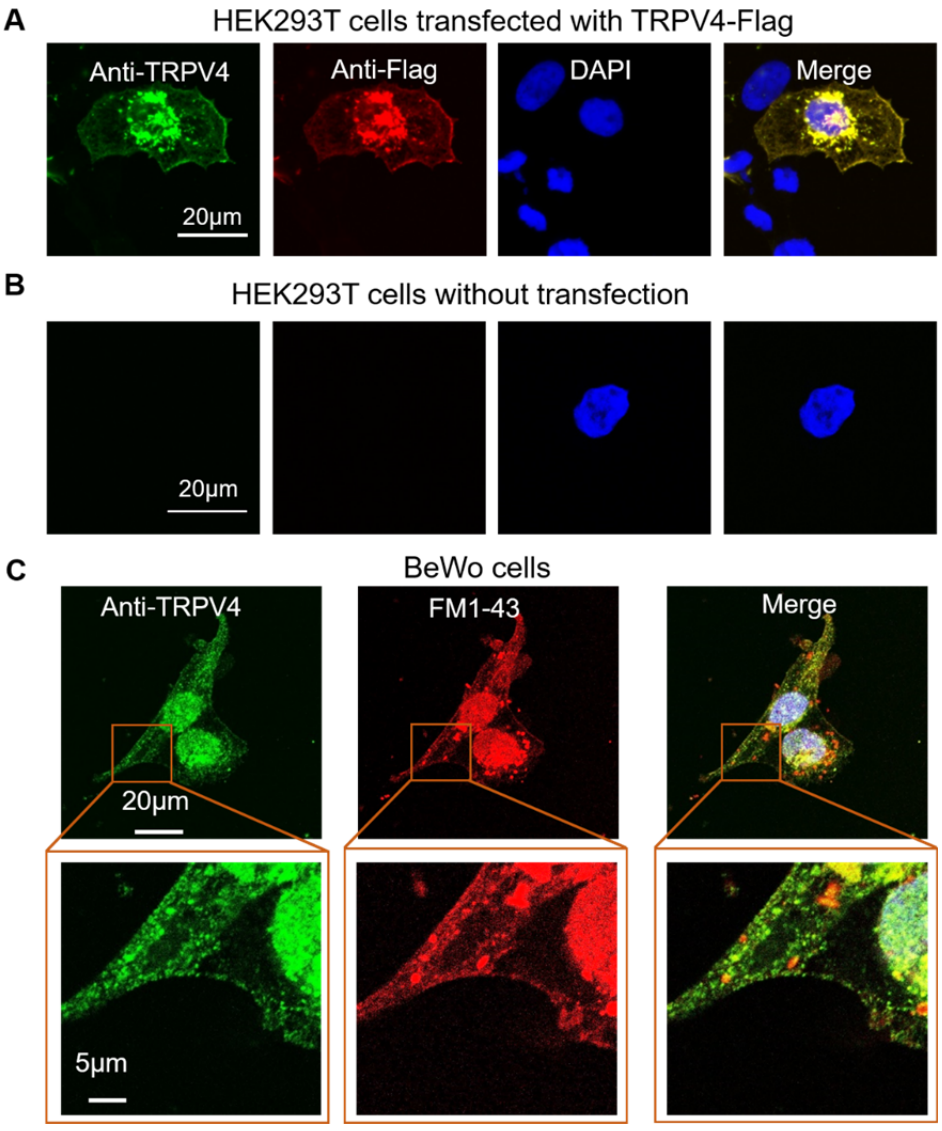

Figure 1—figure supplement 2. Validation of the TRPV4 antibody for immunofluorescence. **(A-B)** Validation of the TRPV4 antibody in HEK293T cells heterologously expressing a Flag-tagged TRPV4 plasmid. Immunofluorescence of TRPV4 (anti-TRPV4, green) and Flag tag (anti-Flag, red) in HEK293T cells transfected with a Flag-tagged TRPV4 plasmid (A) and non-transfected control (B). DAPI-stained nuclei are shown in blue. **(C)** Representative immunofluorescence of TRPV4 (green) in BeWo cells. The nuclei were stained with Hoechst (blue) and a plasma membrane marker, FM1-43 dye, is shown in red. All fluorescence images are the representatives of at least three biological replicates.

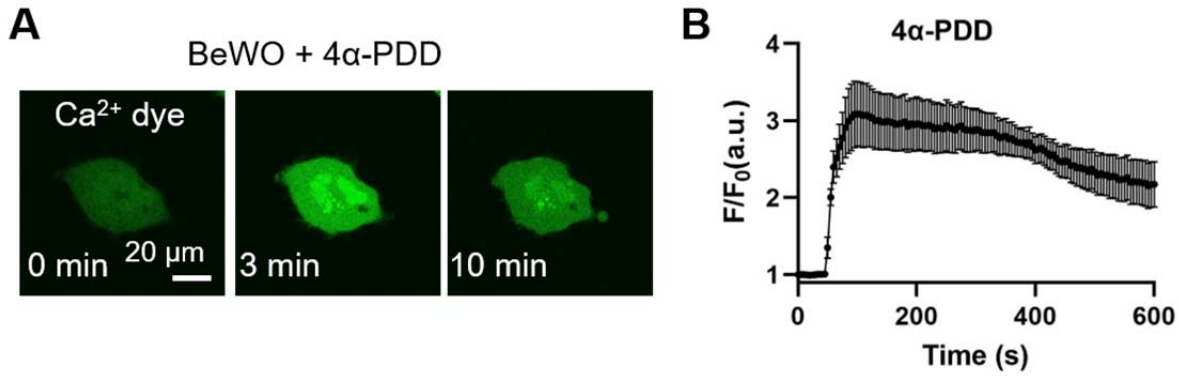

Figure 1—figure supplement 3. 4α-phorbol-12, 13-didecanoate (4α-PDD, 20 μM), a TRPV4 agonist, triggers intracellular Ca^{2+} elevation in BeWo cells. (A) Ca^{2+} dye (Calbryte 520, green) was used to monitor the dynamics of intracellular Ca^{2+}. All fluorescence images are the representatives of at least three biological replicates. **(B)** Time course of 4α-PDD triggered Ca^{2+} influx in BeWo cells (n = 7).

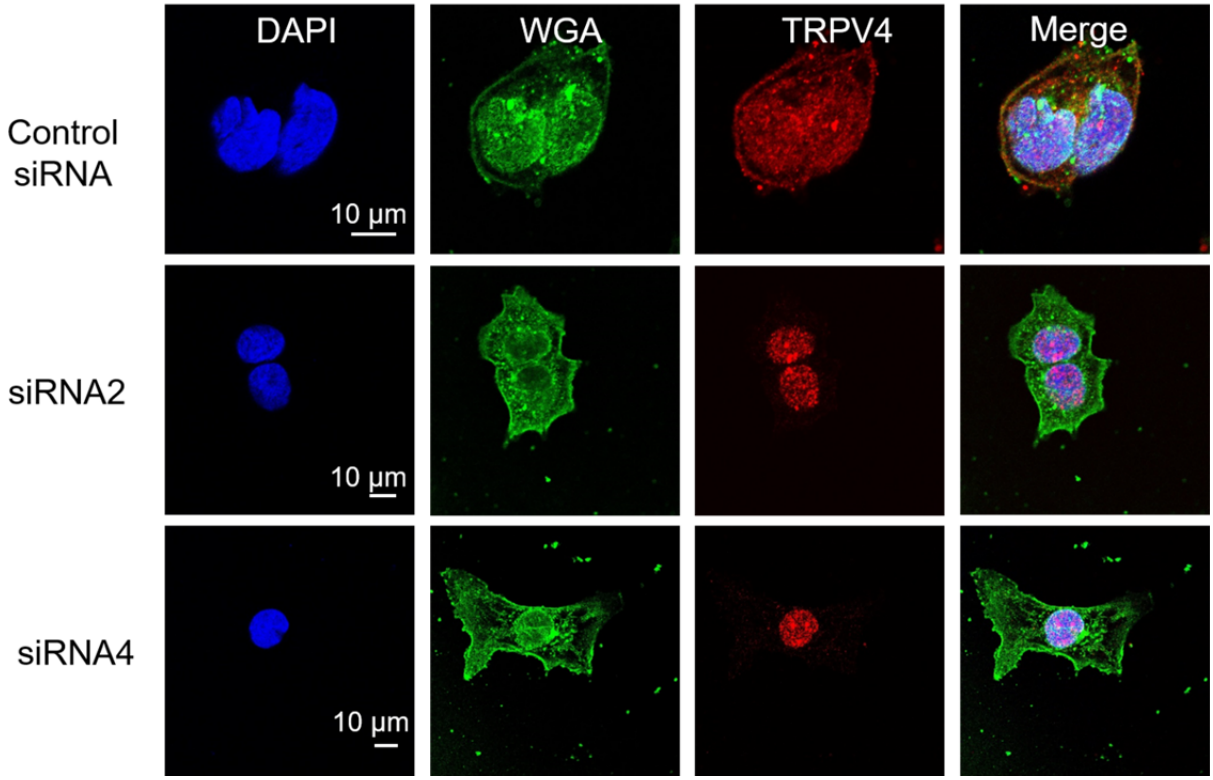

Figure 1—figure supplement 4. Immunofluorescence of TRPV4 in BeWo cells transfected with *TRPV4* siRNAs. Representative immunofluorescence of TRPV4 (red) in scrambled control siRNA and *TRPV4* siRNA knockdown BeWo cells. The nuclei were stained with Hoechst (blue). The plasma membrane was labeled with WGA dye (green). All fluorescence images are the representatives of at least three biological replicates.

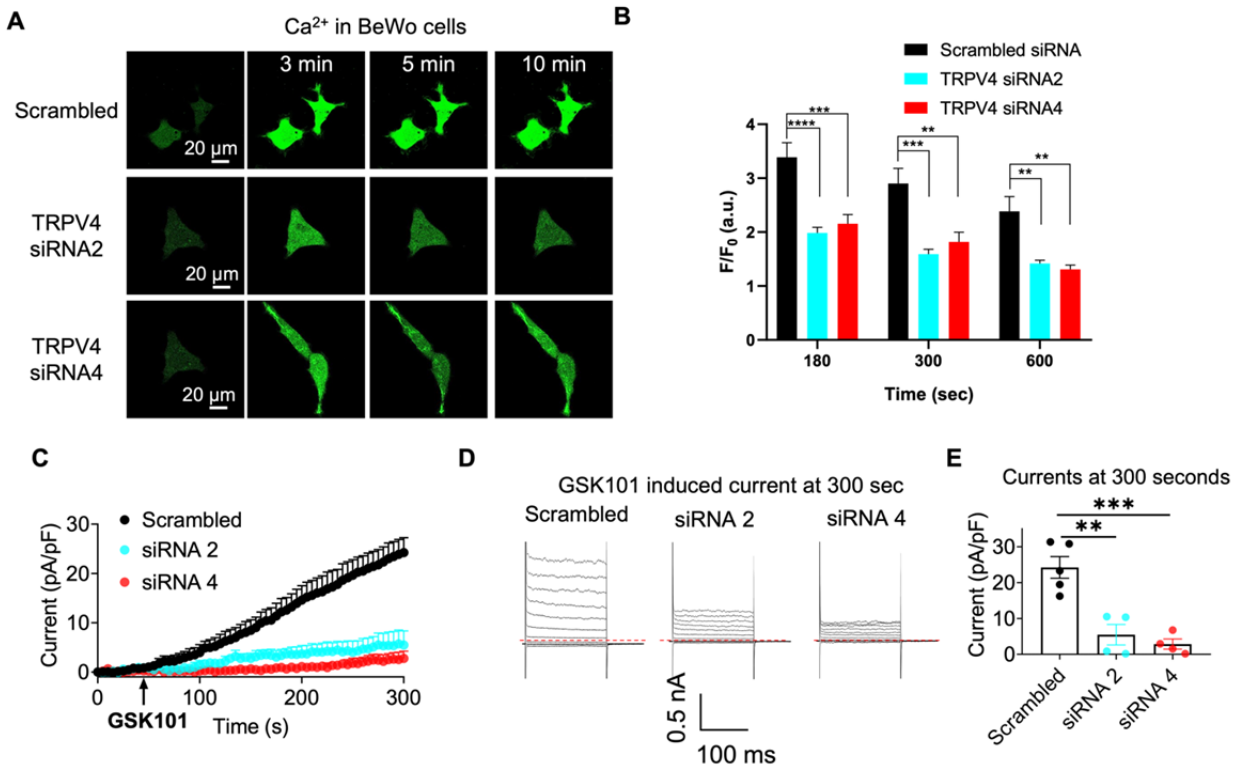

Figure 1—figure supplement 5. siRNA knockdown supports TRPV4 functional expression in BeWo cells. (A) Representative Ca^{2+} imaging in BeWo cells transfected with scrambled siRNA and *TRPV4* siRNAs. Calbryte 590 was used to monitor cytosolic Ca^{2+} dynamics. All fluorescence images are the representatives of at least three biological replicates. **(B)** Quantification of GSK101-induced Ca^{2+} influx in BeWo cells transfected with scrambled siRNA (n= 50), *TRPV4* siRNA2 (n = 55), or siRNA4 (n = 51) from at least three biological replicates. Values represent mean ± SEM and statistics were done using two-way ANOVA followed by Tukey's test. (**: $p<0.01$, ***: $p<0.001$, and ****: $p<0.0001$). **(C)** Time course of 30 nM GSK101-induced currents from scrambled siRNA and *TRPV4* siRNAs transfected BeWo cells. Whole-cell current was elicited by a ramp protocol from -100 mV to +100 mV every 5 seconds and is plotted at +100 mV. Error bar represents SEM. n=4-5. **(D)** Representative GSK101-

induced currents at 300 second after GSK101 stimulation in (C). Whole-cell current was elicited by a voltage step protocol (200 ms) from -100 mV to +140 mV. **(E)** Currents densities at +140 mV after 300 second after GSK101 application. Current densities from BeWo cells treated with scrambled siRNA, *TRPV4*-siRNA2 and *TRPV4*-siRNA4 were 24.24±3.02, 5.47±2.86 and 24.24±3.02 pA/pF, respectively. Values represent mean ± SEM and statistics were done using one-way ANOVA followed by Tukey's test. (**: $p<0.01$ and ***: $p<0.001$, n=4-5).

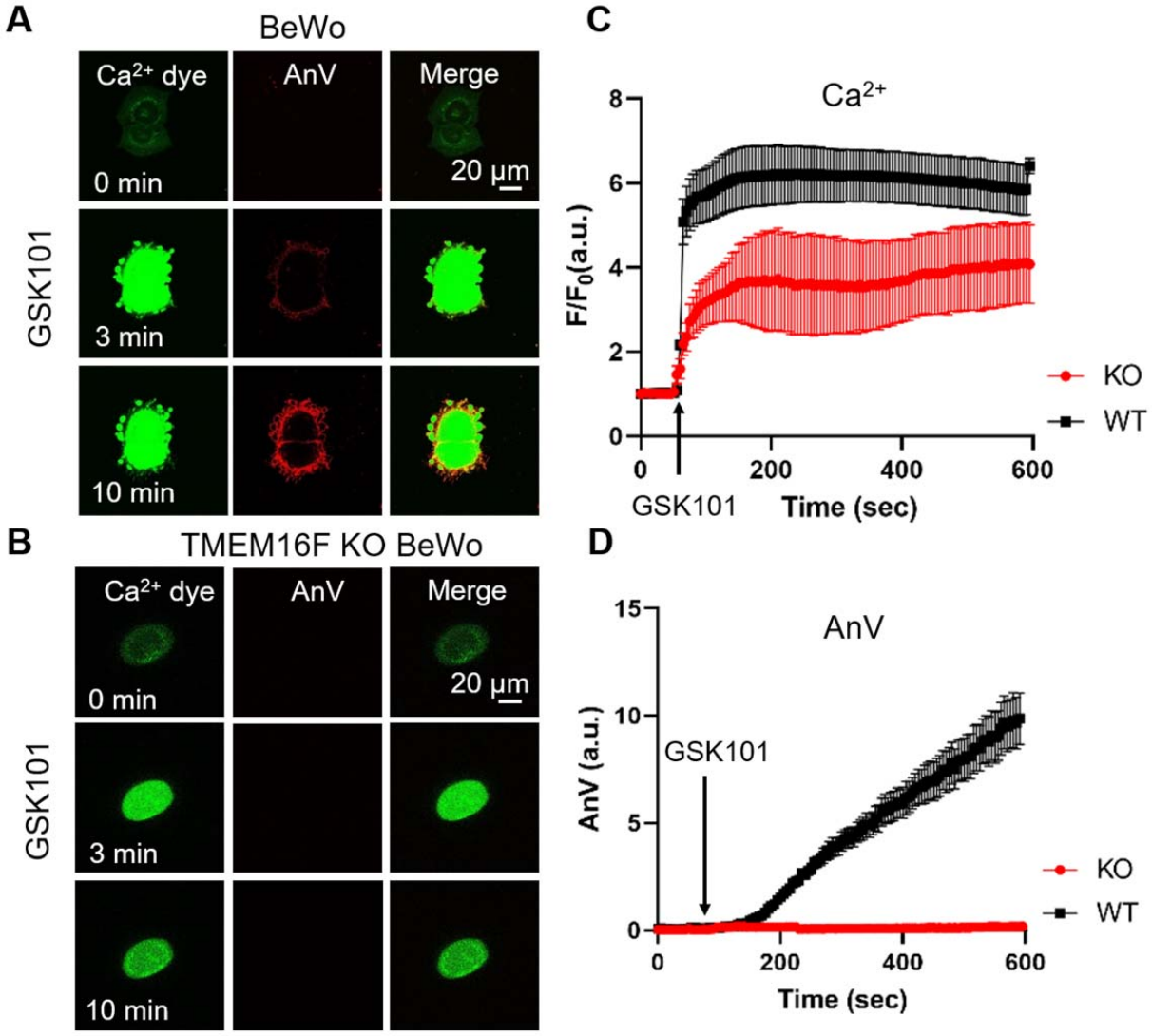

Figure 2. Ca^{2+} influx through TRPV4 activates TMEM16F scramblase in BeWo cells. (A) 20 nM GSK101 triggers Ca^{2+} influx and PS exposure (labeled by AnV) in wildtype (WT) BeWo cells. **(B)** 20 nM GSK101 induces Ca^{2+} influx, but fails to trigger PS exposure in TMEM16F knockout (KO) BeWo cells. Ca^{2+} dye (Calbryte 520, green) and fluorescently tagged AnV (AnV-CF594, red) were used to monitor the dynamics of intracellular Ca^{2+} and PS externalization, respectively. (**C-D**) Time course of GSK101-triggered Ca^{2+} influx (C) and PS exposure (D) in BeWo WT (n = 5) and TMEM16F KO cells (n = 5).

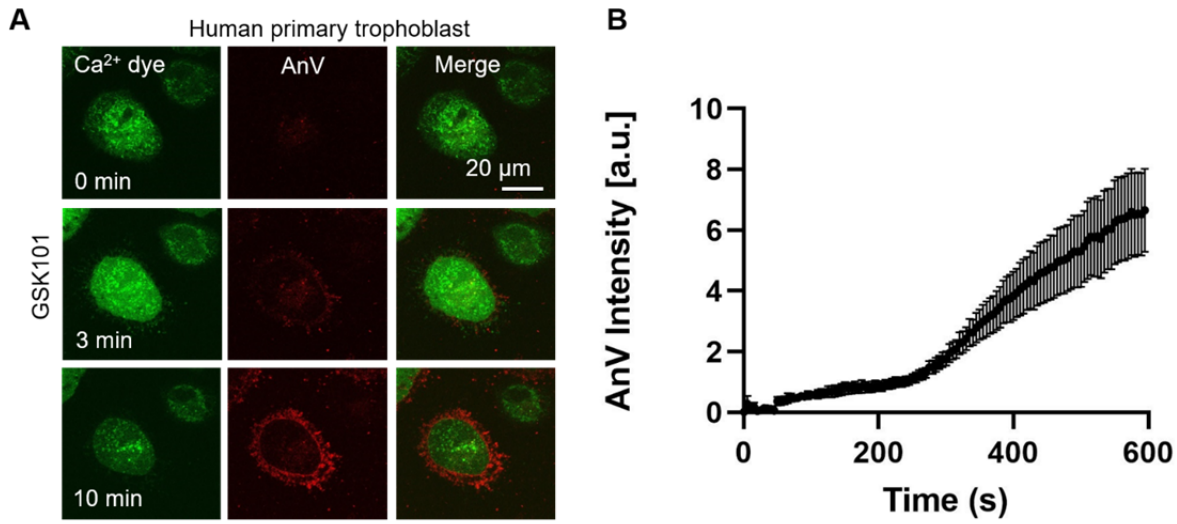

765

766 **Figure 2—figure supplement 1. 20 nM GSK101 triggers Ca^{2+} increase and subsequent**
767 **CaPLSase activities in primary human placental trophoblasts. (A)** Ca^{2+} dye (Calbryte 520)
768 and fluorescently tagged AnV (AnV-CF594) were used to measure the dynamics of intracellular
769 Ca^{2+} and PS externalization, respectively. All fluorescence images are the representatives of at
770 least three biological replicates. **(B)** Time course of GSK101 triggered PS exposure in primary
771 human placental trophoblasts. n = 6. Error bar represents ±SEM.

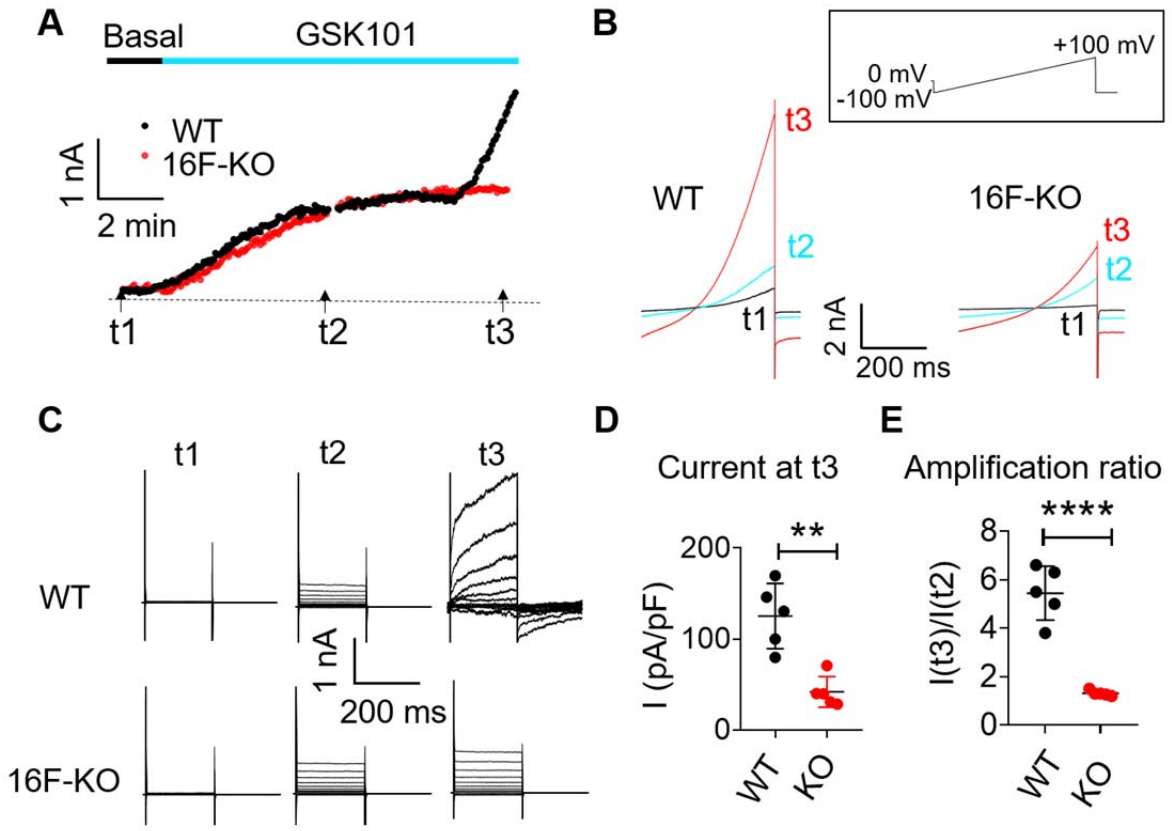

Figure 3. TRPV4 activation elicits TMEM16F current in BeWo cells. (A-B) Time course of whole-cell currents in response to 30 nM GSK101 stimulation in WT and TMEM16F-KO BeWo cells. The currents were elicited with the ramp protocol shown in Panel B (top). (A) The current amplitudes at +100 mV were plotted every 5 seconds. (B) Representative currents at three different time points as shown in Panel A. **(C)** Representative current traces elicited by a voltage step protocol (200 ms) from -100 mV to +140 mV at three different time points t1, t2 and t3 as indicated in Panel A. **(D)** Statistical analysis of current density (+100 mV) at t3 in WT and TMEM16F-KO BeWo cells. The current was elicited by the voltage steps shown in (C). Values represent mean ± SEM and statistics were done using Student's t-test (n=5 for each group, **: $p<0.01$). **(E)** Statistical analysis of amplification ratio (current amplitude ratio at t3 and t2 in (C)) in WT and TMEM16F-KO BeWo cells. Values represent mean ± SEM and statistics were done using Student's t-test (n=5 for each group, ****: $p<0.0001$).

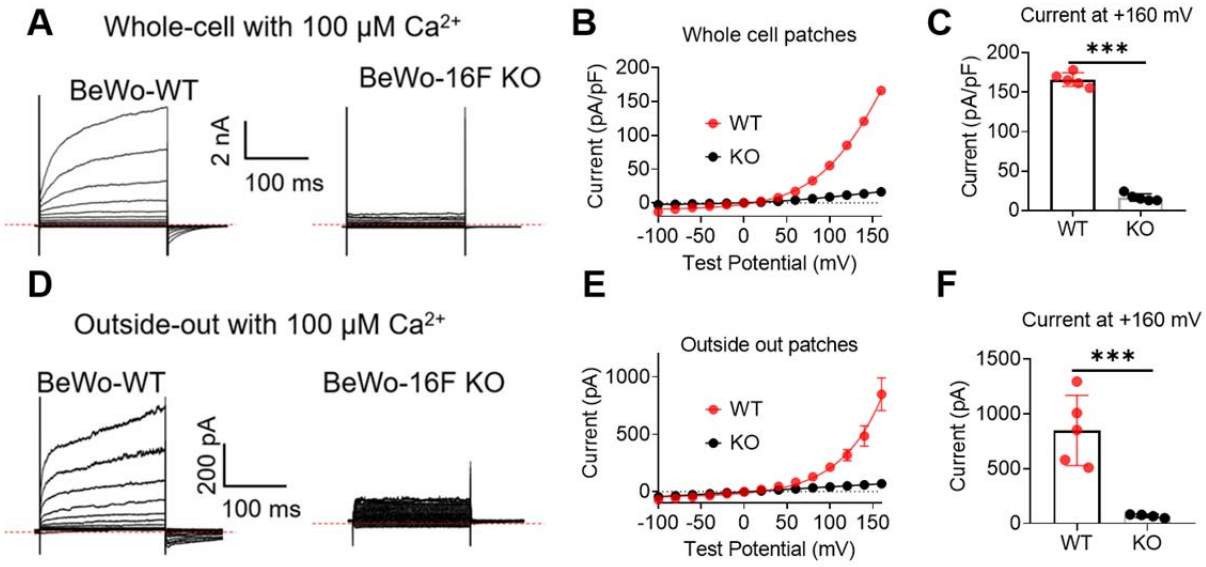

Figure 3—figure supplement 1. Ca^{2+}-activated current in BeWo WT and TMEM16F KO BeWo cells. (A) Representative whole cell recordings elicited by a voltage step protocol (200 ms) from -100 mV to +140 mV. The currents were recorded at ~7-10 minutes after whole-cell patches were formed. The free Ca^{2+} inside the pipette was 100 µM. **(B)** *I-V* relation of current recorded in WT and TMEM16F-KO BeWo cells under whole cell configuration. **(C)** Peak whole-cell current at +160 mV was compared with Student's t-test. (***p<0.001, n=5). **(D)** Representative outside-out patch recordings elicited by a voltage step protocol (200 ms) from -100 mV to +140 mV. The currents were recorded immediately after outside-out patches were formed. The free Ca^{2+} inside the pipette was 100 µM. **(E)** *I-V* relation of current recorded in WT and TMEM16F-KO BeWo cells under outside-out configuration. **(F)** Peak outside-out current at +160 mV was compared with Student's t-test. (***p<0.001, n=5 for WT and n=4 for TMEM16F-KO).

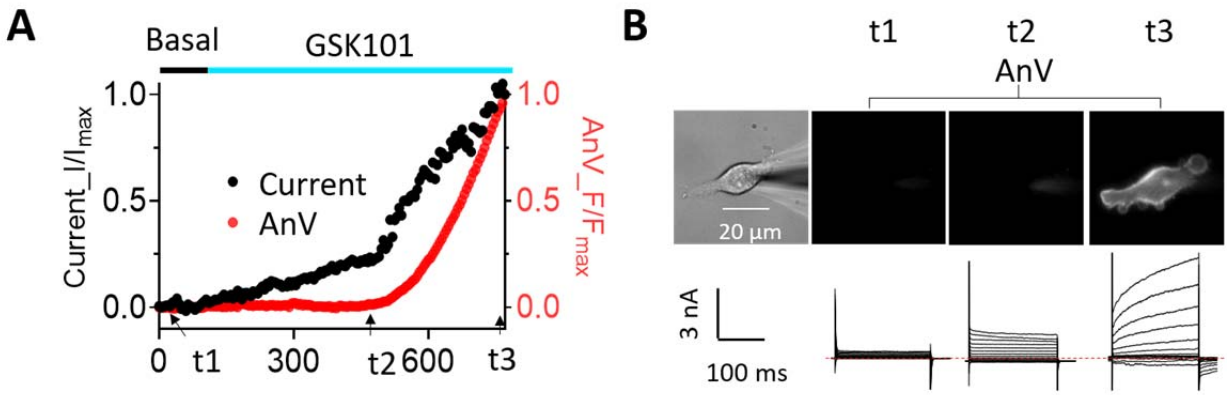

Figure 3—figure supplement 2. Simultaneous monitoring of GSK101-triggered channel and lipid scramblase activities in BeWo cells. (A) Time course of 30 nM GSK101-induced current and PS exposure recorded using patch clamp-lipid scramblase fluorometry. **(B)** Representative data of PS exposure (top) and current traces (bottom) at different time points as indicated in (A). t1 was during baseline recording. t2 demarcates the time point right before the time-dependent, outward rectifying TMEM16F current started to develop. t3 was 10 minutes after GSK101 application. Current and AnV signal were both normalized to their maximum values at t3. n= 4.

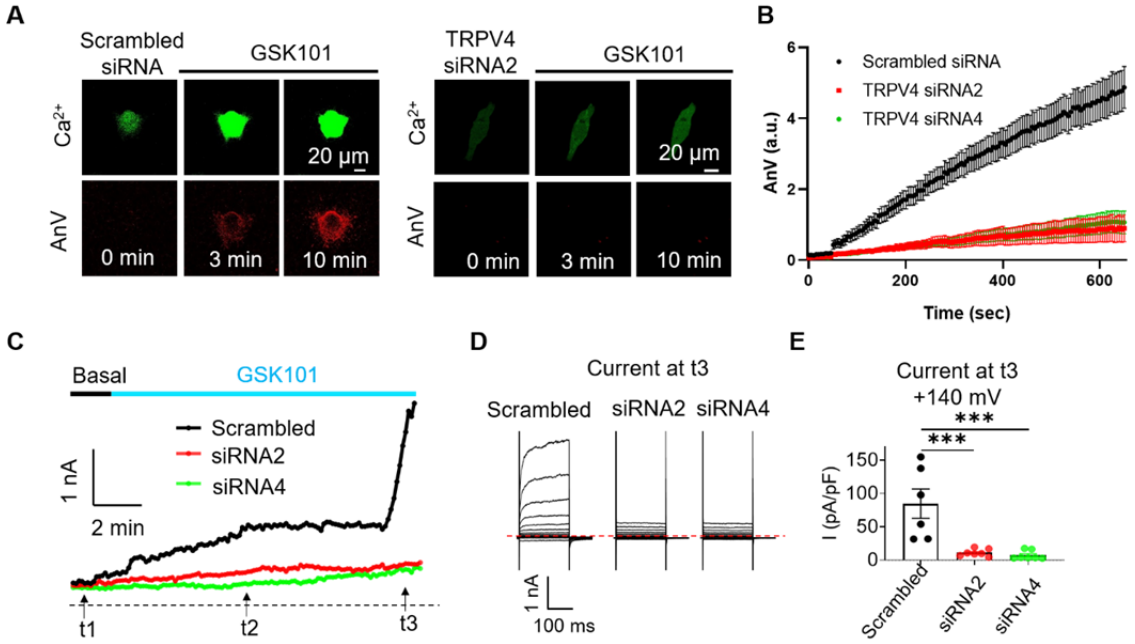

Figure 4. siRNA knockdown of *TRPV4* abolishes GSK101-induced Ca^{2+} influx and subsequent TMEM16F CaPLSase activation in BeWo cells. (A) Representative images of Ca^{2+} and AnV in scrambled siRNA and *TRPV4* siRNA2 treated BeWo cells in response to 20 nM GSK101 stimulation. Fluorescently-tagged AnV labels exposed PS, serving as an indicator of CaPLSase activity. **(B)** Time course of CaPLSase activities for scrambled siRNA (n = 50), *TRPV4* siRNA2 (n = 55) and siRNA4 (n = 51) treated BeWo cells. **(C)** Time course of whole-cell currents elicited in response to 30 nM GSK101 in scrambled siRNA or *TRPV4* siRNAs treated BeWo cells. The currents were elicited with a ramp protocol from -100 mV to +100 mV and plotted every 5 seconds at +100 mV. **(D)** Representative current traces elicited by a voltage step protocol (200 ms) from -100 mV to +140 mV at three different time points t1, t2 and t3 as indicated in (C). **(E)** Statistical analysis of current density at t3 (+140 mV) in WT and *TRPV4*-siRNA knockdown BeWo cells. Current densities after scrambled siRNA, *TRPV4*-siRNA2 and *TRPV4*-siRNA4 treatment are 84.72±21.97, 11.12±2.03 and 7.32±2.53 pA/pF, respectively.

824 Values represent mean ± SEM and statistics were done using Student's t-test (n=6 for scrambled
825 group and n=7 for TRPV4 siRNA groups, ***: $p<0.001$).

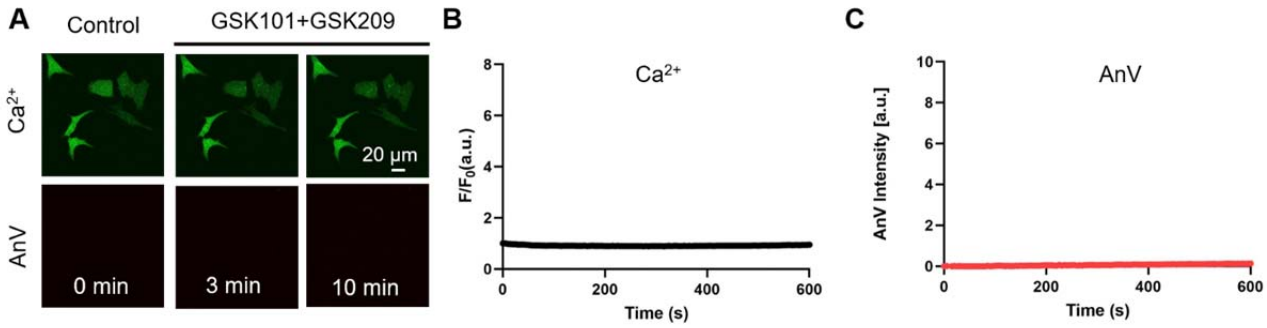

Figure 4—figure supplement 1. Pharmacological inhibition of TRPV4 abolishes GSK101-induced Ca^{2+} influx and subsequent TMEM16F activation in BeWo cells. (A) Representative images Ca^{2+} and PS exposure in BeWo cells treated with 20 nM TRPV4 agonist GSK101 and by 500 nM TRPV4 antagonist GSK219. Ca^{2+} dye (Calbryte 488) and fluorescently tagged AnV proteins (AnV-CF594) were used to measure the dynamics of intracellular Ca^{2+} and PS externalization, respectively. **(B-C**) Time course of intracellular Ca^{2+} (B) and PS exposure (C) in BeWo cells treated with 20 nM GSK101 and by 500 nM GSK219. n= 9. All fluorescence images are the representatives of at least three biological replicates.

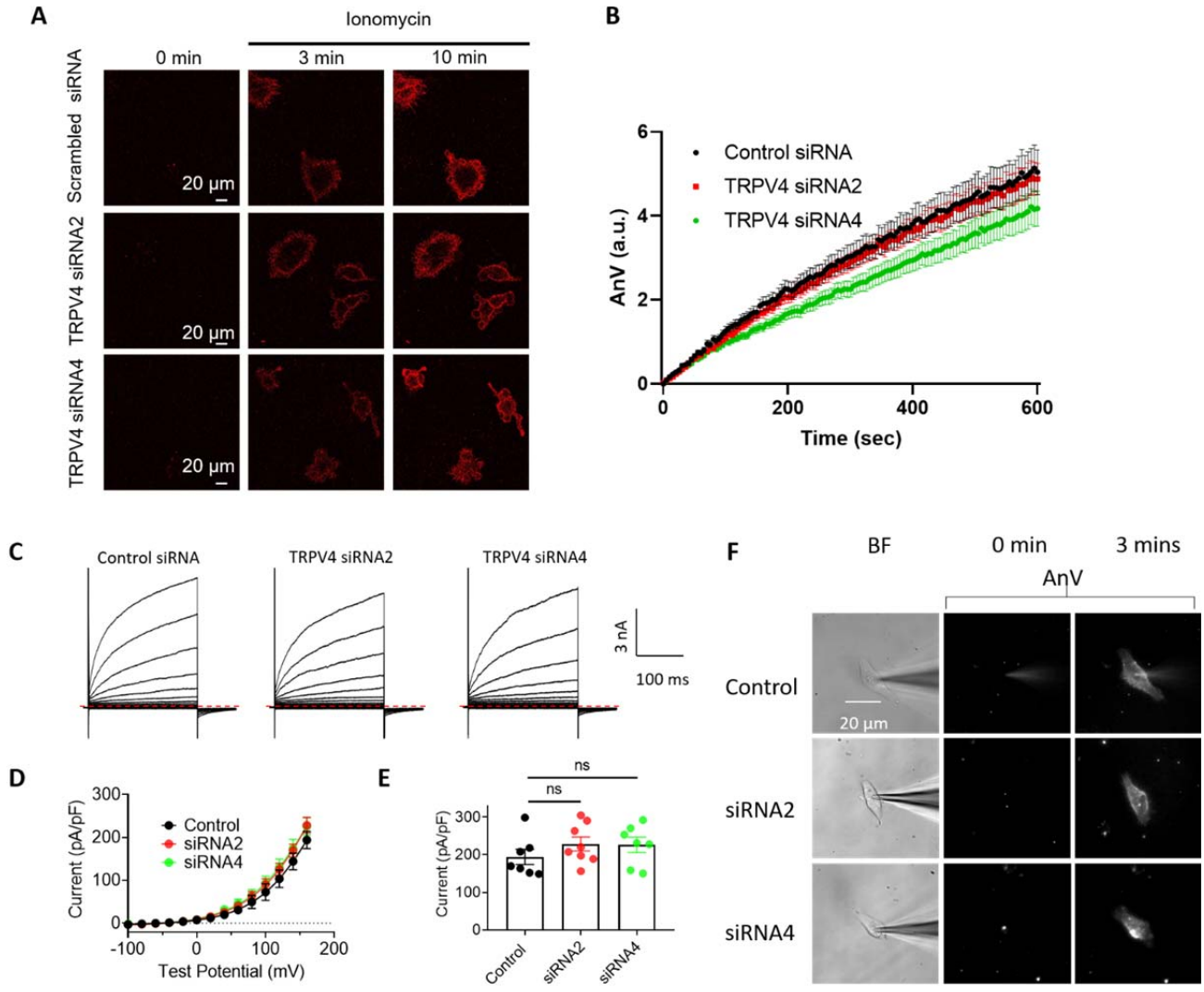

Figure 4—figure supplement 2. TMEM16F CaPLSase and channel activity in BeWo cells is not affected by *TRPV4* knockdown. (A) Representative images showing 5 μM ionomycin triggers similar levels of PS exposure in scrambled, *TPRV4* siRNA2, and siRNA4 knockdown BeWo cells. **(B)** Quantification of ionomycin-induced AnV intensities increase in BeWo cells transfected with scrambled siRNA (n= 25), *TRPV4* siRNA2 (n = 25), or siRNA4 (n = 27). All fluorescence images are the representatives of at least three biological replicates. **(C)** Representative TMEM16F current traces from control siRNA and the *TRPV4* siRNAs treated BeWo cells recorded with whole cell patch clamp or patch clamp-lipid scrambling fluorometry

(PCLSF). 1000 μM Ca^{2+} was included in the pipette solution, and the current was elicited by a voltage step protocol from -100 mV to +160 mV with holding potential at -60 mV. **(D)** I-V relation of TMEM16F current recorded from the control siRNA and the *TRPV4* siRNAs treated BeWo cells. **(E)** Statistics of the TMEM16F current density at +160 mV shown in (D). Student's t-test. (ns: not significant, n = 7 for control siRNA, n = 8 for *TRPV4* siRNA2 and n = 7 for *TRPV4* siRNA4). **(F)** Representative lipid scrambling activities recorded using PCLSF to simultaneously record TMEM16F channel and lipid scramblase activities. The cells are the same ones shown in (C). n = 3.

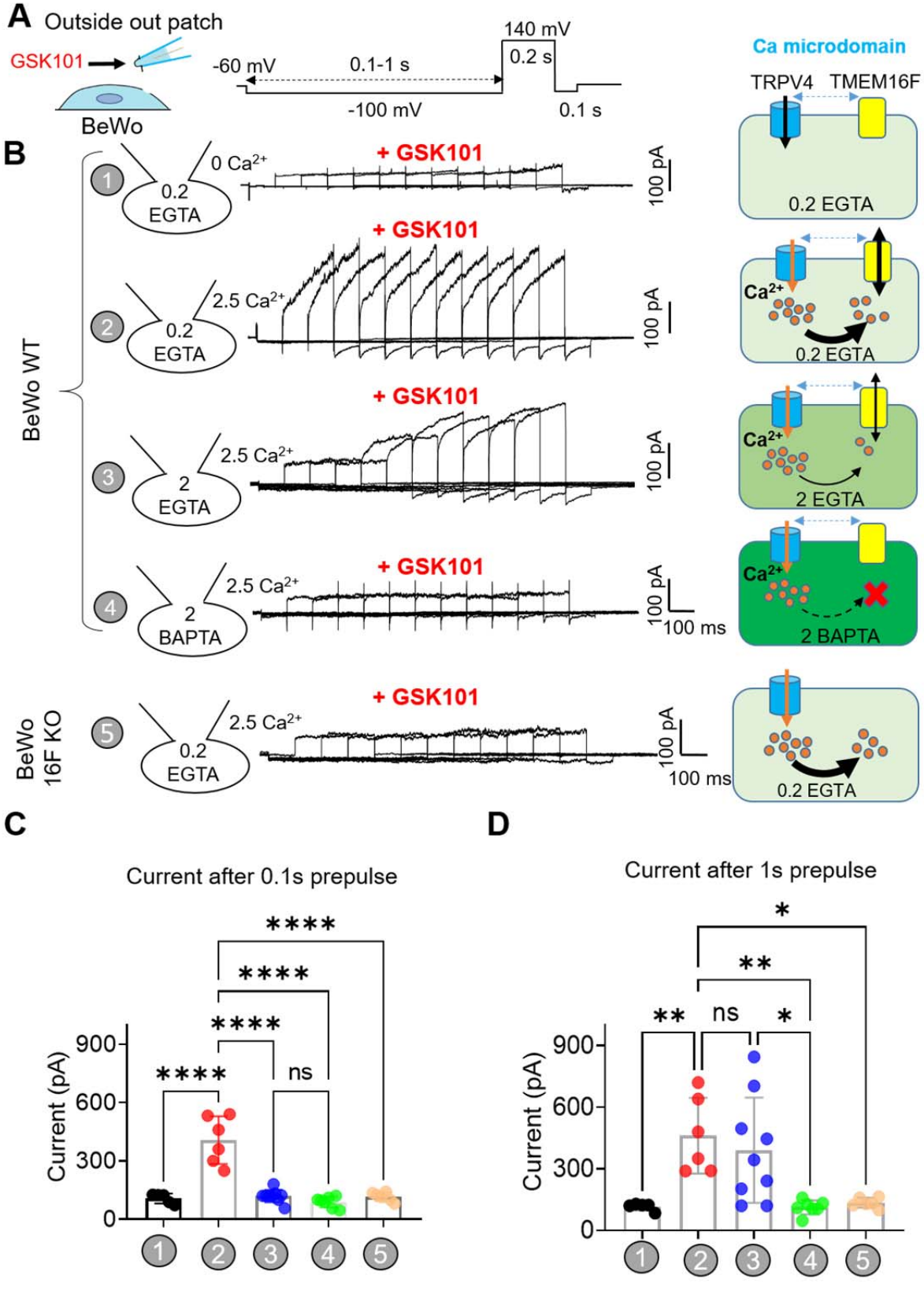
A
Outside out patch
GSK101
BeWo
-60 mV
0.1-1 s
-100 mV
140 mV
0.2 s
0.1 s
B
BeWo WT
BeWo 16F KO
1
0.2 EGTA
0 Ca2+
+ GSK101
2
0.2 EGTA
2.5 Ca2+
+ GSK101
3
2 EGTA
2.5 Ca2+
+ GSK101
4
2 BAPTA
2.5 Ca2+
+ GSK101
5
0.2 EGTA
2.5 Ca2+
+ GSK101
100 pA
100 ms
Ca microdomain
TRPV4
TMEM16F
0.2 EGTA
Ca2+
0.2 EGTA
Ca2+
2 EGTA
Ca2+
2 BAPTA
0.2 EGTA
C
Current after 0.1s prepulse
Current (pA)
900
600
300
0
****
****
****
****
ns
1
2
3
4
5
D
Current after 1s prepulse
Current (pA)
900
600
300
0
*
**
**
ns
*
1
2
3
4
5

Figure 5. TRPV4 and TMEM16F are functionally coupled within microdomain in BeWo cells. (A) Outside-out patch configuration and voltage protocols used to demonstrate TRPV4-TMEM16F coupling. The holding potential was set at -60 mV. A -100 mV pre-pulse with varied length from 0.1 second to 1 second with 0.1 second increment was applied along with perfusion of 30 nM GSK101 to induce Ca^{2+} influx. Following the pre-pulse, a depolarized pulse with 0.2 second duration and 140 mV amplitude was applied to record TMEM16F current. **(B)** Left: Representative outside-out patch recordings from wildtype (WT) BeWo cells under different conditions: 1) intracellular 0.2 mM EGTA, extracellular 0 Ca^{2+} with 30 nM GSK101 (n=5); 2) intracellular 0.2 mM EGTA, extracellular 2.5 mM Ca^{2+} with 30 nM GSK101 (n=6); 3) intracellular 2 mM EGTA, extracellular 2.5 mM Ca^{2+} with 30 nM GSK101 (n=9); 4) intracellular 2 mM BAPTA, extracellular 2.5 mM Ca^{2+} with 30 nM GSK101 (n=7). 5) Intracellular 0.2 mM EGTA, extracellular 2.5 mM Ca^{2+} with 30 nM GSK101 for TMEM16F-KO BeWo cells (n=6). Right: Diagrams demonstrating TRPV4-TMEM16F coupling under each condition on the left. The intensity of green color depicts Ca^{2+} chelating capacity and kinetics with BAPTA as the most efficient Ca^{2+} chalator. **(C-D)** Quantification of peak current amplitudes at +140 mV after 0.1 second pre-pulse (C) and 1 second pre-pulse (D). Values represent mean ± SEM and statistics were done using Student's t-test (****: $p<0.0001$, **: $p<0.01$, *: $p<0.05$, ns: not significant).

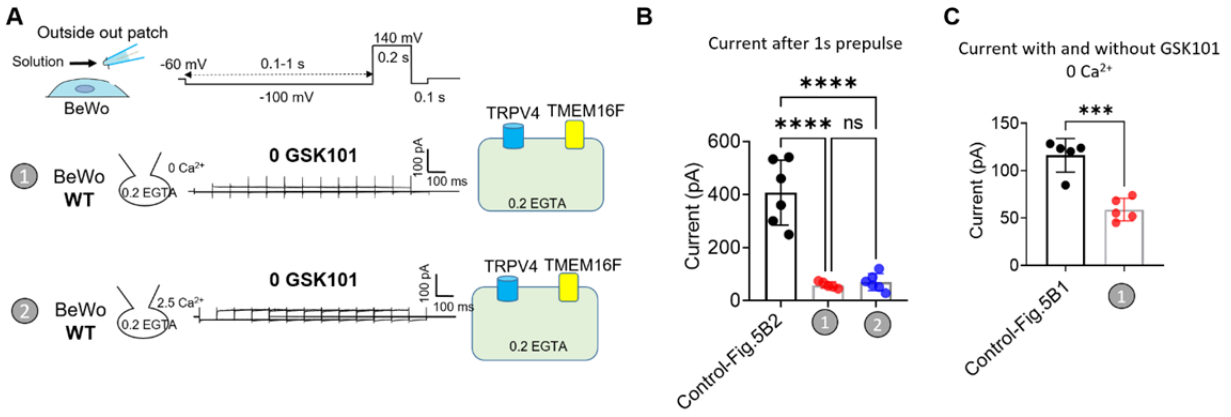

876

877 **Figure 5—figure supplement 1. Lack of TRPV4-TMEM16F coupling in BeWo**
878 **trophoblast cells in the absence of GSK101. (A)** Outside-out patch recording of BeWo cells in
879 the absence of GSK101. 1) 0 extracellular Ca^{2+}; 2) 2.5 mM extracellular Ca^{2+}. 0.2 mM EGTA
880 was included in the pipette. **(B)** Comparison of outside-out patch current with (Figure 5B, #2,
881 with 2.5 mM Ca^{2+}) and without GSK101 after 1 sec of prepulse. **(C)** Comparison of outside-out
882 patch current with (Figure 5B, #1, with 0 Ca^{2+}) and without GSK101 after 1 sec of prepulse.
883 Values represent mean ± SEM and statistics were done using Student's t-test (****: $p<0.0001$,
884 ***: $p<0.001$, ns: not significant).

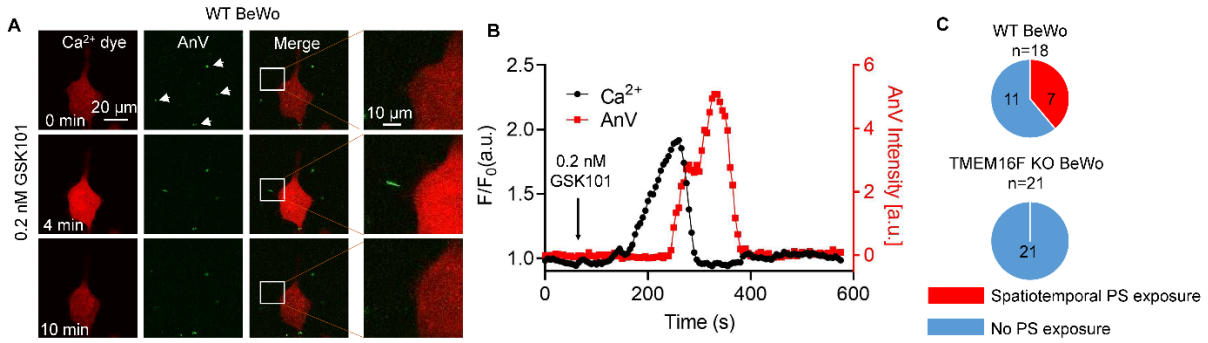

Figure 6. Transient Ca^{2+} influx through TRPV4 induces local PS exposure in BeWo cells. **(A)** Representative images of Ca^{2+} and PS exposure from the BeWo cells stimulated with low concentration of GSK101 (0.2 nM). Ca^{2+} dye (Calbryte 594) and fluorescently tagged AnV proteins (AnV-CF488) were used to measure the dynamics of intracellular Ca^{2+} and PS externalization, respectively. The white box highlights transient and reversible PS exposure in a membrane process in response to TRPV4 stimulation. The arrow heads label the PS positive debris in the cell culture, which existed before TRPV4 stimulation. All fluorescence images are the representatives of at least three biological replicates. **(B)** The dynamics of global Ca^{2+} (black) and local AnV signal (red) upon 0.2 nM GSK101 stimulation in WT BeWo cells. **(C)** Quantification of WT (7/18) and TMEM16F KO (0/21) BeWo cells that showed local PS exposure in response to 0.2 nM GSK101.

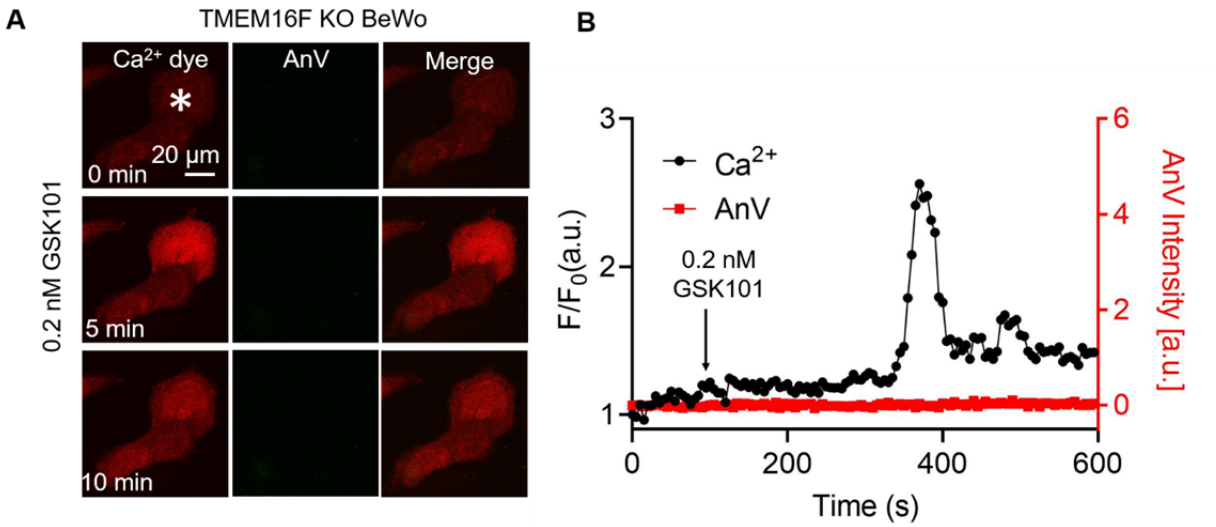

900

901 **Figure 6—figure supplement 1. Simultaneous imaging of Ca^{2+} increase and phospholipid**
902 **scrambling in TMEM16F knockout (KO) BeWo cells in response to low concentration**
903 **GSK101. (A)** Stimulation of TRPV4 with low concentration of GSK101 (0.2 nM) triggers
904 transient Ca^{2+} increase without spatiotemporal PS exposure in TMEM16F KO BeWo cells.
905 Ca^{2+} dye (Calbryte 594) and fluorescently tagged AnV proteins (AnV-CF488) were used to
906 measure the dynamics of intracellular Ca^{2+} and PS externalization, respectively. All
907 fluorescence images are the representatives of at least three biological replicates. **(B)** The
908 dynamics of Ca^{2+} (black) and AnV signal (red) of a TMEM16F KO BeWo cell in A (*).

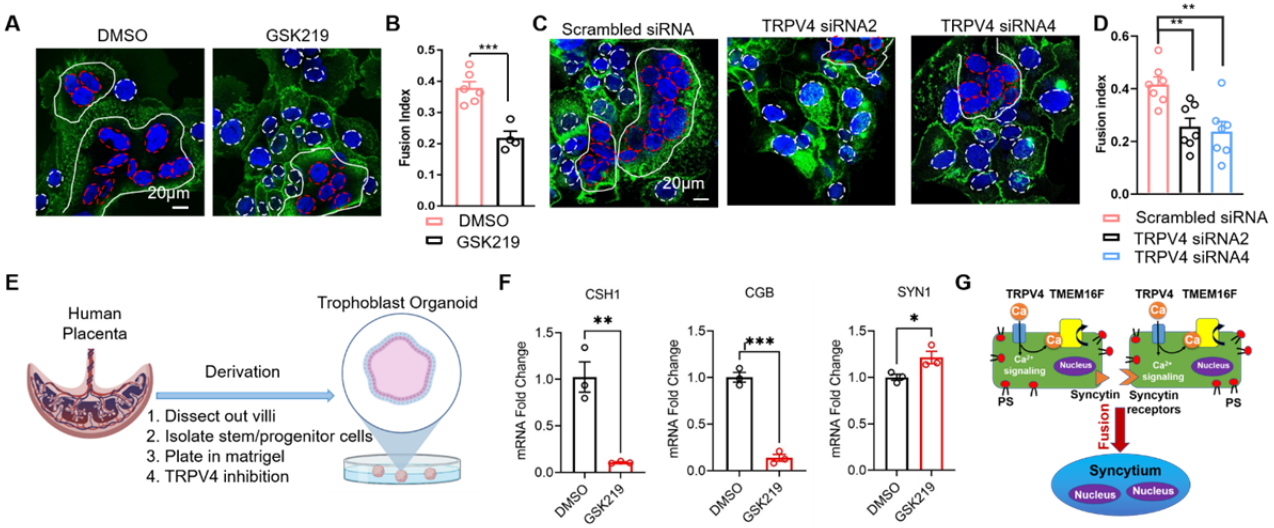

Figure 7. TRPV4 inhibition hinders human trophoblast fusion *in vitro*. (A) Representative images of control and GSK219 treated BeWo cells after 48-hour forskolin treatment. Nuclei and membranes were labelled with Hoechst (blue) and Di-8-ANEPPS (green), respectively. **(B)** GSK219 inhibits forskolin-induced BeWo cell fusion. Unpaired two-sided Student's *t*-test. ***: $p < 0.001$. Error bars indicate ± SEM. Each dot represents the average of fusion indexes of six random fields from one cover glass. **(C)** Representative images of control (scrambled siRNA) and *TRPV4* knockdown (*TRPV4* siRNA 2 and 4) BeWo cells after 48-hour forskolin treatment. **(D)** *TRPV4* siRNA knockdown inhibits forskolin-induced BeWo cell fusion. Unpaired two-sided Student's *t*-test. **: $p < 0.01$. Error bars represent ± SEM. Each dot represents the average of fusion indexes of six random fields from one cover glass (See Methods for details). All fluorescence images are the representatives of at least three biological replicates. **(E)** Schematic of 3-D culture of human placenta trophoblast-derived organoid. **(F)** The mRNA changes of placental syncytiotrophoblast marker genes *CSH1, CGB* and the fusogenic gene *SYNCITIN-1(SYN1)* after TRPV4 inhibition. Unpaired two-sided Student's *t*-test. ***: $p < 0.001$, **: $p <$

925 0.01. *: $p < 0.05$. Error bars indicate ± SEM. **(G)** A cartoon demonstration of TRPV4-
926 TMEM16F coupling in regulating trophoblast fusion.

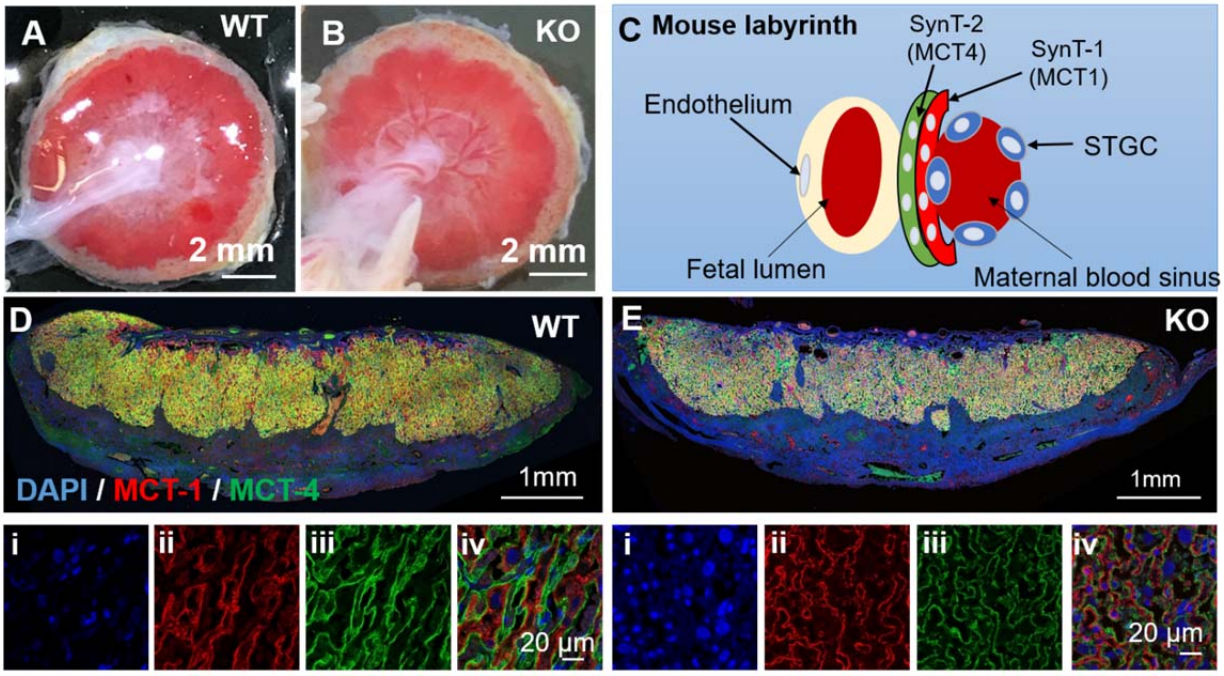

Figure 7—figure supplement 1. TRPV4 knockout placentas do not show obvious defects in trophoblast syncytialization in mice. (A-B) Representative images of placentas from wild-type (WT, A) and TRPV4 knockout (KO, B) mice at E18.5. **(C)** Anatomical diagram of fetomaternal exchange in mouse placentas. **(D-E)** MCT1 and MCT4 immunofluorescence staining of the *TRPV4* WT (D) and KO (E) placentas at E18.5. MCT1 (red) specifically stains the SynT-1 layer that faces maternal blood sinuses, while MCT4 (green) specifically stains the SynT-2 layer that encloses fetal blood vessels. Panel (i-iv) at the bottom show enlarged views of the placentas on top. All fluorescence images are the representatives of at least three biological replicates.

Supplementary File 1. qPCR primer list used in this study.

Videos:

Video 1: Time lapse video showing wildtype BeWo cells in response to 20 nM GSK101 stimulation. Ca^{2+} dye (Calbryte 520, green) and fluorescently tagged AnV (AnV-CF594, red) were used to monitor the dynamics of intracellular Ca^{2+} and PS externalization, respectively. Related to Figure 2A.

Video 2: Time lapse video showing TMEM16F knockout (KO) BeWo cells in response to 20 nM GSK101 stimulation. Ca^{2+} dye (Calbryte 520, green) and fluorescently tagged AnV (AnV-CF594, red) were used to monitor the dynamics of intracellular Ca^{2+} and PS externalization, respectively. Related to Figure 2B.

Video 3: Time lapse video showing wildtype BeWo cells in response to 0.2 nM GSK101 stimulation. Ca^{2+} dye (Calbryte 594, red) and fluorescently tagged AnV (AnV-CF488, green) were used to monitor the dynamics of intracellular Ca^{2+} and PS externalization, respectively. Related to Figure 6A.

Video 4: Time lapse video showing TMEM16F knockout (KO) BeWo cells in response to 0.2 nM GSK101 stimulation. Ca^{2+} dye (Calbryte 594, red) and fluorescently tagged AnV (AnV-CF488, green) were used to monitor the dynamics of intracellular Ca^{2+} and PS externalization, respectively. Related to Figure 6—figure supplement 1.

Source Data Files:

1. Source Data-Figure 1.xls
2. Source Data-Figure 2.xls
3. Source Data-Figure 3.xls

4. Source Data-Figure 4.xls
5. Source Data-Figure 5.xls
6. Source Data-Figure 6.xls
7. Source Data-Figure 7.xls

A

Chorionic villus

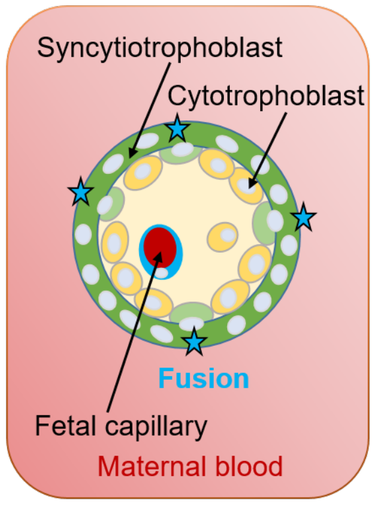

B

Human trophoblasts

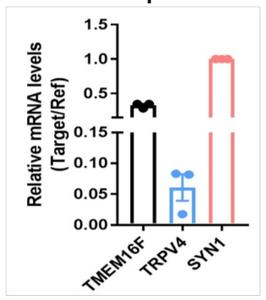

C

BeWo cells

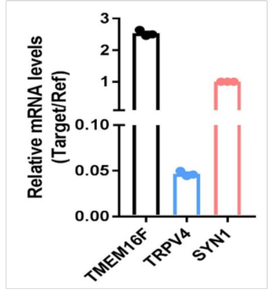

D

Chorionic villus

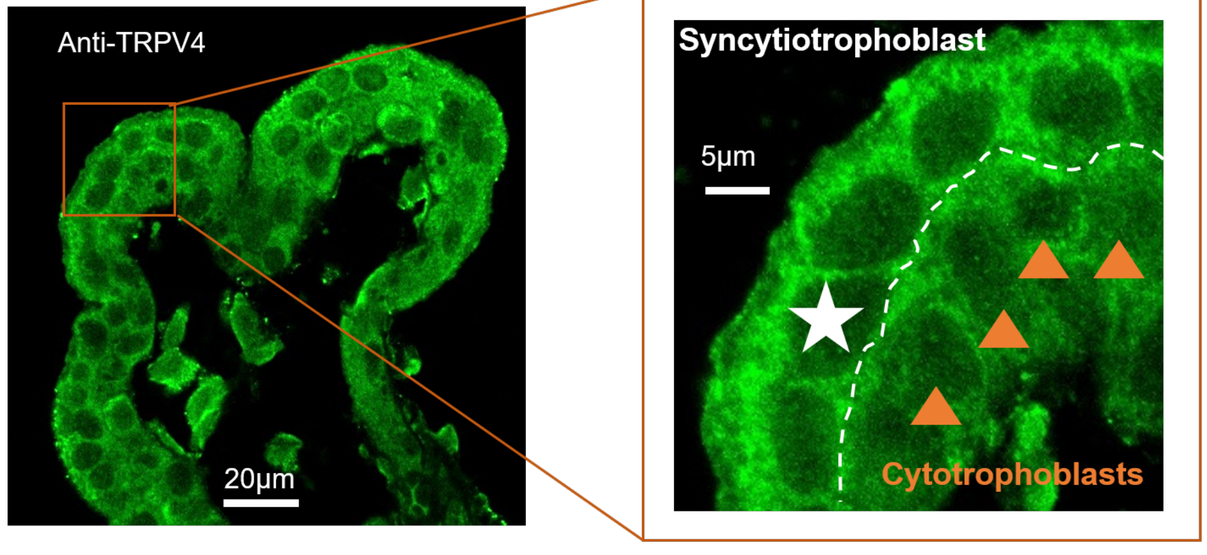

E

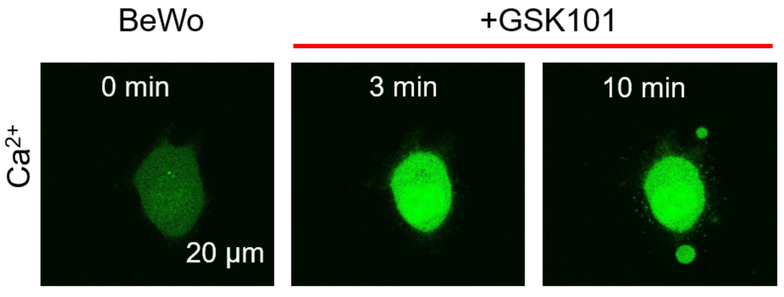

F

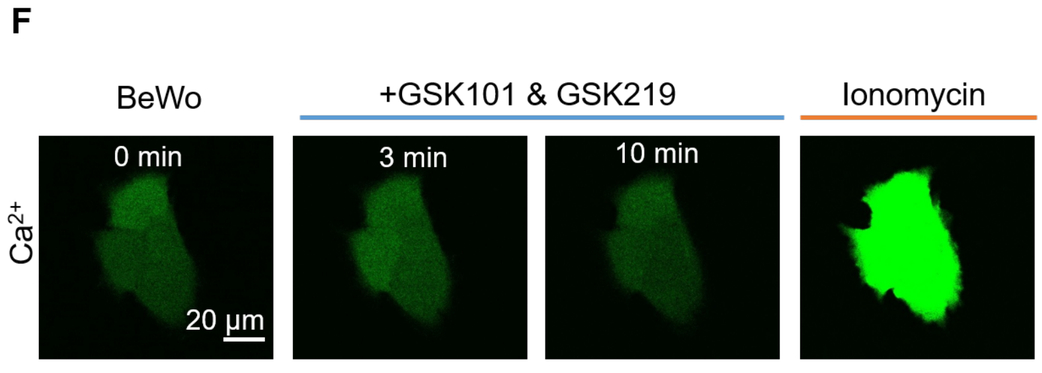

G

Ca^{2+}

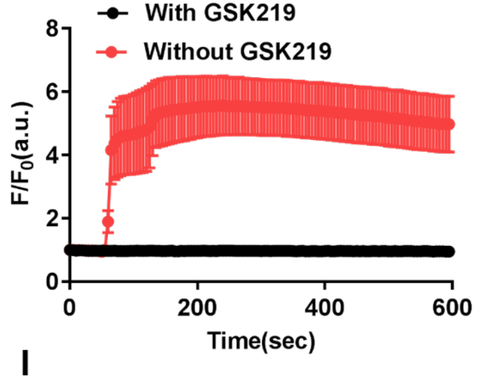

H

Patch clamp

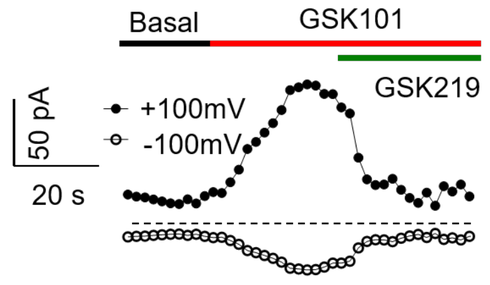

I

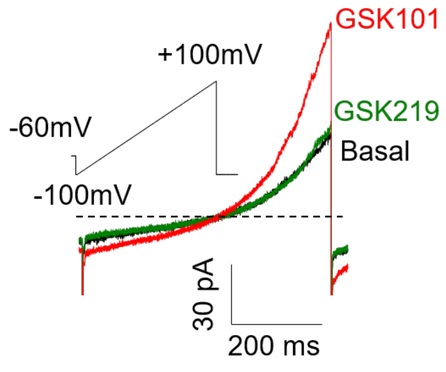

J

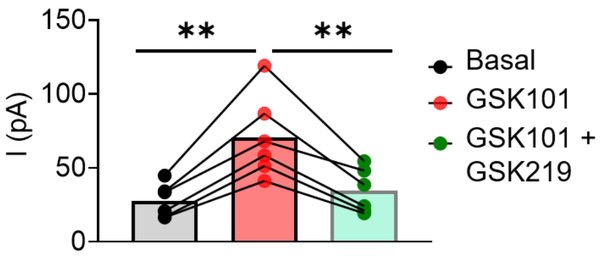

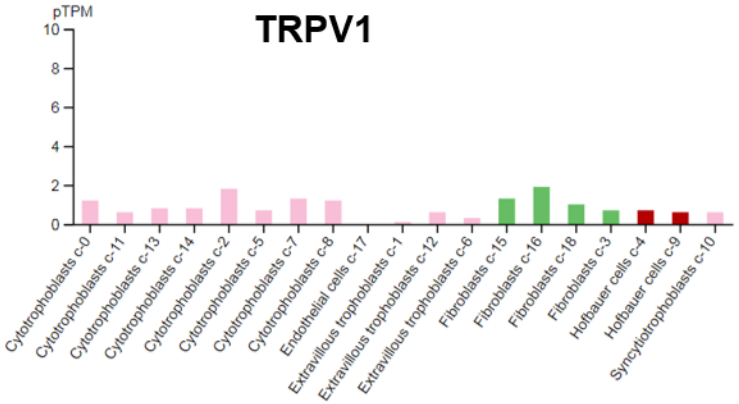
TRPV1
pTPM
10
8
6
4
2
0
Cytotrophoblasts c-0
Cytotrophoblasts c-11
Cytotrophoblasts c-13
Cytotrophoblasts c-14
Cytotrophoblasts c-2
Cytotrophoblasts c-5
Cytotrophoblasts c-7
Cytotrophoblasts c-8
Endothelial cells c-17
Extravillous trophoblasts c-1
Extravillous trophoblasts c-12
Extravillous trophoblasts c-6
Fibroblasts c-15
Fibroblasts c-16
Fibroblasts c-18
Fibroblasts c-3
Hofbauer cells c-4
Hofbauer cells c-9
Syncytiotrophoblasts c-10

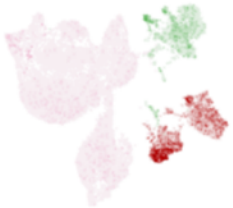

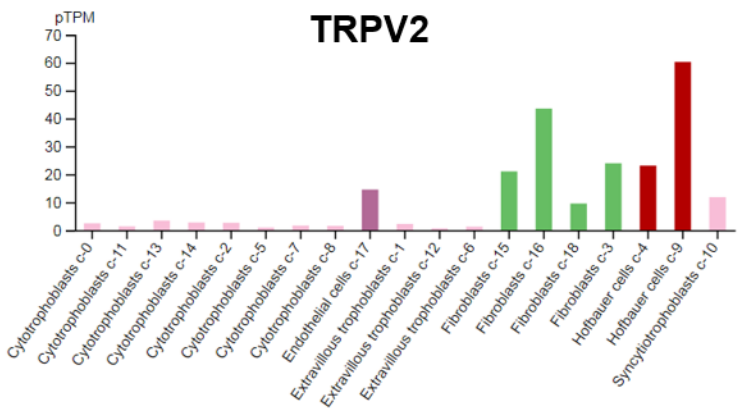
TRPV2
pTPM
70
60
50
40
30
20
10
0
Cytotrophoblasts c-0
Cytotrophoblasts c-11
Cytotrophoblasts c-13
Cytotrophoblasts c-14
Cytotrophoblasts c-2
Cytotrophoblasts c-5
Cytotrophoblasts c-7
Cytotrophoblasts c-8
Endothelial cells c-17
Extravillous trophoblasts c-1
Extravillous trophoblasts c-12
Extravillous trophoblasts c-6
Fibroblasts c-15
Fibroblasts c-16
Fibroblasts c-18
Fibroblasts c-3
Hofbauer cells c-4
Hofbauer cells c-9
Syncytiotrophoblasts c-10

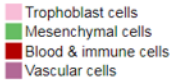
Trophoblast cells
Mesenchymal cells
Blood & immune cells
Vascular cells

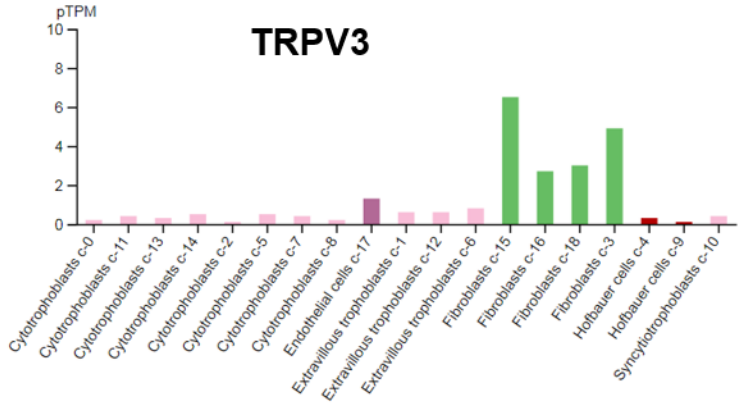
TRPV3
pTPM
10
8
6
4
2
0
Cytotrophoblasts c-0
Cytotrophoblasts c-11
Cytotrophoblasts c-13
Cytotrophoblasts c-14
Cytotrophoblasts c-2
Cytotrophoblasts c-5
Cytotrophoblasts c-7
Cytotrophoblasts c-8
Endothelial cells c-17
Extravillous trophoblasts c-1
Extravillous trophoblasts c-12
Extravillous trophoblasts c-6
Fibroblasts c-15
Fibroblasts c-16
Fibroblasts c-18
Fibroblasts c-3
Hofbauer cells c-4
Hofbauer cells c-9
Syncytiotrophoblasts c-10

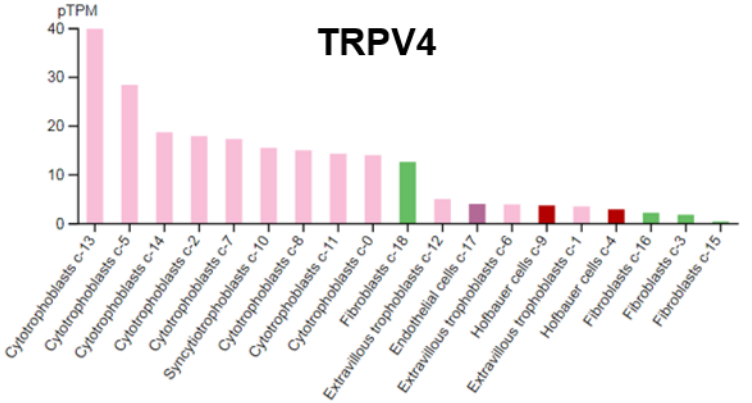
TRPV4
pTPM
40
30
20
10
0
Cytotrophoblasts c-13
Cytotrophoblasts c-5
Cytotrophoblasts c-14
Cytotrophoblasts c-2
Cytotrophoblasts c-7
Syncytiotrophoblasts c-10
Cytotrophoblasts c-8
Cytotrophoblasts c-11
Cytotrophoblasts c-0
Fibroblasts c-18
Extravillous trophoblasts c-12
Endothelial cells c-17
Extravillous trophoblasts c-6
Hofbauer cells c-9
Extravillous trophoblasts c-1
Hofbauer cells c-4
Fibroblasts c-16
Fibroblasts c-3
Fibroblasts c-15

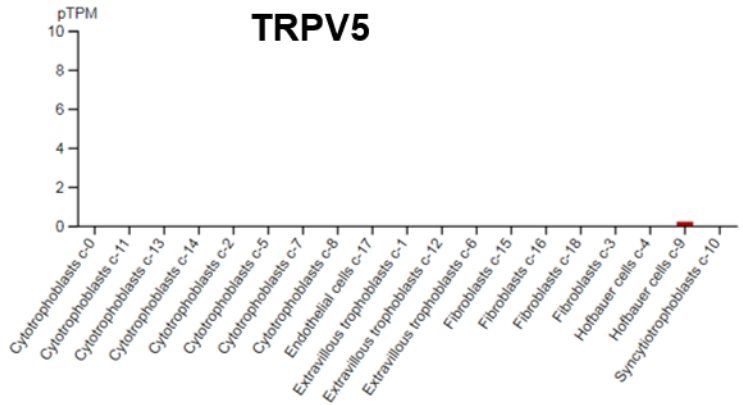
TRPV5
pTPM
10
8
6
4
2
0
Cytotrophoblasts c-0
Cytotrophoblasts c-11
Cytotrophoblasts c-13
Cytotrophoblasts c-14
Cytotrophoblasts c-2
Cytotrophoblasts c-5
Cytotrophoblasts c-7
Cytotrophoblasts c-8
Endothelial cells c-17
Extravillous trophoblasts c-1
Extravillous trophoblasts c-12
Extravillous trophoblasts c-6
Fibroblasts c-15
Fibroblasts c-16
Fibroblasts c-18
Fibroblasts c-3
Hofbauer cells c-4
Hofbauer cells c-9
Syncytiotrophoblasts c-10

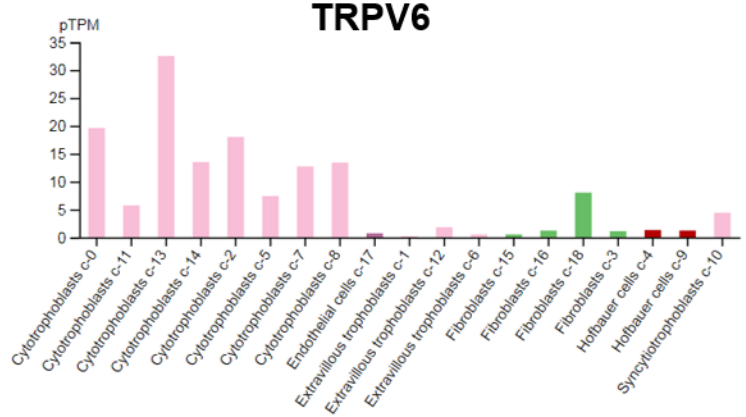
TRPV6
pTPM
35
30
25
20
15
10
5
0
Cytotrophoblasts c-0
Cytotrophoblasts c-11
Cytotrophoblasts c-13
Cytotrophoblasts c-14
Cytotrophoblasts c-2
Cytotrophoblasts c-5
Cytotrophoblasts c-7
Cytotrophoblasts c-8
Endothelial cells c-17
Extravillous trophoblasts c-1
Extravillous trophoblasts c-12
Extravillous trophoblasts c-6
Fibroblasts c-15
Fibroblasts c-16
Fibroblasts c-18
Fibroblasts c-3
Hofbauer cells c-4
Hofbauer cells c-9
Syncytiotrophoblasts c-10

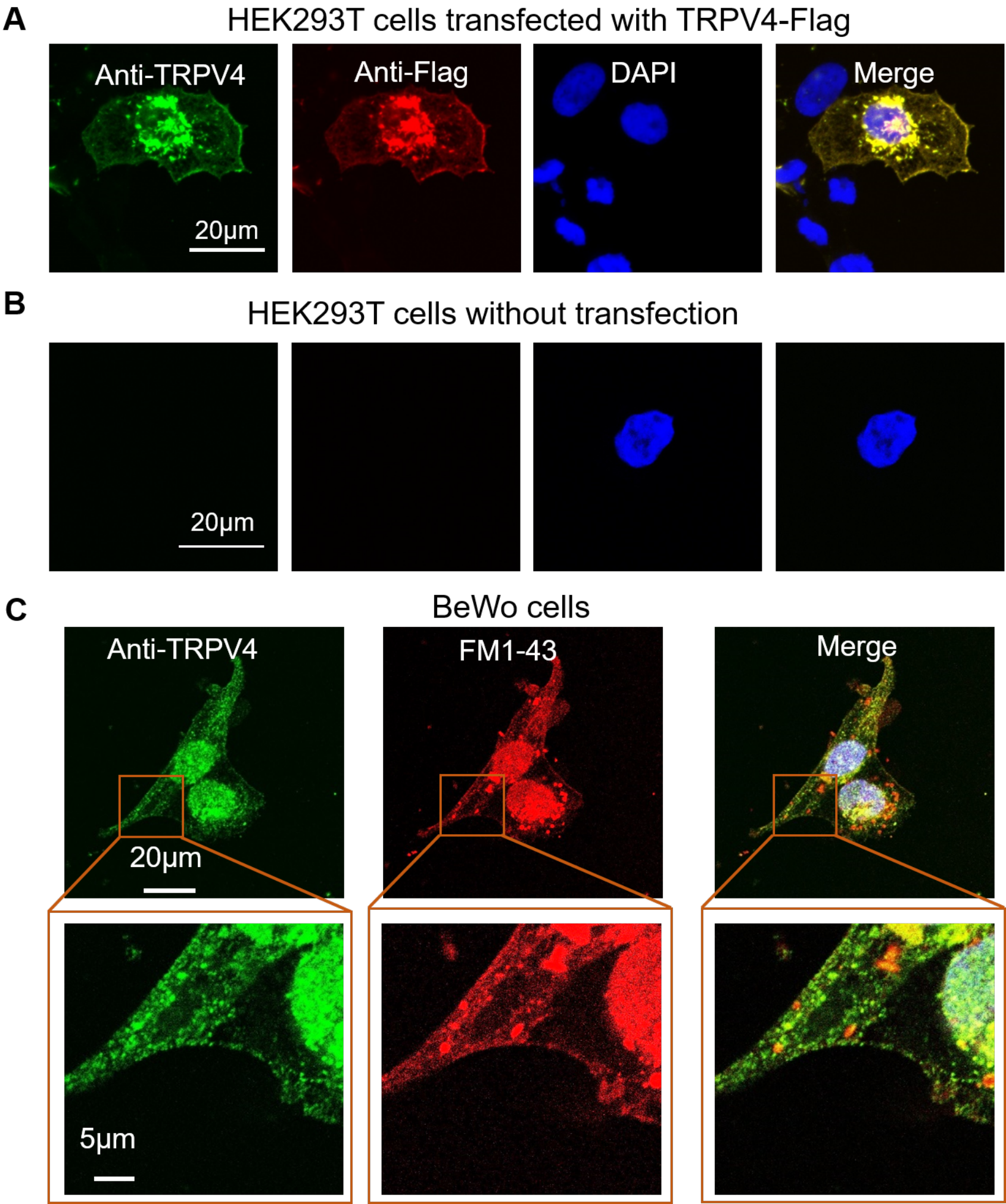
A
HEK293T cells transfected with TRPV4-Flag
Anti-TRPV4
Anti-Flag
DAPI
Merge
20μm
B
HEK293T cells without transfection
20μm
C
BeWo cells
Anti-TRPV4
FM1-43
Merge
20μm
5μm

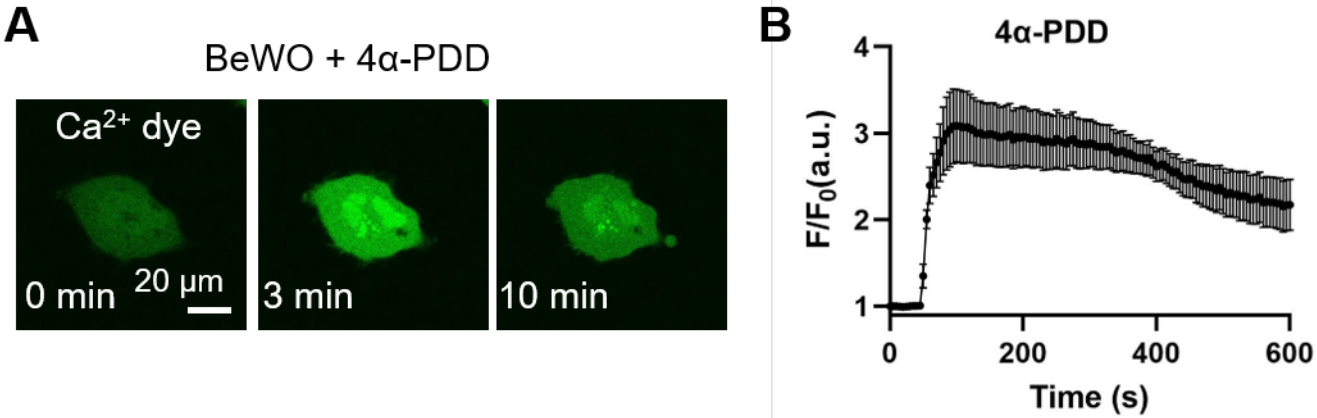
A
BeWO + 4α-PDD
Ca2+ dye
0 min
20 μm
3 min
10 min
B
4α-PDD
F/F0(a.u.)
4
3
2
1
0
200
400
600
Time (s)

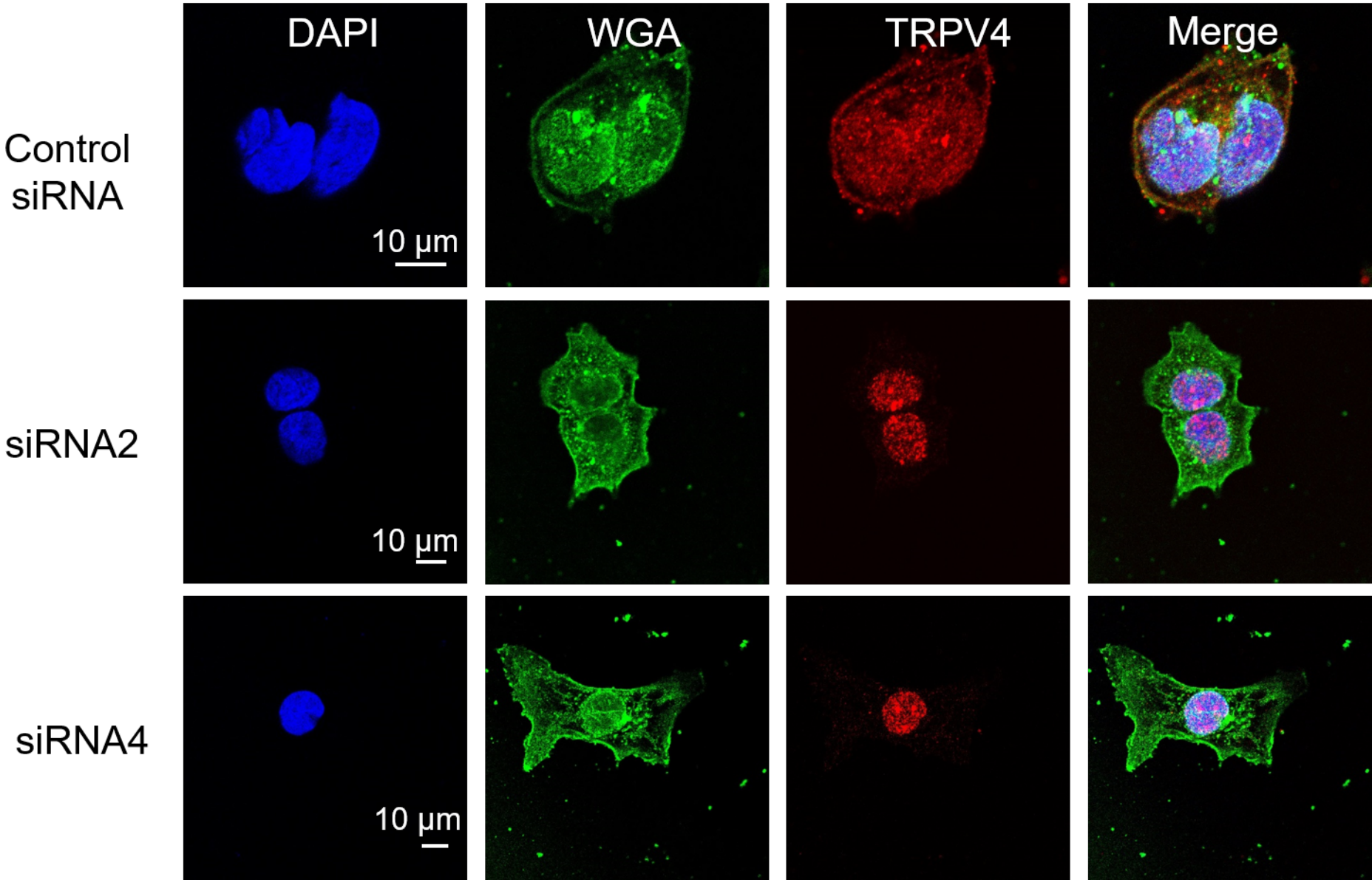
DAPI
WGA
TRPV4
Merge
Control siRNA
siRNA2
siRNA4
10 μm
10 μm
10 μm

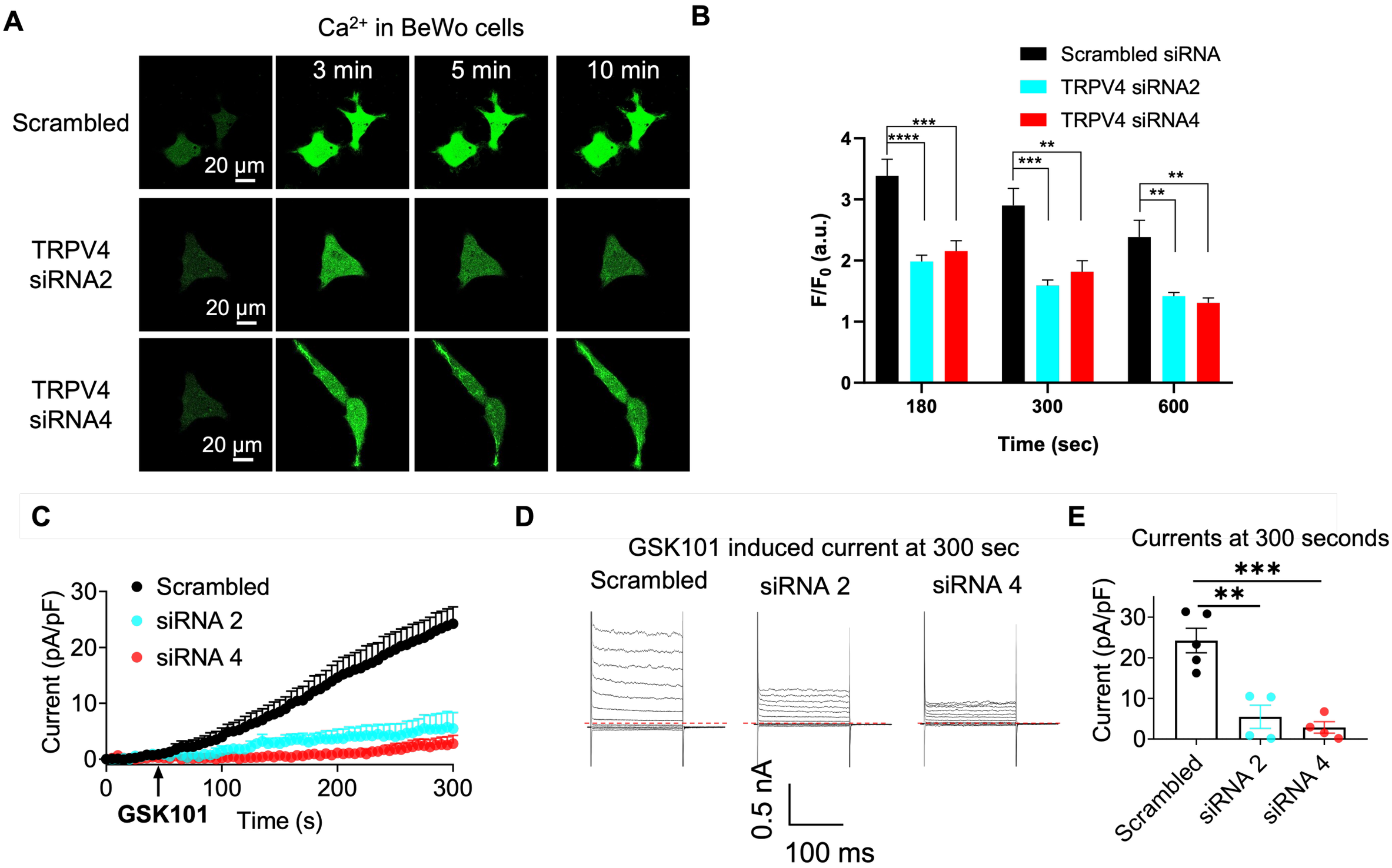
A
Ca2+ in BeWo cells
3 min
5 min
10 min
Scrambled
TRPV4 siRNA2
TRPV4 siRNA4
20 µm
20 µm
20 µm
B
Scrambled siRNA
TRPV4 siRNA2
TRPV4 siRNA4
F/F0 (a.u.)
Time (sec)
180
300
600
***
****
**
***
**
**
C
Scrambled
siRNA 2
siRNA 4
Current (pA/pF)
GSK101
Time (s)
D
GSK101 induced current at 300 sec
Scrambled
siRNA 2
siRNA 4
0.5 nA
100 ms
E
Currents at 300 seconds
Current (pA/pF)
Scrambled
siRNA 2
siRNA 4

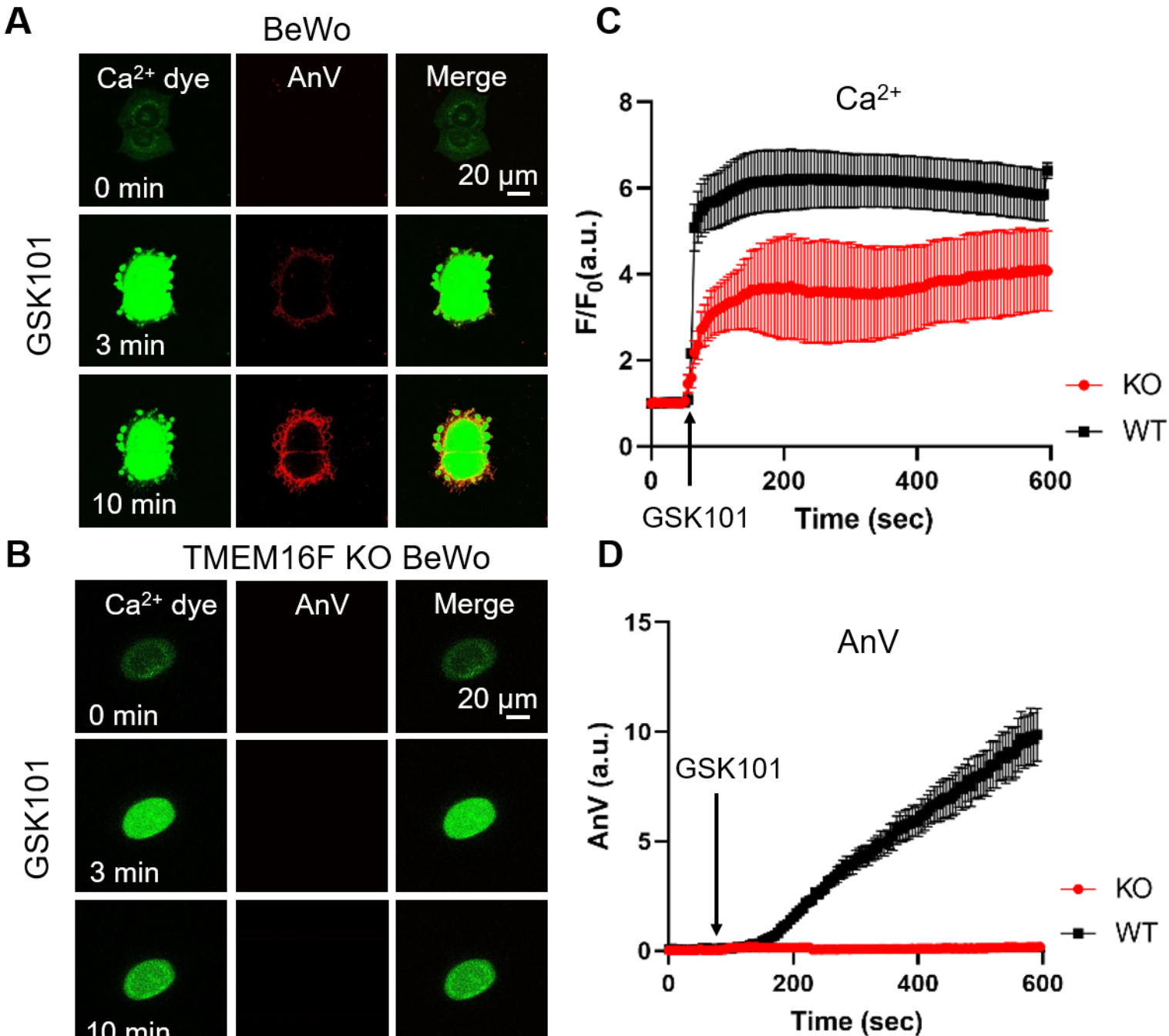
A
BeWo
Ca2+ dye
AnV
Merge
0 min
20 μm
GSK101
3 min
10 min
B
TMEM16F KO BeWo
Ca2+ dye
AnV
Merge
0 min
20 μm
GSK101
3 min
10 min
C
Ca2+
F/F0(a.u.)
8
6
4
2
0
0
200
400
600
GSK101
Time (sec)
KO
WT
D
AnV
AnV (a.u.)
15
10
5
0
GSK101
0
200
400
600
Time (sec)
KO
WT

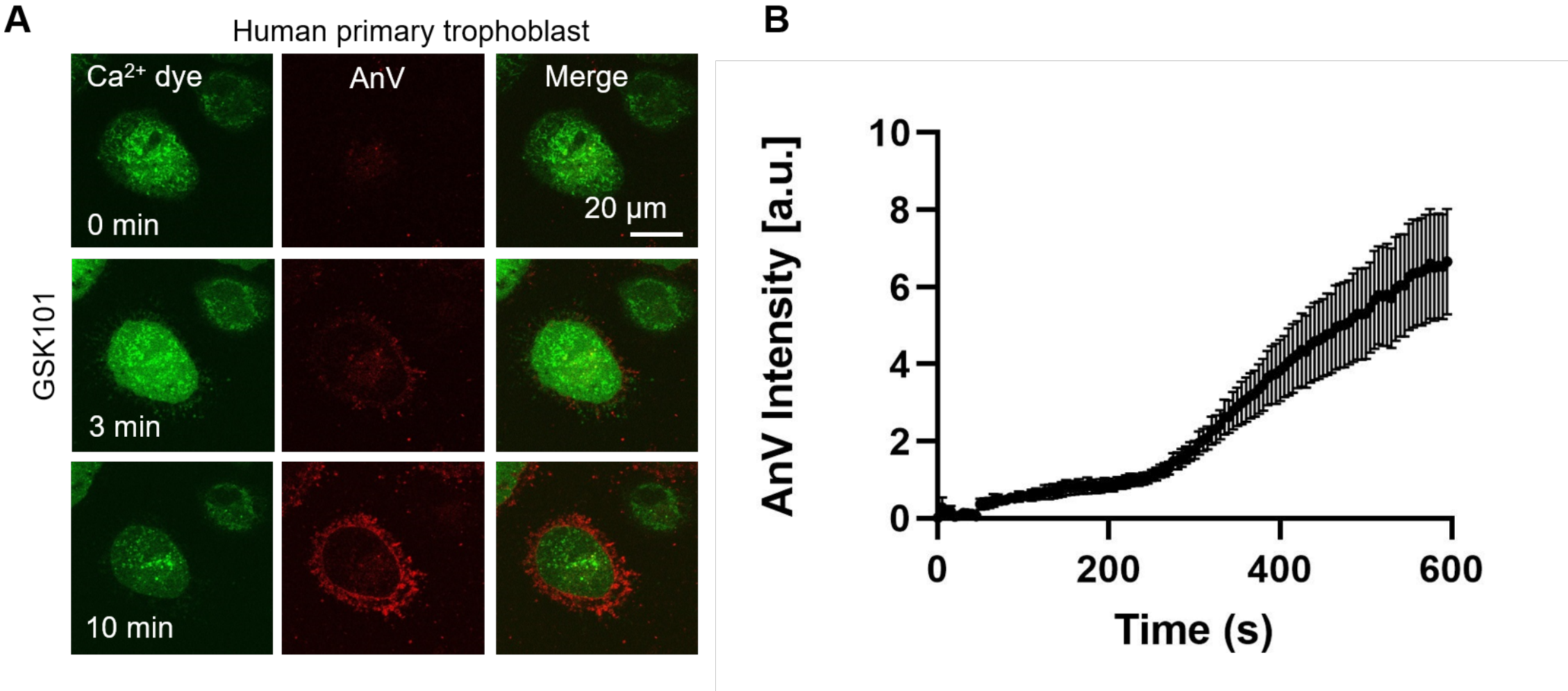
A
Human primary trophoblast
Ca2+ dye
AnV
Merge
20 µm
0 min
3 min
10 min
GSK101
B
AnV Intensity [a.u.]
10
8
6
4
2
0
0
200
400
600
Time (s)

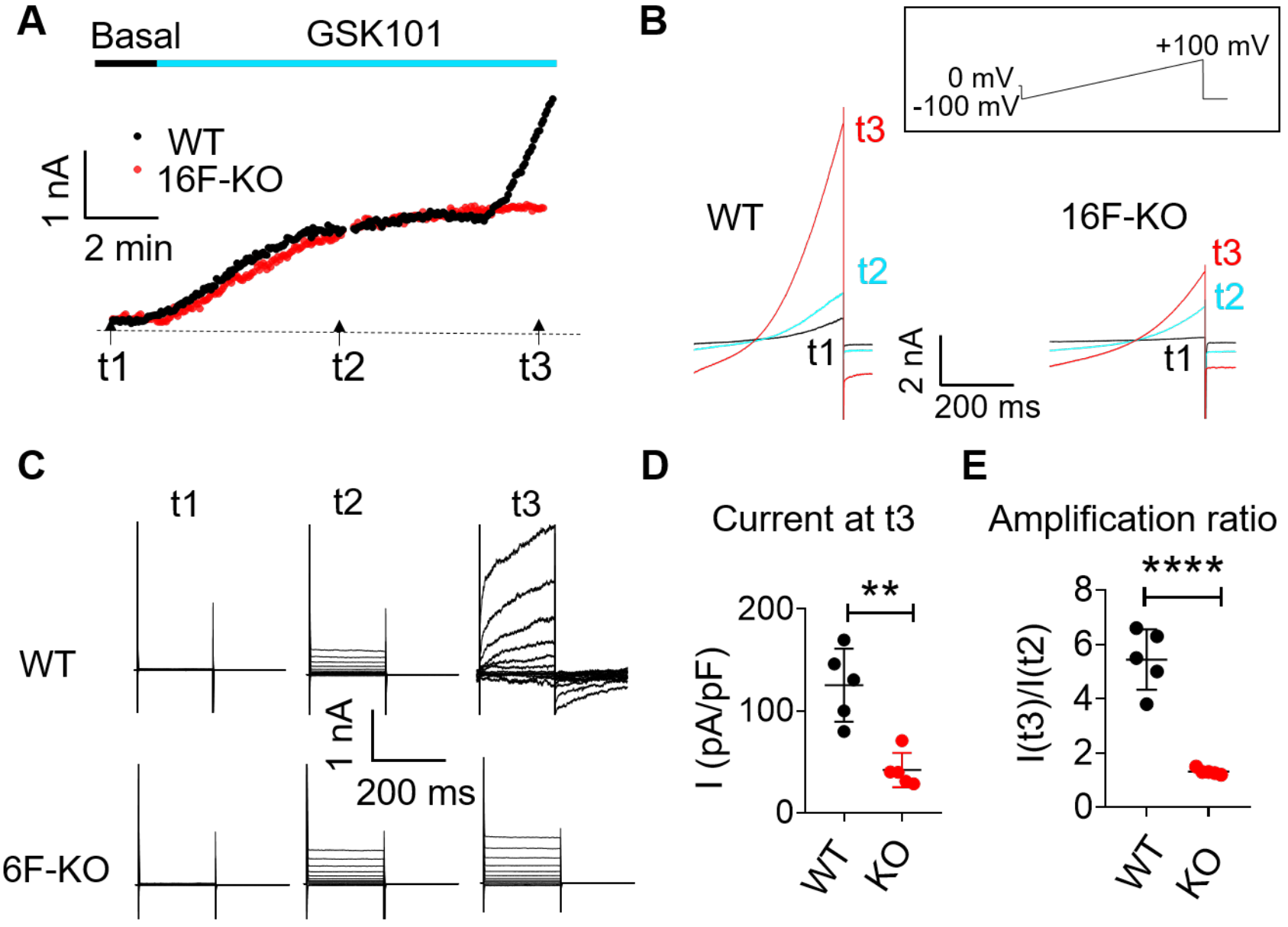
A
Basal
GSK101
WT
16F-KO
1 nA
2 min
t1
t2
t3
B
+100 mV
0 mV
-100 mV
t3
WT
t2
t1
16F-KO
t3
t2
t1
2 nA
200 ms
C
t1
t2
t3
WT
1 nA
200 ms
16F-KO
D
Current at t3
**
200
100
0
I (pA/pF)
WT
KO
E
Amplification ratio
****
8
6
4
2
0
I(t3)/I(t2)
WT
KO

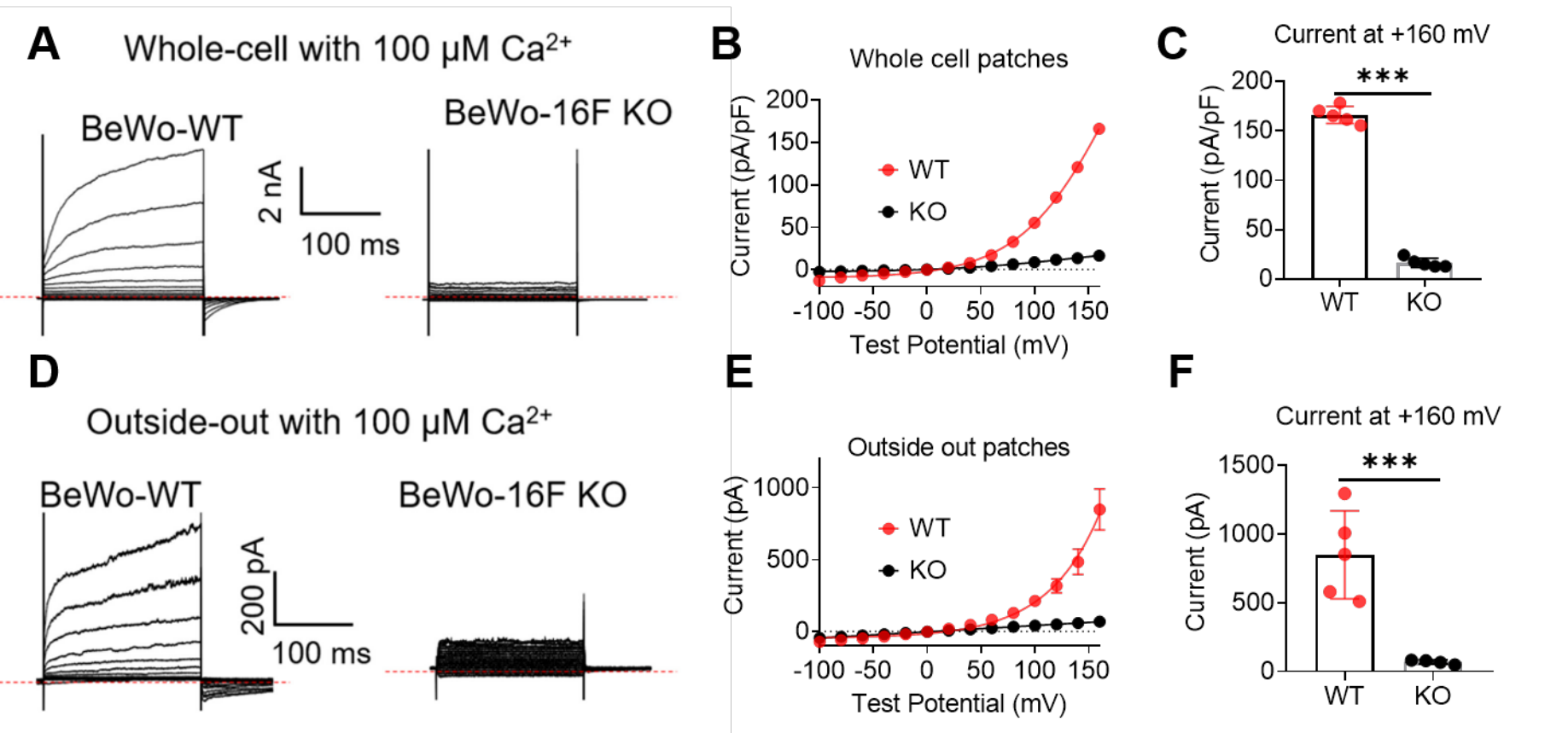
A
Whole-cell with 100 μM Ca2+
BeWo-WT
BeWo-16F KO
2 nA
100 ms
B
Whole cell patches
Current (pA/pF)
WT
KO
Test Potential (mV)
C
Current at +160 mV
***
Current (pA/pF)
WT
KO
D
Outside-out with 100 μM Ca2+
BeWo-WT
BeWo-16F KO
200 pA
100 ms
E
Outside out patches
Current (pA)
WT
KO
Test Potential (mV)
F
Current at +160 mV
***
Current (pA)
WT
KO

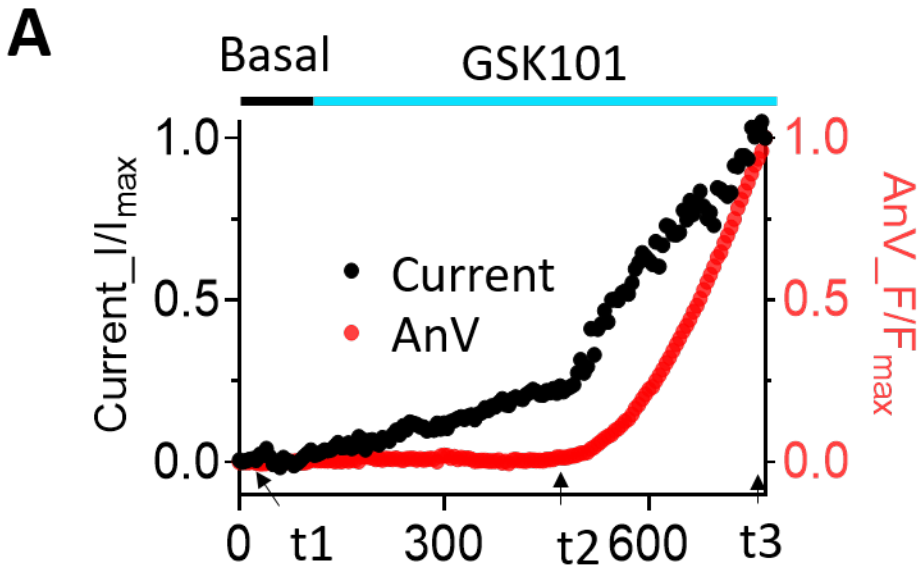
A
Basal
GSK101
Current_I/I$_{max}$
1.0
0.5
0.0
Current
AnV
AnV_F/F$_{max}$
1.0
0.5
0.0
0
t1
300
t2
600
t3

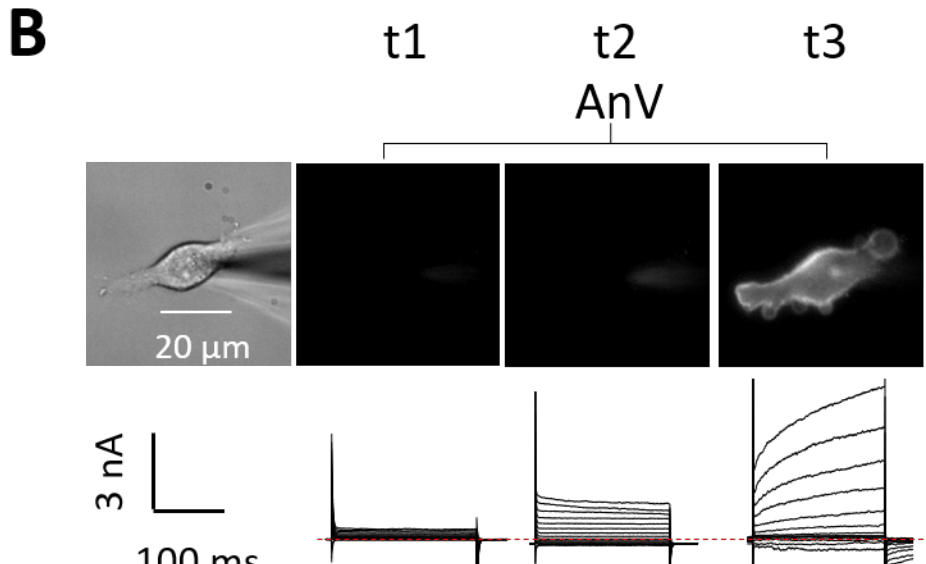
B
t1
t2
t3
AnV
20 µm
3 nA
100 ms

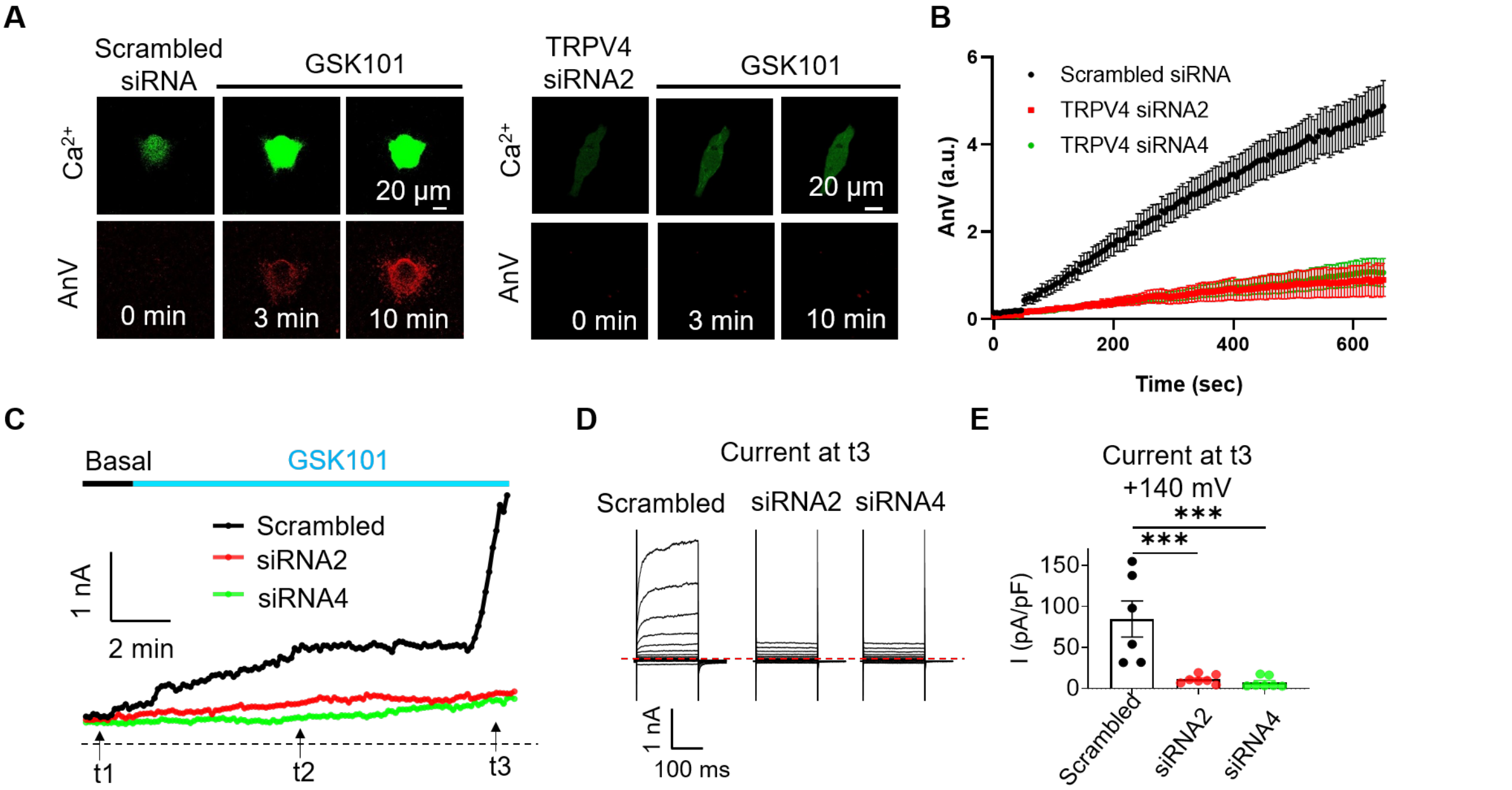
A
Scrambled siRNA
GSK101
TRPV4 siRNA2
GSK101
Ca2+
AnV
20 μm
0 min
3 min
10 min
B
Scrambled siRNA
TRPV4 siRNA2
TRPV4 siRNA4
AnV (a.u.)
Time (sec)
C
Basal
GSK101
Scrambled
siRNA2
siRNA4
1 nA
2 min
t1
t2
t3
D
Current at t3
Scrambled
siRNA2
siRNA4
1 nA
100 ms
E
Current at t3
+140 mV
***
***
I (pA/pF)
Scrambled
siRNA2
siRNA4

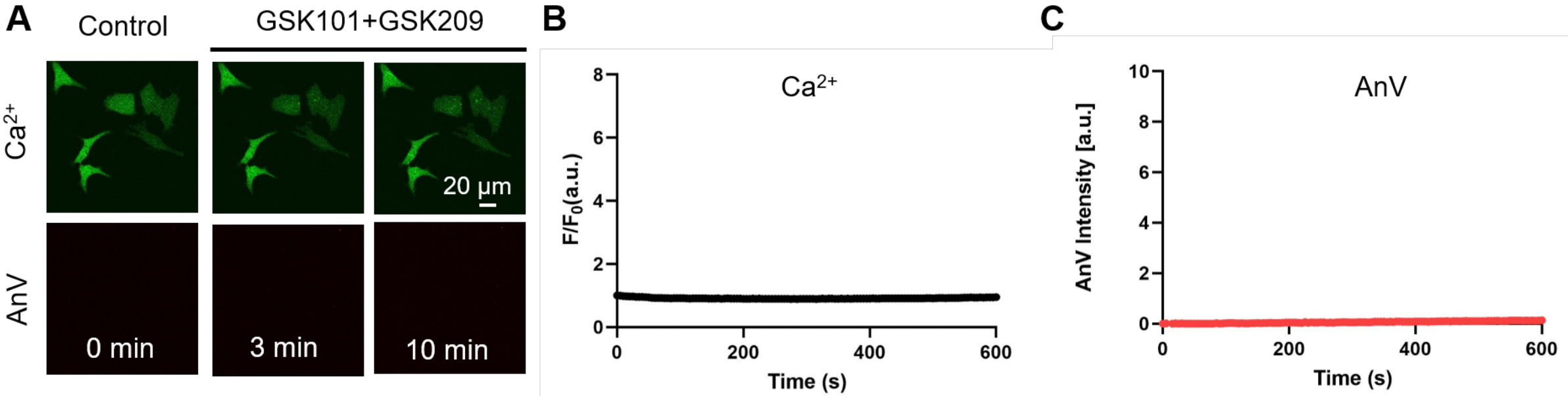
A
Control
GSK101+GSK209
Ca2+
AnV
20 μm
0 min
3 min
10 min
B
Ca2+
F/F0(a.u.)
Time (s)
C
AnV
AnV Intensity [a.u.]
Time (s)

A

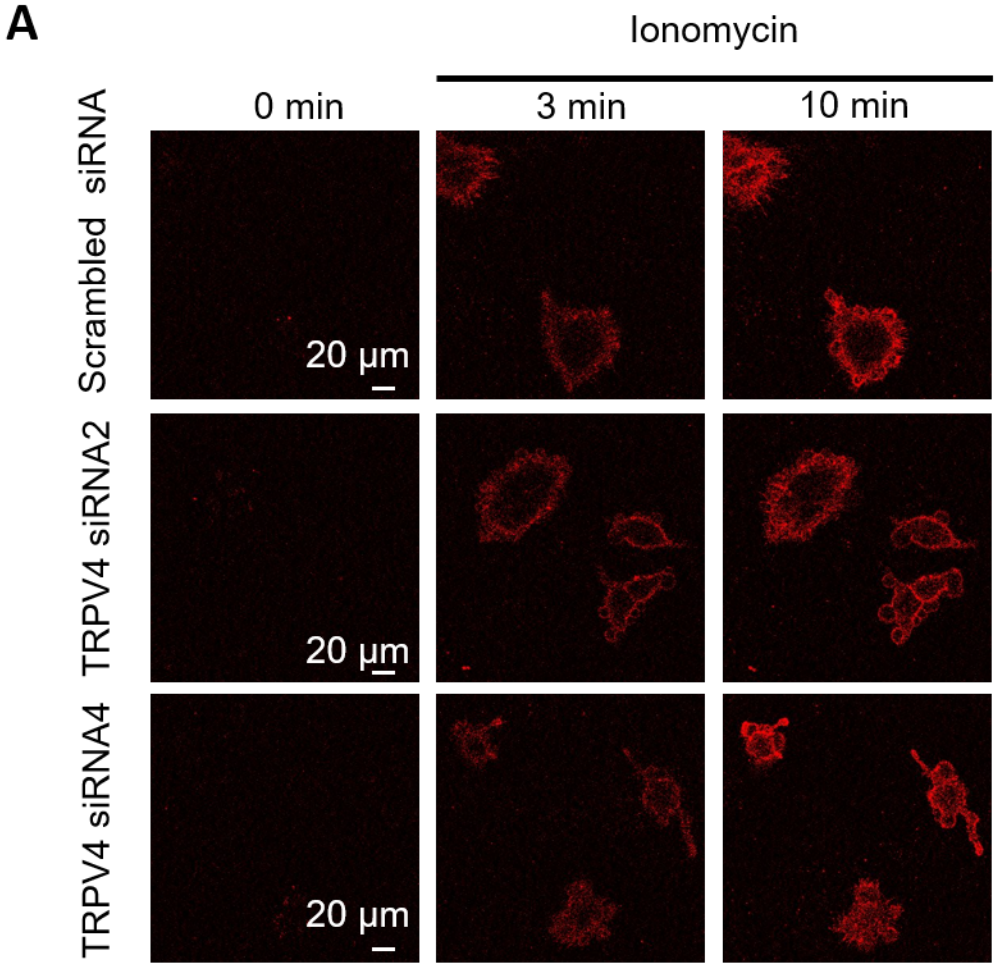
Ionomycin
0 min
3 min
10 min
Scrambled siRNA
TRPV4 siRNA2
TRPV4 siRNA4
20 µm
20 µm
20 µm

B

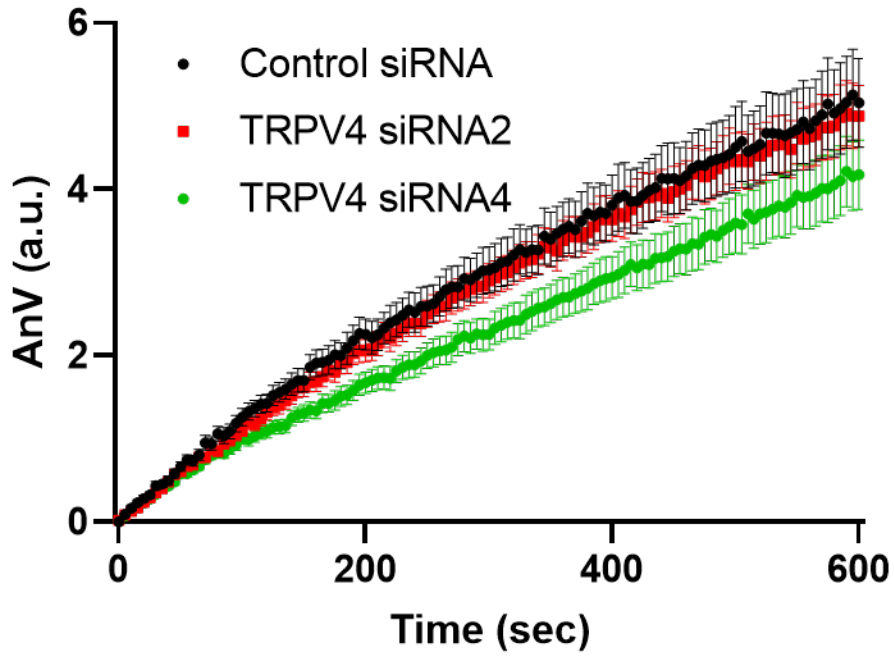
Control siRNA
TRPV4 siRNA2
TRPV4 siRNA4
AnV (a.u.)
Time (sec)
0
2
4
6
0
200
400
600

C

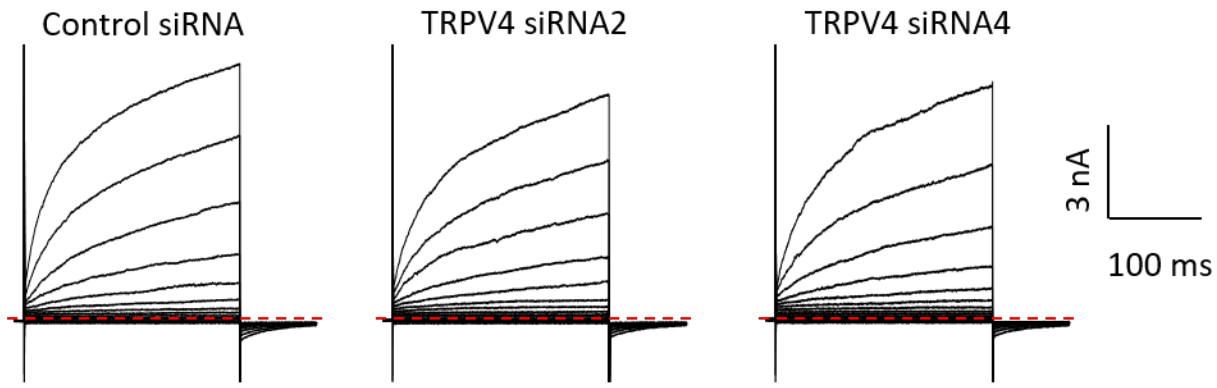
Control siRNA
TRPV4 siRNA2
TRPV4 siRNA4
3 nA
100 ms

D

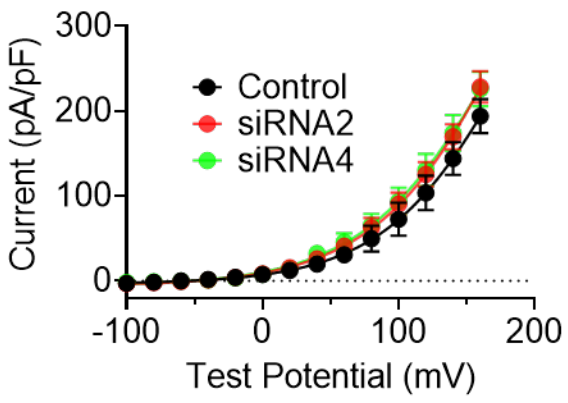
Control
siRNA2
siRNA4
Current (pA/pF)
Test Potential (mV)
300
200
100
0
-100
0
100
200

E

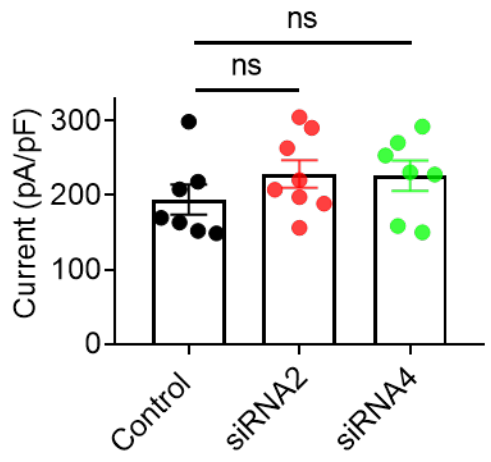
ns
ns
Current (pA/pF)
300
200
100
0
Control
siRNA2
siRNA4

F

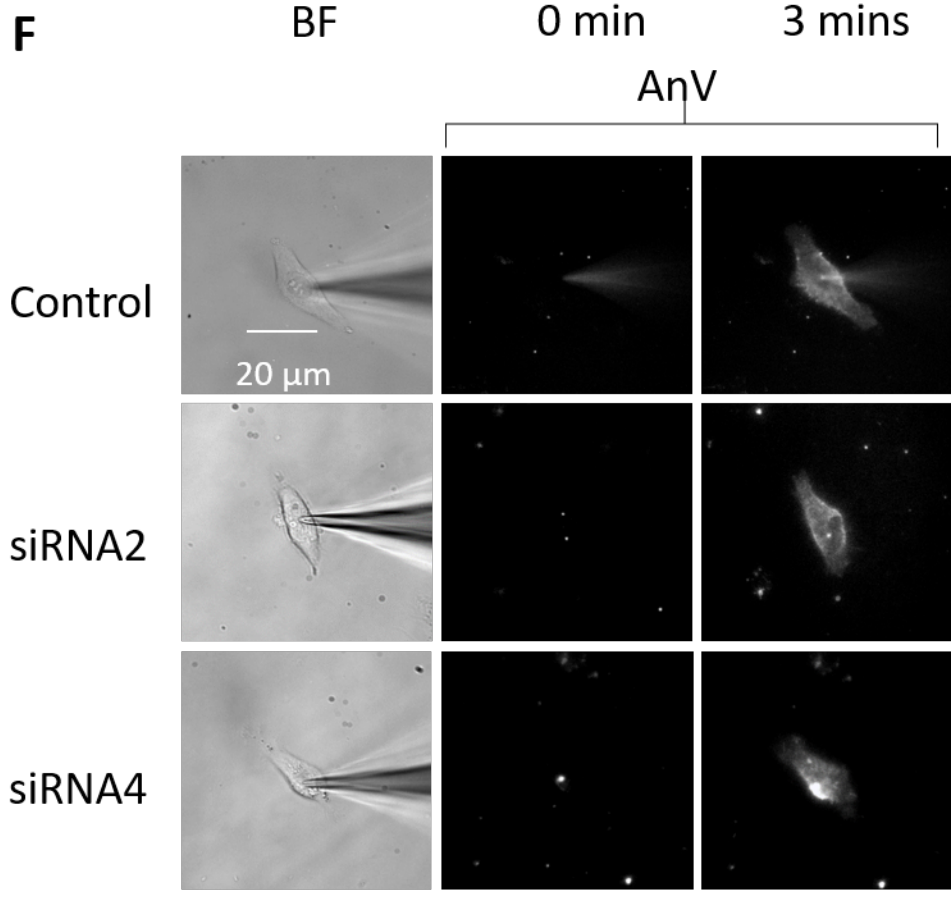
BF
0 min
3 mins
AnV
Control
siRNA2
siRNA4
20 µm

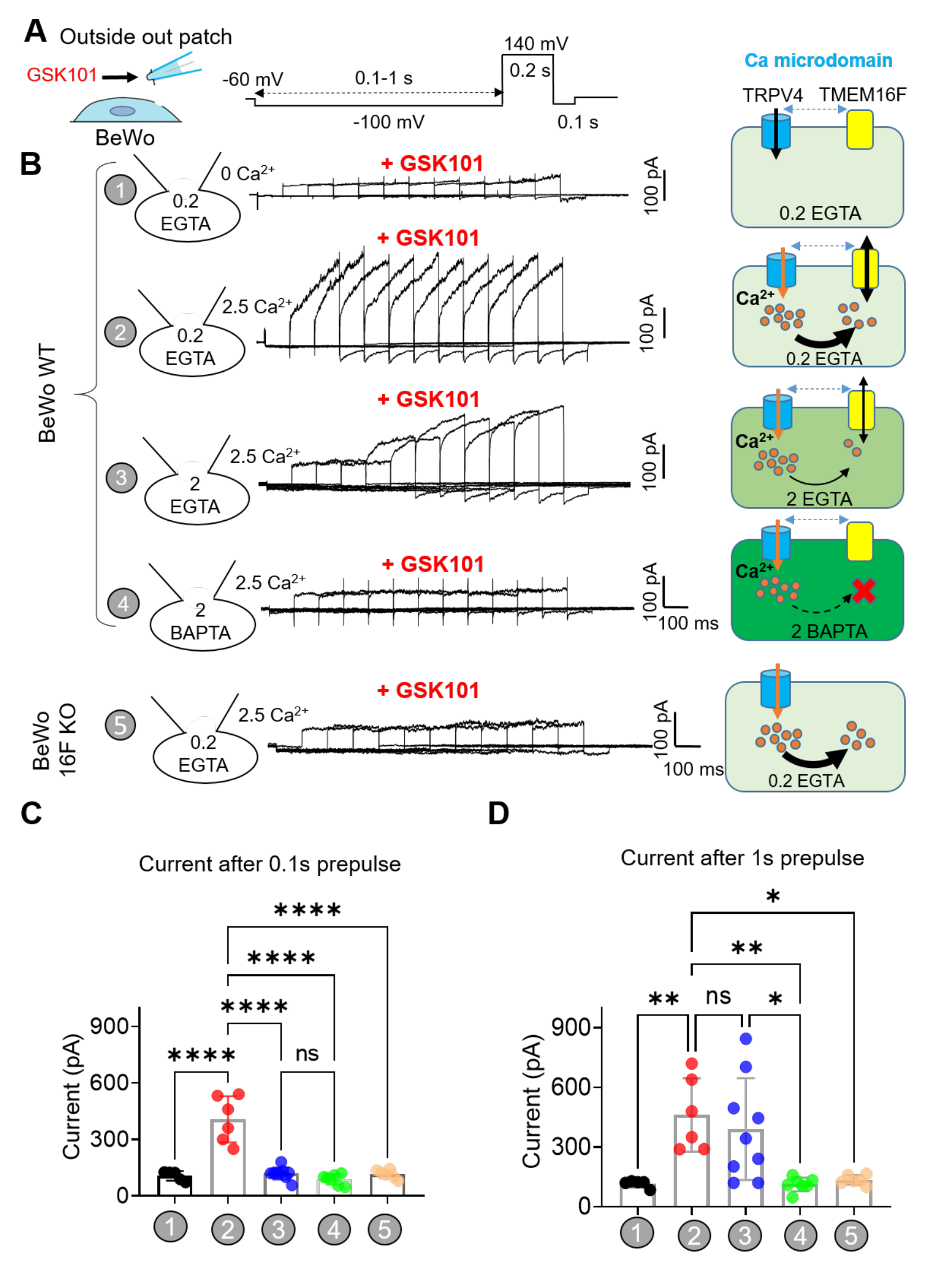
A
Outside out patch
GSK101
BeWo
-60 mV
0.1-1 s
-100 mV
140 mV
0.2 s
0.1 s
B
BeWo WT
BeWo 16F KO
1
0.2 EGTA
0 Ca2+
+ GSK101
100 pA
2
0.2 EGTA
2.5 Ca2+
+ GSK101
100 pA
3
2 EGTA
2.5 Ca2+
+ GSK101
100 pA
4
2 BAPTA
2.5 Ca2+
+ GSK101
100 pA
100 ms
5
0.2 EGTA
2.5 Ca2+
+ GSK101
100 pA
100 ms
Ca microdomain
TRPV4
TMEM16F
0.2 EGTA
Ca2+
0.2 EGTA
Ca2+
2 EGTA
Ca2+
2 BAPTA
0.2 EGTA
C
Current after 0.1s prepulse
Current (pA)
900
600
300
0
****
****
****
****
ns
1
2
3
4
5
D
Current after 1s prepulse
Current (pA)
900
600
300
0
*
**
**
ns
*
1
2
3
4
5

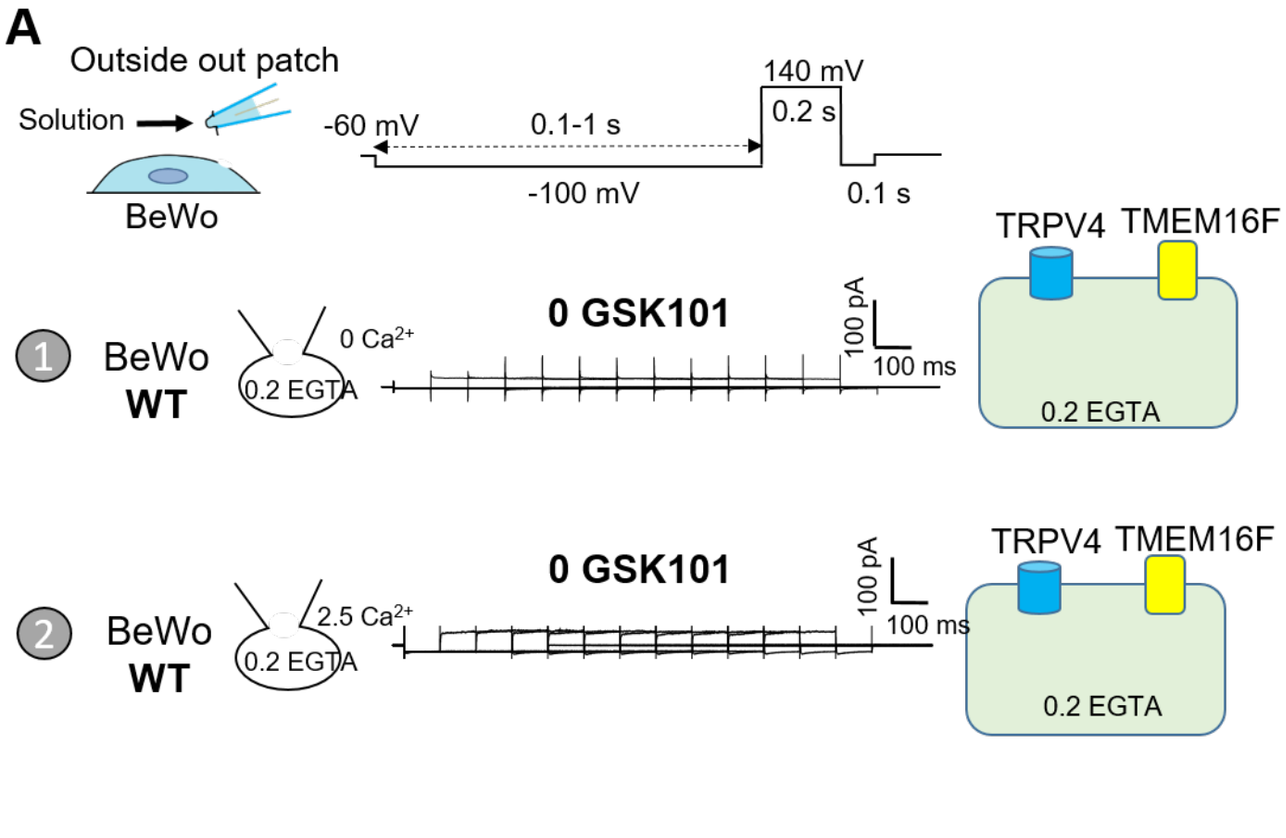
A
Outside out patch
Solution
BeWo
-60 mV
0.1-1 s
140 mV
0.2 s
-100 mV
0.1 s
1
BeWo
WT
0 Ca2+
0.2 EGTA
0 GSK101
100 pA
100 ms
TRPV4 TMEM16F
0.2 EGTA
2
BeWo
WT
2.5 Ca2+
0.2 EGTA
0 GSK101
100 pA
100 ms
TRPV4 TMEM16F
0.2 EGTA

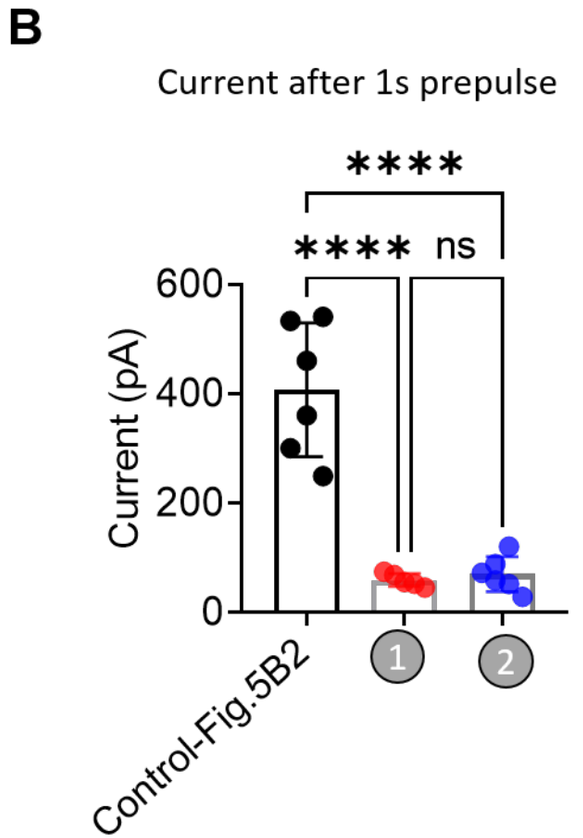
B
Current after 1s prepulse
****
**** ns
Current (pA)
600
400
200
0
Control-Fig.5B2
1
2

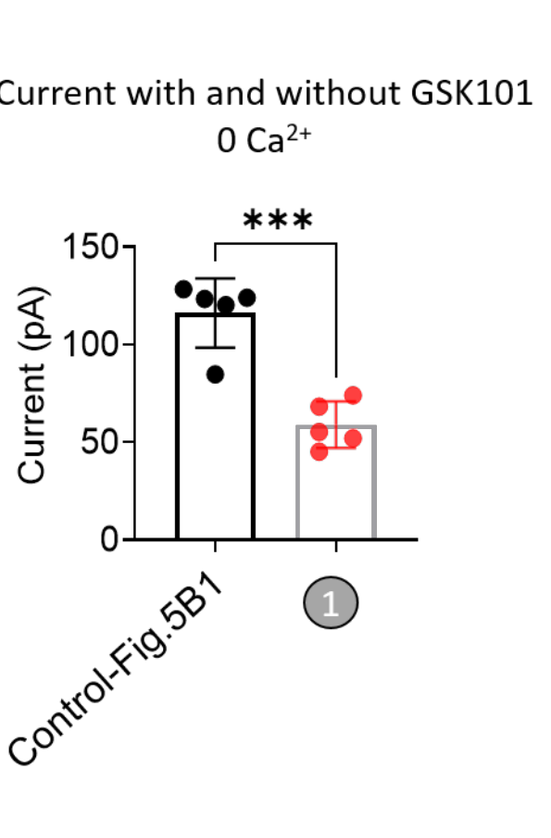
C
Current with and without GSK101
0 Ca2+
***
Current (pA)
150
100
50
0
Control-Fig.5B1
1

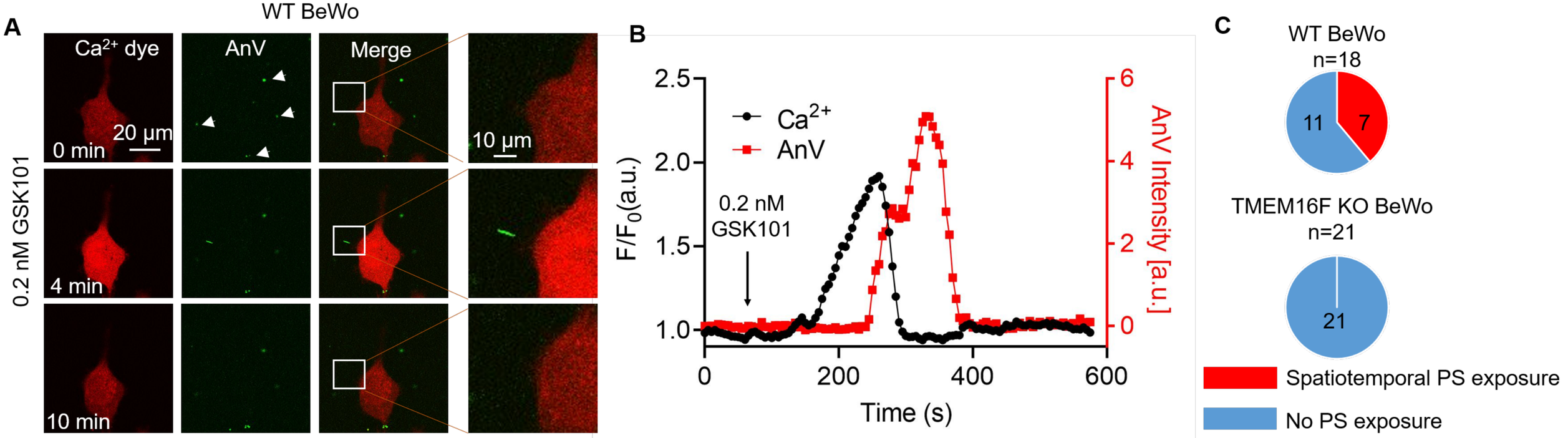
A
WT BeWo
Ca2+ dye
AnV
Merge
20 μm
10 μm
0 min
4 min
10 min
0.2 nM GSK101
B
Ca2+
AnV
0.2 nM
GSK101
F/F0(a.u.)
AnV Intensity [a.u.]
Time (s)
C
WT BeWo
n=18
11
7
TMEM16F KO BeWo
n=21
21
Spatiotemporal PS exposure
No PS exposure

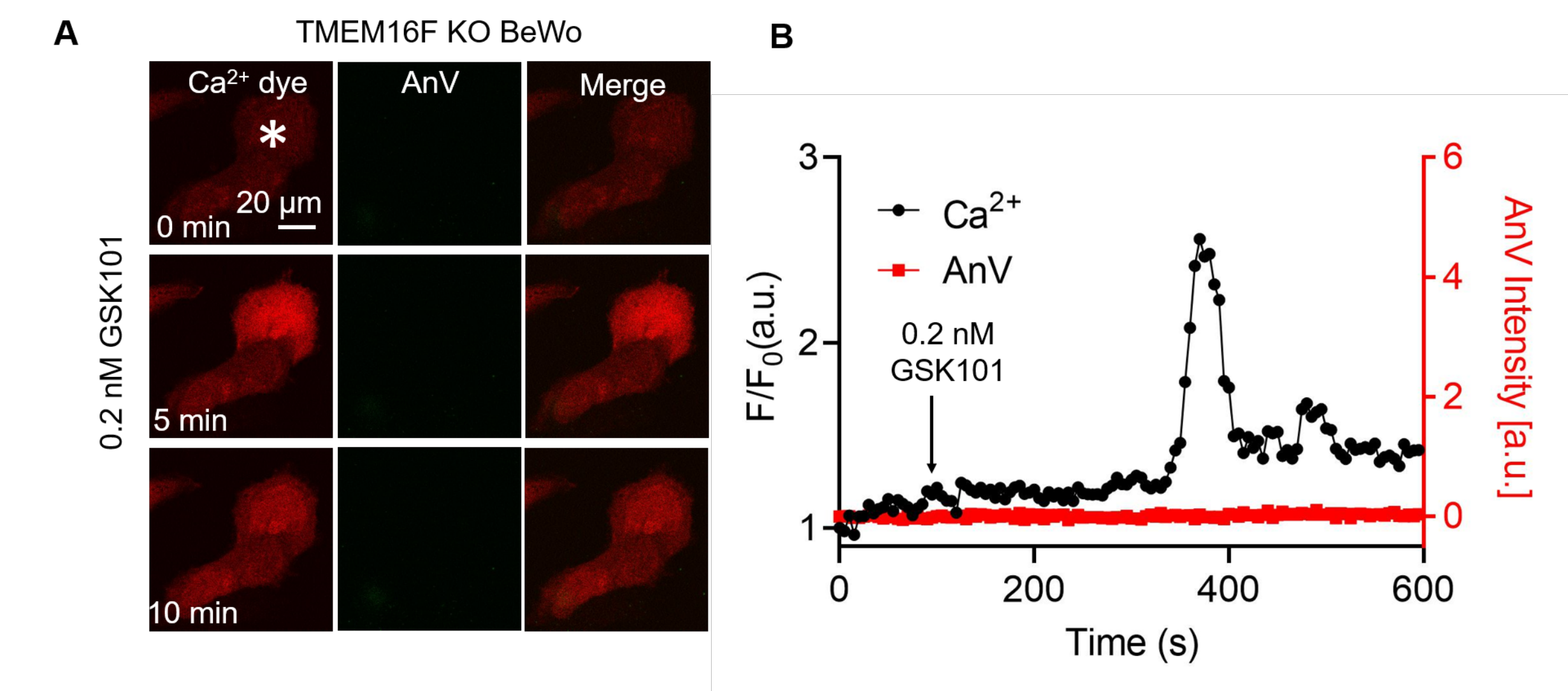
A
TMEM16F KO BeWo
Ca2+ dye
AnV
Merge
20 µm
0 min
5 min
10 min
0.2 nM GSK101
B
Ca2+
AnV
0.2 nM
GSK101
F/F0(a.u.)
AnV Intensity [a.u.]
Time (s)
0
200
400
600
1
2
3
0
2
4
6

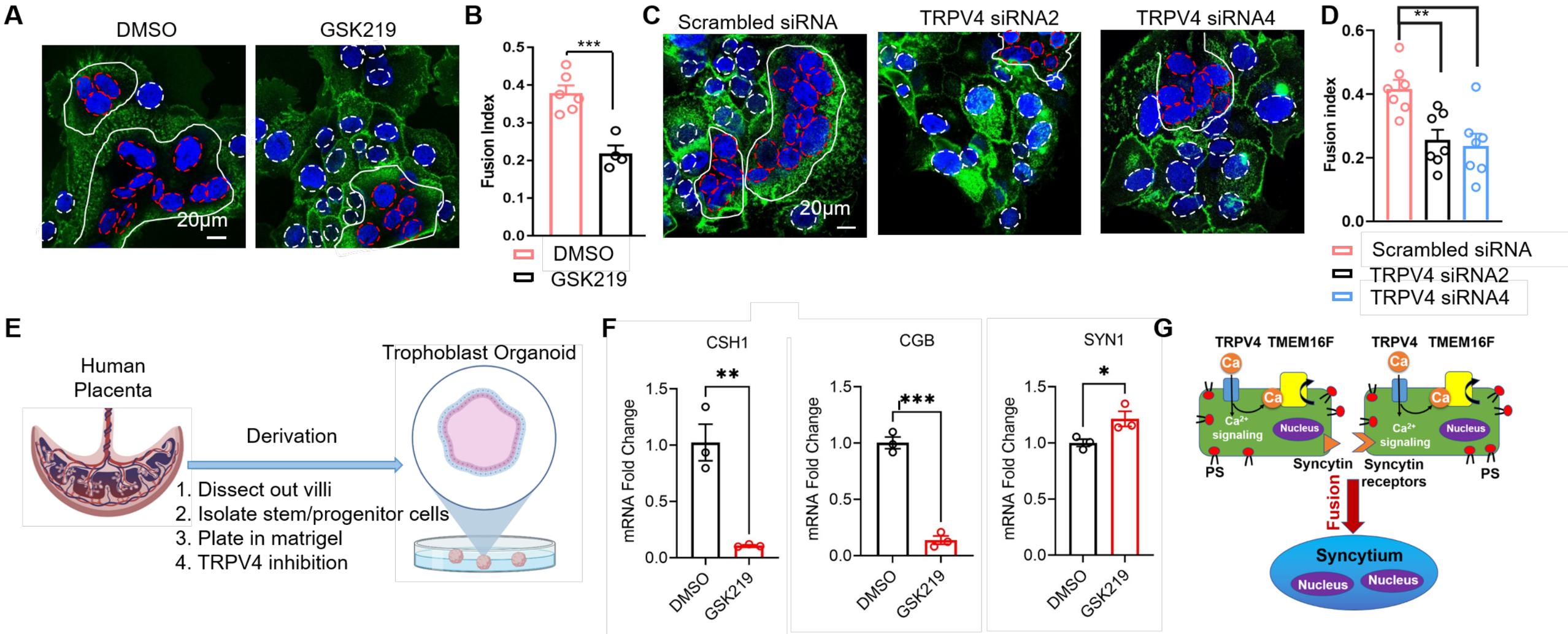
A
DMSO
GSK219
20μm
B
Fusion Index
0.5
0.4
0.3
0.2
0.1
0.0
***
DMSO
GSK219
C
Scrambled siRNA
TRPV4 siRNA2
TRPV4 siRNA4
20μm
D
Fusion index
0.6
0.4
0.2
0.0
**
**
Scrambled siRNA
TRPV4 siRNA2
TRPV4 siRNA4
E
Human Placenta
Derivation
1. Dissect out villi
2. Isolate stem/progenitor cells
3. Plate in matrigel
4. TRPV4 inhibition
Trophoblast Organoid
F
CSH1
CGB
SYN1
mRNA Fold Change
1.5
1.0
0.5
0.0
**
***
*
DMSO
GSK219
G
TRPV4 TMEM16F
Ca
Ca2+ signaling
Nucleus
PS
Syncytin
Syncytin receptors
Fusion
Syncytium
Nucleus
Nucleus

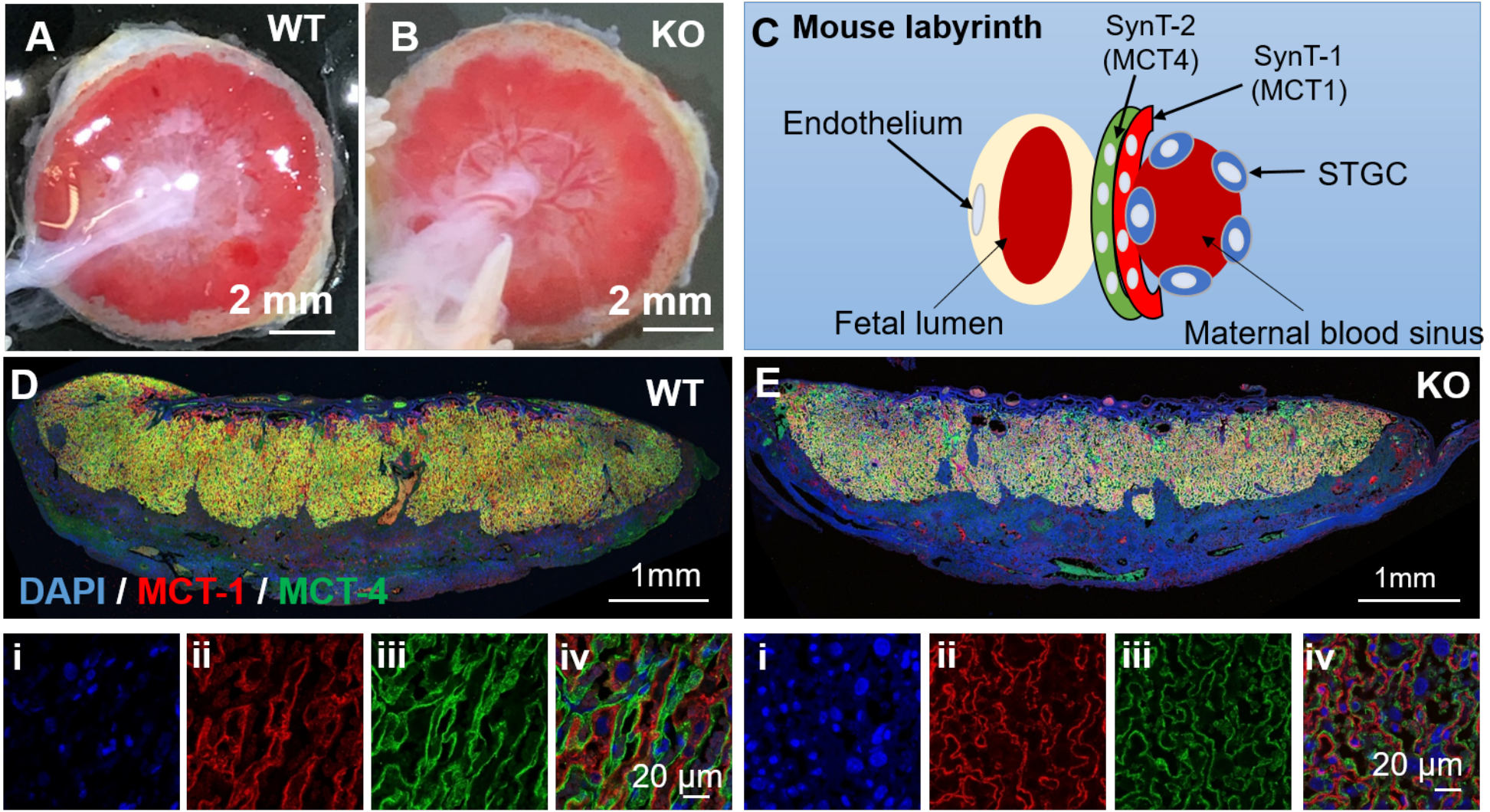
A
WT
2 mm
B
KO
2 mm
C Mouse labyrinth
SynT-2
(MCT4)
SynT-1
(MCT1)
Endothelium
STGC
Fetal lumen
Maternal blood sinus
D
WT
DAPI / MCT-1 / MCT-4
1mm
E
KO
1mm
i
ii
iii
iv
20 µm
i
ii
iii
iv
20 µm